The Henryk Niewodniczański Institute of Nuclear Physics
Polish Academy of Sciences

Characterization of cell surface structure and its relation to cytoskeleton elasticity in cancer cells

Justyna Bobrowska

Thesis submitted for the Degree of Doctor of Philosophy in Physics
Prepared under the supervision of
dr hab. Małgorzata Lekka (thesis supervisor)
dr hab. Jakub Rysz (auxiliary supervisor)

Kraków 2016

You must have long-range goals to keep you
from being frustrated by short-range failures.

Charles C. Noble

Acknowledgements

Undertaking this PhD has been a truly life-changing experience and it would not have been possible to do without all the support and guidance that I received from many people. I am lucky to have met them.

First of all, I would like to express my deepest gratitude to my thesis supervisor Assoc. Prof. Małgorzata Lekka. I am grateful for her help, encouragement, constructive criticism, and guidance. With her immense knowledge and excitement in regard to research, she shows me what does it mean to be a real researcher.

I would also like to thank my co-supervisor, Assoc. Prof. Jakub Rysz, for his help, insightful comments and expertise that greatly assisted the research.

My deepest thanks to all my colleagues from the Division of Applications of Physics and Interdisciplinary Research (IFJ PAN) headed by Prof. Wojciech Kwiatek and the Department of Advanced Materials Engineering (UJ) under the supervision of Prof. Andrzej Budkowski. Working with you, as a team, was a real honour for me. Kasia and Szymon, you were the best labmates I could have. I would like to thank Mrs. Joanna Wiltowska-Zuber and Mrs. Joanna Pabijan for their laboratory support and Dr Kamil Awsiuk for his help with PCA.

I am also grateful to Assoc. Prof. Franciszek Krok and Dr Benedykt R. Jany for their help with recording SEM images and to Dr Jonathan Moffat, and Prof. Mike Reading for sharing PTMS spectra.

Sincere thanks to the group of Prof. Peter Hinterdorfer from the University of Linz, where I spent a few months as an intern.

For my family and friends for their love and patience. Especially, during last months, when my duties were consuming all my time, but you never said a word. I know I owe you.

And, finally, to my husband Piotr, who always believes in me, even when I do not. Without you I would not be here.

Abstract

The alterations observed in tumour cells include the number of processes introducing abnormalities in cellular morphology, structure and growth profiles. Despite continuous efforts, the molecular mechanism of the metastasis is still not understood completely. That is the reason why there is an urgent need for the search of new scientific approaches in the cancer progression investigations. The development of various biochemical and biological methods increases the chance to detect cancer, however, in past decades, single cell biomechanics has gained large significance since certain diseases are known to manifest in altered biomechanical properties. Stiffness of single cells is one of the major properties that changes during cancerous progression. Studies have demonstrated that biomechanics can bring both data describing mechanisms underlying cancer progression and tools for its detection and diagnosis at the single cell level. However, one of the emerging directions is to correlate cellular biomechanics with biochemical and biophysical properties of single cells.

The main objective of the presented thesis is to study how single cell deformability is linked with cellular surface properties, and how these changes correlate with cancer progression. Thus, the elasticity of melanoma cells was measured by means of atomic force microscopy (AFM). Measurements were carried out for three groups of cells encompassing cells originating from primary tumour sites i.e. from radial and vertical growth phases (RGP and VGP, respectively), and those derived from skin and lung metastasis. The results were compared with properties of melanocytes (cells from which melanoma originates). The surface properties were determined using time of flight secondary ions mass spectrometry (ToF SIMS). The use of ToF SIMS has required to develop a dedicated sample preparation protocol enabling measurements of biological material in the high vacuum environment.

The final results show the correlation between single cell deformability and surface biochemical properties of melanoma cells. They confirm the hypothesis that cancer progression causes alterations in the morphological and mechanical properties of cancerous cells and these differences are connected with changes in the cellular surface composition.

Streszczenie

Zmiany obserwowane w komórkach nowotworowych obejmują szereg procesów wprowadzających zaburzenia w ich morfologii, strukturze i wzroście. Pomimo ciągłych badań, molekularny mechanizm procesu przerzutowania wciąż nie został do końca wyjaśniony. Dlatego wciąż istnieje potrzeba poszukiwania nowych rozwiązań w badaniach dotyczących nowotworów. Rozwój zaawansowanych metod biochemicznych i biologicznych zwiększa szanse na wczesne wykrywanie zmian nowotworowych. Jednakże, w ostatnich dekadach, biomechanika pojedynczej komórki zyskuje na znaczeniu, ponieważ okazuje się, że wiele chorób wpływa na zmianę właściwości biomechanicznych już na poziomie komórkowym. Sztywność pojedynczych komórek zmienia się podczas progresji nowotworowej. Liczne badania wykazują, że biomechanika może dostarczać zarówno danych opisujących mechanizm progresji nowotworu jak i narzędzi do jego detekcji na poziomie pojedynczej komórki. Niemniej jednak, jednym z istotnych kierunków badań jest korelacja biomechaniki z biochemicznymi i biofizycznymi właściwościami komórek.

Głównym celem niniejszej rozprawy jest zbadanie w jaki sposób elastyczność komórki jest związana budową biochemiczną jej powierzchni i czy zmiany te są skorelowane ze stopniem progresji nowotworowej. W tym celu, elastyczność komórek czerniaka została wyznaczona za pomocą mikroskopii sił atomowych (AFM). Pomiary zostały wykonane dla komórek wywodzących się z linii komórkowych pochodzących z pierwotnego ogniska czerniaka - z radialnej i wertykalnej fazy wzrostu, oraz z przerzutu czerniaka do skóry i płuc. Jako linię referencyjną wykorzystano prawidłowe melanocyty. Budowę biochemiczną powierzchni komórek zbadano za pomocą spektrometrii mas jonów wtórnych za analizatorem czasu przelotu (ToF SIMS). Wykorzystanie ToF SIMS wymagało opracowania protokołu preparatyki umożliwiającego pomiary materiału biologicznego w warunkach wysokiej próżni.

Uzyskane rezultaty, przedstawione w niniejszej rozprawie, wskazują na związek pomiędzy deformowalnością a budową biochemiczną powierzchni komórek czerniaka. Tym samym potwierdzają hipotezę, że progresja nowotworowa powoduje różnice w morfologii i nanomechanice komórek nowotworowych, które są związane ze zmianami w budowie biochemicznej ich powierzchni.

Table of contents

List of abbreviations

1205Lu - melanoma cell line derived from the lungs metastasis of WM793 cells
A375P - melanoma cell line derived from the lungs metastasis
A_C *- surface area of an average single cell*
A_N *- surface area of an average single nucleus*
AFM - atomic force microscope
ECM – extracellular matrix
EMEM - cell culture medium
HCV29 – non-malignant epithelial cells of ureter
HEMa-LP - human, epidermal, adult melanocytes - primary cell line
HTB-9 - urinary bladder carcinoma
HT1376 - urinary bladder carcinoma
N/C - nucleus-to-cell ratio
PBS - phosphate buffer saline
PC - principal component
PCA - principal component analysis
PTMS - photothermal microspectroscopy
RGP - radial growth phase
RPMI - cell culture medium
SD - standard deviation
SEM - scanning electron microscope
T24 - transitional cell carcinoma
ToF SIMS - time of flight secondary ions mass spectrometry
VGP - vertical growth phase
WM115 – melanoma cell line from vertical growth phase (VGP)
WM266-4 - melanoma cell line derived from the skin metastasis of WM115 cells
WM239 - melanoma cell line derived from the skin metastasis
WM35 - melanoma cell line from radial growth phase (RGP)
WM793 - melanoma cell line from vertical growth phase (VGP)

1. Introduction

Nowadays, the development of advanced spectroscopic techniques, working at the nanoscale, achieved through enhancing the sensitivity and through coupling with other complementary techniques, enables measurements of biological samples at the single cell level. Many of the processes, occurring at the cellular level, play an important role in the variety of biological functions at macroscale. The example is the carcinogenesis that starts with the alterations occurring in single cells. These changes encompass, among others, distinct cellular morphology, cytoskeleton organization, biochemical composition, biophysical and biomechanical properties. Such an observation leads to the conclusion that cancer progression is a complex process that cannot be explained with a single biomarker. Therefore, the employment of various techniques, including molecular biology and physical approaches, delivers distinct characteristics of cancer-related changes in single cells.

Since several decades, the atomic force microscopy (AFM) can serve not only as a tool for the measurements of the cellular morphology with a high resolution but also, working in the force spectroscopy mode, it delivers the quantitative description of mechanical properties of living cells in conditions close to their physiological environment. Thus, within the frame of the presented thesis, the goal was to characterize mechanical properties of various melanoma cells lines originating from distinct stages of melanoma progression, namely, from radial/vertical growth phases and from metastasis to skin and lung. The obtained results were compared to properties of melanocytes being the cells of origin for malignant melanoma.

On the other hand, the altered biomechanics is only one of many distinct features characteristic for cancerous cells. The other changes include modifications in adhesive properties of single cells occurring at the cell surface. Thus, one can expect that, instead of searching for specific molecules responsible for malignant phenotype, the alterations in the overall composition of cell’s surface are distinct enough to be identified using techniques probing sample surface and, further, to be used as a diagnostic marker. Among various techniques used to study the composition of cell surface, a time of flight secondary ions mass spectrometry (ToF SIMS) appears to be the optimal one to measure the biophysical/biochemical changes on the surface of cancerous cells. The recorded information is derived from a layer of a few nm, that is comparable to the thickness of the cell membrane. In this thesis, the ToF SIMS technique was applied to measure the surface composition of individual melanoma cells in an attempt to detect these changes occurring at the sub-cellular and cellular levels. The goal was to study whether there is a correlation between biomechanical and biophysical/biochemical properties of cell surface.

The layout of the presented thesis is the consequence of the proposed research plan. *Chapter 2* introduces the basic information on melanoma progression, basic terms used in biomechanics of cells, followed by significance of cellular deformability and chemical properties. The *Chapter 2* ends with the presentation of the aims of the thesis. Subsequently, in *Chapter 3*, the biological samples are characterized together with the applied methodology of the sample preparation. In particular, the protocol devoted to ToF SIMS sample preparation was developed as a one of specific work objectives. Its validation involved the AFM based topography imaging after each step of preparation protocol and cellular structure and surface visualization by fluorescence and environmental scanning electron (ESEM) microscopes. The basics for all employed experimental methods are shortly described in the *Chapter 4.* Mass spectra of biological samples are very complex, that is why various statistical methods are usually used to resolve characteristic fingerprints in these samples. Here, the principal component analysis (PCA) was chosen, as it allows for the search of the biggest variances in the analysed data. Moreover, PCA was performed for the whole collected range of mass spectra without a pre-definition of any particular mass peaks *a priori*. Using such an approach, it is possible to determine those masses that cause the strongest differentiation between studied cell populations, afterwards. Next chapter, i.e. *Chapter 5*, contains the results of ToF SIMS measurements demonstrating the functionality of this technique. It was applied to determine chemical properties of human bladder cells. These cells are characterized by large deformability difference occurring between non-malignant and cancerous bladder cells. The large deformability of these cells was accompanied by visible separation among the studied cell lines. Characterizing cells that are clearly distinguishable by cellular morphology, biomechanical, biophysical, and biochemical properties with the use of various techniques bears traces of proof-of-concept approach, thus, in further studies melanoma cells were chosen (*Chapters 6–8*). First, two types of cells were analysed, namely, WM115 cells originating from vertical growth phase and from the metastasis of WM115 to skin (WM266-4 melanoma cells). Their nanomechanical characterization in relation to both, surface structure and actin cytoskeleton organization, is presented in *Chapter 6*. The measurements of surface chemical composition with identified molecular masses causing the strongest differentiation between these cell lines is presented in the *Chapter 7*. These studies were verified by the use of photothermal microspectroscopy (PTMS). The latter technique delivers the photothermal spectra that resemble the infrared spectra observed in Fourier Transform Infrared Spectroscopy (FTIR). The final chapter,

Chapter 8, presents the results of biomechanical and biophysical characterization of various melanoma cells. The findings show that the alterations of mechanical properties observed in various melanoma groups (radial/vertical growth phase, metastasis to skin, metastasis to lung, melanocytes) are accompanied by the alterations in their surface composition.

Results, included in the presented thesis, were obtained thanks to the close collaboration of two research groups, namely, between the Department of Biophysical Microstructures at the Institute of Nuclear Physics (Polish Academy Sciences) and the Department of Advanced Materials Engineering at the Institute of Physics (Jagiellonian University).

This work was partially supported by National Science Centre (NCN) Project Number **DEC-2013/11/N/ST4/01860**. The author is grateful to Polish National Science Center (NCN) for the financial support of the ETIUDA scholarship no **DEC-2015/16/T/ST4/00358** and to the Institute of Nuclear Physics PAS for a healthy work environment and KNOW for PhD scholarship.

2. Fundamentals and state of the art

2.1 Melanoma progression

Cutaneous melanoma is the most aggressive and lethal malignancy of the skin. Despite advances in melanoma treatment [1], mortality from melanoma is still increasing [2]. Thus, there is an urgent need to develop prognostic biomarkers that can differentiate between malignant and non-malignant skin lesions and that can identify melanoma patients with high-risk primary lesions to facilitate greater surveillance [3]. That is why, the discovery of biomarkers and their application, in conjunction with traditional cancer diagnosis, staging, and prognosis, could improve early diagnosis and patient care [4]. Melanoma arises from melanocytes [5]. Melanocytes are neural crest-derived cells endowed with defined morphological and biochemical markers. They are mainly located within the basal layer of the epidermis, just superficial to the basement membrane. Normal melanocytes produce and subsequently transfer pigment-producing melanosomes to neighbouring keratinocytes, which are thought to protect the keratinocytes against UV radiation. When the functioning of melanocytes is impaired, the UV irradiation can lead to the formation of melanoma.

Melanoma is characterized by high rate of invasion resulting at various metastatic sites in, for example, skin and lung. Such behaviour of cells requires the interaction of the tumour cells with the extracellular matrix (ECM) trough cell adhesion, cell migration, and cell-mediated tissue proteolysis [6]. During melanoma development and progression, cancerous cells encounter several basal membranes (BMs) being the sheets of ECM mainly composed of laminins, type IV collagen, nidogens and perlecan [7–9]. The BMs are lost or penetrated by tumour cells during invasion and metastasis: firstly melanoma cells penetrate the dermo-epidermal junction, and invade the BM of dermal lymphatic vessels, entering the lymphatic circulation and lodging into regional lymph nodes. After obtaining access to the blood circulation system, the melanoma cells interact with the blood vessel wall and invade target organs, causing metastasis [6].

Tumour growth and dissemination involve specific interactions with tumour cell surface adhesion receptors and multiple adhesive components of the ECM. The receptors that mediate the cellular adhesive interactions with the ECM are derived from a large family of heterodimeric molecules referred to as the integrins [10]. Today it is clear, that these molecules play key roles in the regulation of tumour cell migration and survival in dependency of their ligands.

Alterations in the number and composition of integrins is a result of changes in surface receptors linked with cancer progression [11]. In addition, many proteins participating in normal biochemical processes are glycosylated i.e. they have attached oligosaccharide moieties. The variations of this glycosylation pattern often lead to changes in their functions. It has been reported for many tumours that the plasma membrane oligosaccharides linked to proteins or lipids are altered during cancer transformation. Changes in the expression and the structure of oligosaccharides seem to be a characteristic feature of the malignant transformation. All together, these characteristics can be attributed to alterations in adhesion and communication between cancerous cells and the normal cells in their nearest environment. Malignant transformation is also characterized by disruption of cytoskeletal organization, decreased adhesion, and altered adhesion–dependent responses. It has been already reported that the deformability of a cell in response to external forces is mainly determined by cytoskeleton and governed by adhesive molecules, usually linked to the cell cytoskeleton [12,13].

Melanoma has been already classified into well-described clinical stages as illustrated in the Figure 2.1.

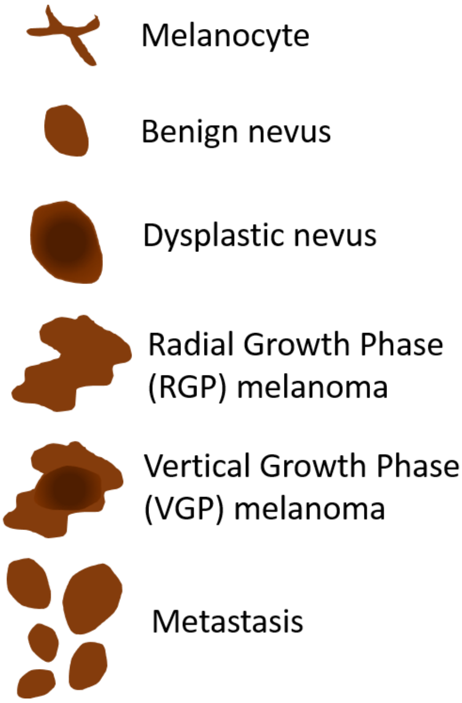

Figure 2.1. *Schematic model for melanoma progression.* [5]

Starting from benign lesions to highly metastatic ones. At the first step, due to oncogenic mutations, melanocytes can transform, through nevus stages, to a flat tumour, growing horizontally (radial growth phase, RGP). It is followed by the acquisition of the ability to invade deeper layers of the skin (vertical growth phase, VGP), what finally leads to the metastasis [14].

The transition, from radial to vertical growth phase, is a crucial step in the melanoma progression. It is correlated with the diversity of alterations that allow for distinguishing between RGP and VGP melanoma cells. As it was already described in the literature, the VGP melanoma cells change their phenotype, for example, BRAF and NRAS mutations towards more invasive one that lead to further metastatic progress [15,16]. Cells derived from vertical growth phase express surface receptors involved in the metastasis. These molecules are a part of the large family of heterodimeric receptors called integrins, that play crucial roles in the regulation of cell survival and migration [10,17].

Around 60% of melanoma cases had tumour thickness below 1 mm, it is important because they are frequently diagnosed as a non-invasive melanoma and there is a clear need for novel screening strategies [18]. Nevertheless, the incidence of thin metastasizing melanomas is still increasing [19]. It creates an urgent necessity for the determination of other significant criteria and novel melanoma characteristics, molecular as well as mechanical ones, especially on the correlation between their deformability and metastatic potential. It is already well-known, that melanoma cells deformability is related to their metastatic potential, for example, the more invasive melanoma cells, the larger deformability was observed [20].

2.2 Basic terms used in cellular biomechanics

There are many various theoretical and phenomenological models describing the properties and behaviour of distinct materials under the influence of external forces [21–23]. However, the mechanistic description of biological systems, in particular single cells, is not easy. In most cases, cells are approximated as a homogenous material without internal structure [24]. Currently applied models describe viscosity and elasticity of cells in a sufficient way to deliver semi-quantitative parameters enabling direct comparison between various populations of cells [25,26]. The mechanistic nature of any materials can be determined through the nature of deformation generated by the external force F. It can be purely elastic, viscoelastic or purely plastic. Most of the deformed biological objects reveal viscoelastic behaviour as observed phenomenologically [27–29], however, theoretical models are not easy to be applied. Thus, very frequently only elastic contribution is studied.

Purely elastic material has an ability to resist an external force and to return to its original size and shape when the stress is removed. In contrary, purely plastic materials undergo irreversible changes of shape in response to external forces. The remaining types of the deformations include a combination of the elasto-plastic behaviour.

Depending on the value of the external force acting upon the material, different deformation modes may occur. An elastic region, where deformation is reversible, occur up to a certain extent of the strain, the yield strength, where plastic deformation begins.

As it was mentioned above, biological materials, like living cells are not purely elastic. However, in order to the simplifying the theoretical models, usually, they are approximated in such a way that only the elastic contribution is analysed. Then, the Young's modulus parameter is defined to describe their mechanical properties. Nevertheless, the limitations of this approach should be remembered.

In the linear elastic region the deformation of the material can be described using a Hooke's law:

$$\sigma = E\varepsilon$$

where: σ – the applied stress, E - a material constant called the Young's modulus, ε – fractional strain.

In the Figure 2.2 an ideal stress-strain curve in the elastic region is presented.

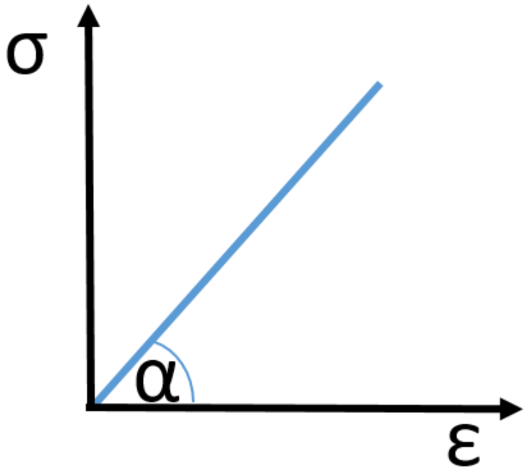

Figure 2.2. *A stress-strain curve in the elastic region.*

The Young's modulus is the basic parameter describing the elastic properties of any investigated material. It is defined as the ratio of the stress along an axis (described as force per unit area) to the strain along that axis (calculated as deformation of the initial length) in the range where Hooke's law is working.

During stretching, a material tends to contract in the directions transverse to the direction of stretching. In this case, the fraction of relative contraction to relative expansion is called the Poisson ratio. The majority of the materials have Poisson's coefficient value between 0 and 0.5.

For living cells, Poisson's ratio equal to 0.5 is usually assumed, as for a perfectly incompressible material deformed elastically at small strains [30,31].

2.3 Significance of cellular deformability

Alterations in the mechanical properties have been shown to accompany molecular changes in the cytoskeleton, as observed in various diseased cells, also in cancerous cells [32,33]. Adhesive interactions, involved in metastatic processes and occurring either between cells (by cadherins) or between cells and their environment (involving integrins) that reflect their individual properties, are mostly governed by the binding/unbinding of appropriate molecules present on a cell surface that frequently require the participation of actin cytoskeleton in their functioning [34]. In all types of eukaryotic cells, the structure responsible for maintaining cytoskeleton network is not only the 3D support, but it also participates in the diversity of cellular processes [35]. What is more, the mechanical properties of cells strongly depend on the cytoskeleton [36]. The cytoskeletal network participates also in the cellular signalling by various surface receptors [37]. As it is already proven, cancerous cells differ from normal ones in many features, such as growth, morphology and cellular adhesion. Also the mechanical resistance maintained by the cytoskeletal network and its organization is altered in cancerous cells in comparison the normal ones [38]. It is well known that the organization of cytoskeleton alters during tumour progression [39,40]. That is the reason why the research on the correlation between cellular structures and nano-mechanical properties of cells would improve the identification of new, potential biomarkers.

The technological progress, made over the last few decades, in the fields of bioengineering, nanotechnology and medicine allows for the determination of the properties of individual cells at the single cell level. Moreover, it is now possible to study the pathological changes occurring within a single cell. Among a variety of scientific apparatuses, atomic force microscope (AFM) seems to be an ideal tool in the research of biological materials ranging from single proteins to living cells [41,42]. It has been shown that the cellular stiffness can be a marker of oncogenic process in various cancer types [43,44]. Different properties of cells derived from the early and late stages of tumour progression may become an indicator of the oncogenic transformation and can be used not only in the diagnosis but also in the cancer treatment and therapy [45]. Taking this into account, studies of cellular biomechanics in the conjunction with the analysis of cellular structure are essential for the progress of advanced diagnostic approaches and the anti-cancer drugs development.

Initially, AFM was mainly used for non-organic samples investigations. However, soon after its invention, it was realized that it can be successfully applied in the measurements of a biological material [46,47]. A significant advantage of AFM, in comparison to other high-resolution microscopic techniques, like electron microscopy, is the possibility to measure biological samples in the environment close to their physiological conditions. It is realized by using a liquid cell-container filled with medium solution with submerged sample in the bottom. Thanks to that fact, measurements on living cells in medium can be performed. Moreover, AFM is not only an excellent tool for measuring the topography of the analysed samples, but also, when working in the force spectroscopy mode, it can give the information about mechanical properties of studied material. Soon after its invention, it was found that AFM can be used for the measurements of nanomechanical properties of biological materials, such as elasticity [46,47].

In 1999 Lekka et al. determined the elastic properties of normal and cancerous human bladder epithelial cells. They showed that the average Young's modulus values for the cancerous cells are much lower than for the benign cell line, what was connected with poorly developed cytoskeletal elements in metastatic cells [46]. Further research in this field confirmed these results and, in present times, it is known that cancer progression correlates with larger deformability of the cancerous cells. The alterations in the cytoskeletal structure in cancerous cells, revealing in the higher deformability, were confirmed in several studies. Ketene et al. showed that ovarian cells are stiffer when they are benign. Moreover, the increase in cell deformability directly correlates with the progression of a transformed phenotype from a non-tumorigenic cell to a malignant one. The decrease in the level of actin in the cytoskeleton and its organization is directly associated with the changes in cellular biomechanical properties [48]. They also indicated that further work is needed to enhance the understanding of the complex architecture of living cells and the interaction of molecular and biomechanical events. The cytoskeletal elements are anchored in the cellular membrane in the focal adhesions - the macromolecular assemblies through which the cytoskeletal elements are connected with the extracellular matrix (ECM). The changes in the cytoskeleton structure in cancerous cells will cause the alterations in the amount and molecular composition of focal adhesion sites in cellular membrane. Lekka et al. in 2006 showed that among many alterations, cancerous cells reveal the expression of different oligosaccharides in cellular membrane than normal ones [49]. By using functionalized AFM tip it was shown i. e. that the amount of sialic acid in cancerous cells is higher than in normal cells, but normal cells have much higher amount of the high-mannose-type glycans on their surface.

2.4 Surface properties

Cancer progression is a multistep process leading to alterations in cellular cytoarchitecture and biophysical properties that are frequently associated with biochemical changes [32,50]. Various studies on cancer progression have shown a wide range of alterations in chemical composition, leading to a conclusion that a general, single change of a specific molecular compound does not exist [3]. Therefore, the characterization of (bio)chemical cancer-related changes in a quantitative manner with respect to normal or benign and cancer cells defines new target area for novel diagnostic approaches.

There are various biochemical methods used to study properties and expression of particular molecule types. The research groups that investigate the overall chemical properties of various biological samples, hope that their deviations from a normal-functioning state will give rise to alterations detectable by methods sensing the chemical composition [52]. These various techniques can be classified as those analysing the molecular masses of molecules or their fragments emitted from the superficial layers of sample surface (mass spectrometry techniques) [53] and as those recording the absorption spectra originating from vibrational oscillations of chemical bonds present in the studied material (infrared based ones such as Raman [54] or Fourier transformed infrared [55] spectroscopies).

Time-of-Flight Secondary Ion Mass Spectrometry (ToF-SIMS) is an excellent tool for analysis of chemical composition of various materials belonging to the former of the abovementioned classes of techniques. ToF-SIMS spectrometer is characterized by its high transmission and mass resolution [56]. It enables to detect different masses simultaneously. Moreover, it is also possible to perform surface maps with good lateral resolution (even 0.1 μm) [57]. The huge advantage of this technique is that, besides information on elements, ToF-SIMS can also be used to probe surface species of higher molecular mass with an extremely high sensitivity [58]. An another advantage of this technique is that measurements are possible without the addition of any additives. Although the experiment performed by J. J. Thomson in the beginning of the 20th century [59], when he observed a release of particles induced by ion bombardment, may be considered as the origin of the mass spectrometry itself, the work of A. Benninghoven in late 1960s [60] could be regarded as the beginning of static SIMS spectrometry in a form used nowadays. The method was primarily applied to inorganic materials but a development of apparatuses allows now for an analysis of biological samples. The technique was originally developed for the analysis of solid state materials in 1960s and soon it was applied for biological samples. In 1970 Galle et al. studied the emission of sodium from red blood cells [61]. SIMS is the first mass spectrometric technique that enables chemical imaging [62]. A. Benninghoven was the pioneer who used this technique to localize ions on a surface [63]. Shortly after its development, the mass resolution and the transmission efficiency of SIMS were improved by Chait and Standing so that this technique, coupled with a time-of-flight analyser, was used to measure masses of biological compounds [64].

The ToF-SIMS is capable of elemental and molecular analysis of complex chemistry on the sub-cellular scale [65]. However, the high vacuum requirements of SIMS prevent the analysis of live cells because of their water content. Therefore, sample preparation protocols are critical in preserving the biochemical architecture of biological samples and extracting meaningful information [66,67]. Biological samples like cells have to be dried or frozen. It is extremely important to remove any contamination from culture medium and to preserve cellular structure intact. The first attempt to achieve this was to apply the same methodology as for scanning electron microscopy for which it has been shown that drying protocols can preserve the biochemical structures [68]. These typically involve drying under argon or freeze drying. Before drying, either chemical (with e.g. parafomaldehyde) or physical (by cryofixation) fixation is necessary to prevent cell degradation, which would be evident in SIMS images as redistribution of diffusible ions like Na+ or K+ [67]. The popular solution is a cryogenic freezing [62]. This approach requires a careful temperature control. An another solution is a chemical fixation using, for example, paraformaldehyde and alcohol substitution. Although it was noticed that drying may cause a cell collapse [62]. Frozen hydrated protocols have also received a lot of interest, possibly due to the fact that chemical fixatives and the drying procedure can potentially distort chemical specificity [69].

The development of cluster and polyatomic ion beams, resulting in the increase of secondary ion yield and broadening of the mass range of molecules, and also highly sensitive ToF analysers, make possible the measurements of molecular composition of extremely complex biological samples, such as cells. However, the lack of reference spectra of relevant bio-compounds is hampering the use of ToF SIMS technique in bioscience [70]. Due to extensive research carried out over the last few decades, the knowledge about organic compounds emitted from cells or tissue surfaces upon primary ions bombardments is still expanding. So far, mass spectra of amino acids [71–73] and lipids [74–77] were established to study protein and lipid contents on cell or tissue surfaces. However, despite this, ToF SIMS data recorded for complex biological samples are still difficult to be interpreted due to the phenomenon of fragmentation of large biomolecules. Moreover, the cellular mass spectra are very similar to each other and, basically, differ only by the maxima intensities, but not, as one could wrongly expect, due to the presence of a unique mass that would be characteristic solely for one cell type. Thus, there is currently no possibility to identify the sample by looking at the ToF SIMS spectrum only [78]. That is the reason why multivariate analysis, such as principal component analysis (PCA), is widely applied to find spectral differences between biological samples [69].

Nowadays, through the extensive research, ToF-SIMS is becoming an important tool; not only for the development of novel chemotherapeutic agents, but also for the diagnosis and prognosis of cancer. Much of the literature pertaining to this area describes the use of this technique to map certain ions within cancerous cells or tissue sections [79,80]. However, increasingly, studies are focusing on the use of multivariate, interdisciplinary techniques to characterize the various cellular differences associated with carcinogenesis. A significant part of the literature on this subject has been provided from dynamic SIMS studies. A particularly active group in this area, Chandra and colleagues, have provided the basis for many of the more recent investigations. After adapting the cryogenic technique to SIMS [81], they have been able to productively apply dynamic SIMS to cancer research. Investigations of various inorganic ions, in cancerous (MCF-7) and normal (MCF-10A) breast cell lines, revealed differences in the ratios of nuclear and cytoplasmic calcium concentrations [52]. Following this, as a part of the same investigation, the same group then progressed on to investigate boron neutron capture therapy (BNCT) of cancer [82]. Quong et al. investigated genotoxic heterocyclic amines produced during certain cooking methods [83]. The most important of these amines is 2-amino-1-methyl-6-phenylimidazo[4,5-b]pyridine (PhIP). The group was able to analyse the distribution of this carcinogen in human breast cancer cells using ToF-SIMS and a dye, specific to the outer leaflet of the cell membrane. This particular study was strongly reliant on the ability of the ToF-SIMS to obtain molecular information, specifically, from large membrane molecules. Furthermore, and more importantly, Fartmann et al. demonstrated the ability of static SIMS to examine molecular distribution without the addition of dyes or isotopic labels [84]. Interestingly, ToF-SIMS was applied to investigate the effects of hederacolchiside A1 (Hcol-A1) – a novel chemotherapeutic agent [85]. The group utilized a range of techniques to assess the ability of Hcol-A1 to permeabilize human melanoma cell membranes. Principally, ToF-SIMS was used to monitor the interaction of the compound with cholesterol and phospholipids. Through the use of imaging ToF-SIMS, the group illustrated the destruction of the cell after prolonged Hcol-A1 exposure. Finally, ToF-SIMS is widely used to investigate the molecular composition of normal and cancerous cell lines. Valuable information regarding the natural history of the disease and metastasis has been obtained from such experiments. One particular research group used this technique to discriminate between malignant and non-malignant prostate cancer cells [86,87]. Baker et al. utilized three prostate cancer cell lines: PC-3, LNCaP and PNT2-C2 - the latter being the non-malignant example [88]. A 40KeV C_{60}^+ primary ion beam was used for the analysis to generate 135 spectra. The complexity of the spectral signatures associated with biological materials, as mentioned previously, is widely known. Interpretation of their spectra was, therefore, aided by the chemometric analysis. Subsequently, the greatest mass spectral differences were rapidly identified. Due to the non-destructive nature of static SIMS, the group was able to discriminate the cell lines according to the phospholipid contents of their cell membranes. This was then illustrated using Principal Component-Discriminant Function Analysis (PC-DFA).

Another use of SIMS results is addressed to the quantitative analysis of chemical alterations in mass spectra between cell lines in order to find differences between them. This approach has already been applied to differentiate three lines of human breast cancer cell types by Kulp et al. [78]. They tested lysed cells and a mass selection range of m/z 58–500. They used ToF-SIMS to classify single cells based on their spectra. For this purpose they applied statistical data reduction on the SIMS data sets. They proved that it is possible to distinguish breast cancer cell lines based on the knowledge about their chemical composition. These results showed also that it is not a single change or modification in a chemical composition that explains the progression of cancer, but rather it is a spectrum of changes that defines the carcinogenesis. In the present times, it is also possible to acquire SIMS images of distribution of certain compounds on cell membranes. Depth profiling can be made, for example, with C_{60} ion beam and followed by analysis with a Bi_3^+. Nygren et al. used this approach to perform 3D imaging of single thyroid tumour cells [89]. They detected and imaged distribution of phosphocholine and inorganic ions in a cellular membrane. In the same study it was also shown that high intensity of potassium can be seen in a cellular membrane. These results may indicate that potassium is compartmentalized in cells of a thyroid tumour. It is clear from the literature, that ToF-SIMS is becoming the valuable tool for the researchers focused on biochemistry. It is important to recognize the strengths and weaknesses of ToF-SIMS. Through this recognition it is hoped that the technique can be used as a significant help in differentiation between cell lines with different metastatic potential.

2.5 Aims of the thesis

Melanoma arises from a disruption of melanocytes that, firstly, grow horizontally forming a superficial tumour (i.e. radial growth phase). Later on, cells invade deep layers of the skin transforming into vertical growth phase [14]. Next, such cells evolve into more invasive ones, leading to metastasis. The cellular conversion from healthy melanocytes to highly invasive melanoma cells is linked with genetic changes that are strongly accompanied by alterations in the expression of cell surface molecules [90], in the actin cytoskeleton organization [91], and indirectly in cellular deformability [92]. Thus, the main objective of the presented thesis is to study the relationship between cellular deformability obtained by means of AFM with alterations in surface chemical compositions measured by ToF SIMS in melanoma cells. The underlying hypothesis assumes that cancer-related changes generated during melanoma progression, namely, cellular deformability and surface chemical properties, are mutually correlated. As the first step of this work, the elaboration of the sample preparation protocol for ToF SIMS measurements, which are carried out in high vacuum conditions, was performed, followed by the acquisition of mass spectra of single cells from human bladder cancer. Bladder cells were chosen due to the gathered knowledge on their mechanical and biochemical properties. These served as basis for the optimisation of ToF SIMS experiments and data analysis using principal component approach (PCA). As next steps, the two melanoma cell lines were characterized using the proposed approach, namely, WM115 cells originated from vertical growth phase and WM166-4 ones derived from skin metastasis. Both cell lines were established from the same patient. Thus, the sample preparation protocol for ToF SIMS experiments was optimized, cellular surface was characterized using both atomic force and fluorescent microscopes, deformability of these cells was quantified through the AFM elasticity measurements, and finally, the mass spectra were recorded and analysed using PCA. The obtained results were validated by applying a data analysis scheme which was analogous to the interpretation of photothermal spectra measured by photothermal microspectroscopy (PTMS). The obtained validation of the proposed methodology, enabled to measure mechanical and chemical properties of seven melanoma cell lines and to compare them to melanocytes. The latter results were used to correlate the deformability of cells with the chemical composition of their surface.

3. Materials

3.1 Cell cultures

The studies performed within the frame of the presented thesis were carried out using cells of human bladder cancer and melanoma cell lines. All cell lines have been cultured for many years at the Department of Biophysical Microstructures (NZ55) at the Institute of Nuclear Physics in Cracow (Poland).

3.1.1 Human bladder cancer cell lines.

As a model system four cell lines representing human bladder cancer were chosen:

(1) non-malignant epithelial cells of ureter (HCV29, this cell line was established at the Fibiger Institute, Copenhagen, Denmark);
(2) urinary bladder carcinoma (HTB-9, ATCC, LGC Standards);
(3) transitional cell carcinoma (HT1376, ATCC, LGC Standards); and
(4) transitional cell carcinoma (T24, ATCC, LGC Standards).

The HCV29 cells represent a non-metastatic cancer while three other cell types are characterized by metastatic phenotype with different histological grades[1]. The higher the grade, the more invasive cancerous cells are. The histological grades for the studied human bladder cancer cell lines are: HTB-9 – grade II, HT1376 – grade III/IV and T24 – grade IV.

All cultures were carried out in 25 cm^2 culture flask (Sarstedt) in the incubator (NuAire) providing 37^{0}C and 95% air/5% CO_2 conditions. The HCV29 and T24 cells were grown in RPMI-1640 medium (Sigma) supplemented with 10% fetal bovine serum (FBS, Sigma). The HTB-9 cells were cultured also in RPMI-1640 medium containing 10% of FBS, but additionally supplemented with 1% HEPES (4-(2-hydroxyethyl)-1-piperazineethanesulfonic acid, Sigma), and 1% sodium pyruvate (Sigma). The culture of HT1376 cells required Eagle’s medium (EMEM, LGC Standards) supplemented only with 10% FBS (LGC Standards). No antibiotics were involved in cell cultures.

---

[1] The histological grade describes a degree of abnormality in cancerous cells (differences in appearance and function in comparison to healthy cells).

3.1.2 Human melanoma cell lines.

To study the properties of cancerous cells, characterized by small differences in their morphology and physic-chemical properties, melanoma cell lines were chosen. In addition, all cell lines originate from very close stages of cancer progression. The measured cell lines were obtained from ESTAB Melanoma Cell Bank:

(1) WM35 cells – these cells were originally isolated from a patient's skin diagnosed with radial growth phase (RGP) primary melanoma,
(2) WM115 cells – cells derived from a 55 year old female skin melanoma at a vertical growth phase (VGP) in the primary melanoma site,
(3) WM793 cells –cells were established from the vertical growth phase (VGP) of a primary skin melanoma lesion,
(4) WM266-4 cells – cells were established from a cutaneous skin metastasis detected in the same patient as WM115 cells,
(5) WM239 cells – cells were collected from a cutaneous skin metastasis,
(6) 1205Lu cells – cells originated from a lung metastasis diagnosed in the same patient as WM793 cells,
(7) A375P – cells were derived from a solid malignant tumour located in the lung.

Since melanoma develops from melanocytes, as a reference cell line, human epidermal melanocytes from adult skin (primary cell line HEMa-LP, ATCC, LGC Standards) were used. All melanoma cell lines, used here, were cultured in the RPMI-1640 medium (Sigma) supplemented with 10% fetal bovine serum (FBS, Sigma). The HEMa-LP melanocytes required a special, dedicated medium i.e. MEDIUM 254 (GIBCO). Also, in melanoma cell cultures, there were not any antibiotics involved.

3.2 Sample preparation for AFM measurements

For elasticity measurements using atomic force microscopy (AFM), cells were seeded on glass coverslips placed in the Petri dishes (Sarstedt) filled with the corresponding culture medium. The culture time was set to 48 hours. Afterwards, prior to AFM measurements, glass coverslips with cells were immersed into the AFM liquid cell setup, filled with corresponding fresh culture medium and placed on the AFM piezo-scanner.

3.3 Sample preparation for PTMS experiments

For photothermal microscopectroscopy (PTMS), cells were cultured in 25 cm^2 culture flasks (Sarstedt) until they reached 70-80% of confluency (corresponding to around 3 millions of cells per 1 ml). Cells were trypsinized with 0.05% EDTA-trypsin solution (Sigma) for 5 minutes. Next, cells were centrifuged at 1800 rpm for 4 minutes in an Eppendorf tube (with volume of 1.5 ml). The supernatant was removed, the culture medium was added and cells were gently mixed. Next, cells were again centrifuged. After the culture medium was removed the phosphate buffered saline (PBS, Sigma) was added to a cell pellet, located at the bottom of the Eppendorf tube. Cells were centrifuged and, again, supernatant was removed in gentle way to keep a cell pellet unbroken. Afterwards, a 2.5% glutaraldehyde solution in PBS was added to each tube for 2 hours, followed by delicate twice rinsing in the sterile PBS buffer. Such prepared cells pellet was used for the PTMS measurements.

3.4 Fluorescent staining

Cells cultured on glass coverslips, immersed in the Petri dish with culture medium, were washed with phosphate buffered saline (PBS, Sigma), and the 3.7% solution of paraformaldehyde (Fluka) was added to fix them at room temperature for 20 minutes. After removing the fixative, cells were incubated with the 0.2% solution of Triton X-100 at 4ºC for 5 minutes, followed by rinsing them with PBS buffer. To visualize the actin filaments, coverslips were incubated with Alexa-Fluor 488 conjugated with phalloidin (0.033 µM in PBS, Molecular Probes) for 35 minutes, and washed again with PBS. The cell nuclei have been stained with Hoechst solution (1 mg/ml in PBS, Sigma) for 15 minutes, followed by washing in PBS buffer.

3.5 Sample preparation for ToF SIMS experiments

Although the sample preparation for AFM-based elasticity measurements is well established at the Department of Biophysical Microstructures, the sample preparation for ToF SIMS experiments required more elaboration. This is due to the fact that these experiments have to be carried out in high vacuum conditions. Thus, a protocol specific for ToF SIMS sample preparation was developed[2].

3.3.1 Substrates for cell culture for ToF SIMS.

To avoid harmful charge deposition on substrates, glass coverslips could not be used as a support for cell cultures. Instead, highly doped silicon was used as a substrate for cell growth due its conductive properties. Here, commercially available silicon wafers (Si-Mat, Germany) were cut into squares with the size of 1 cm × 1 cm. Such prepared substrates were cleaned with pressurized nitrogen and sterilized with a UV lamp for 1 hour on both sides. Afterwards, cells were seeded on these surfaces. Then, silicon slices were moved to Petri dishes (Sarstedt) that were filled with the corresponding culture medium and, further, cultured for 48 h in the CO_2 incubator providing 95%/5% air/CO_2 atmosphere. After 48 h of culture, silicon substrates with cells were washed with phosphate buffered solution (PBS, Sigma) and underwent further steps of sample preparation protocol.

3.3.2 Drying protocol for silicon substrates containing single cells.

After 48 hours of culture on silicon substrates, cells were fixed using 3.7% solution of paraformaldehyde (Fluka) in PBS for 20 minutes, at room temperature (RT). After rinsing them in PBS buffer, steps leading to salt removal were applied (Figure 3.1).

To remove salt, two dilutions were prepared from initial PBS solution containing 150 mM concentrations of NaCl and 27 mM of KCl (pH 7.4). Dilutions were prepared by adding deionized water (Cobrabid purification system, 18 $M\Omega/cm^2$) at ratios 1:2 and 1:4. Samples with cells were washed for 1 minute in each of them. Next, they were immersed in deionized water. As a subsequent part of the protocol, dehydration stage was carried out. Here, to be sure that all water molecules will be removed from the cellular samples, six dilutions of ethyl alcohol (POCH Gliwice) were prepared at concentrations of 40%, 50%, 60%, 70%, 80%, 90%.

---

[2] The ToF SIMS specific sample preparation protocol has been published in the papers by (1) Bobrowska et al. *Analytical Biochemistry* 2016, doi:10.1016/j.ab.2016.06.011 and (2) Bobrowska et al. *Data in Brief, 2016, doi:10.1016/j.dib.2016.07.052.*

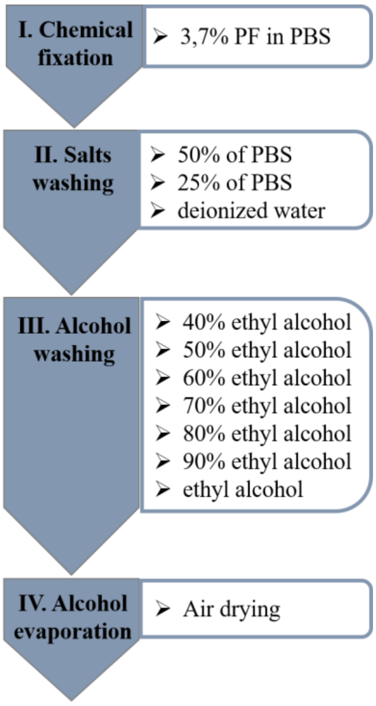

Figure 3.1. *Schematic illustration of the protocol used for sample preparation for ToF SIMS experiments (image adapted from Bobrowska et al. Analytical Biochemistry, 2016, doi:10.1016/j.ab.2016.06.011).*

Afterwards, silicon wafers with cells were immersed subsequently for 30 seconds in each solution, starting from the 40% one. At the end, the anhydrous ethyl alcohol (99.8%, POCH Gliwice) was used for 30 seconds, too. At the final step of the protocol, samples were air dried for 20 minutes in RT. Such prepared samples were transferred into the lock-in chamber of the SIMS apparatus in a vacuum sealed vessel to maintain a sterile environment. All protocol steps were carried out under the laminar flow chamber (NuAire) providing sterile conditions. What is more, for a single batch of experiments, all samples were prepared at once to avoid any differences stemming from the preparation process.

3.3.3 Monitoring changes on cell surface during the preparation protocol.

To study the effects of fixation, salt removal, dehydration and drying steps on cells, the AFM images of cell surface were recorded after each step of the sample preparation protocol. Measurements were carried out for two melanoma cell lines: WM115 from primary tumour site and WM266-4 from skin metastasis (Figure 3.2).

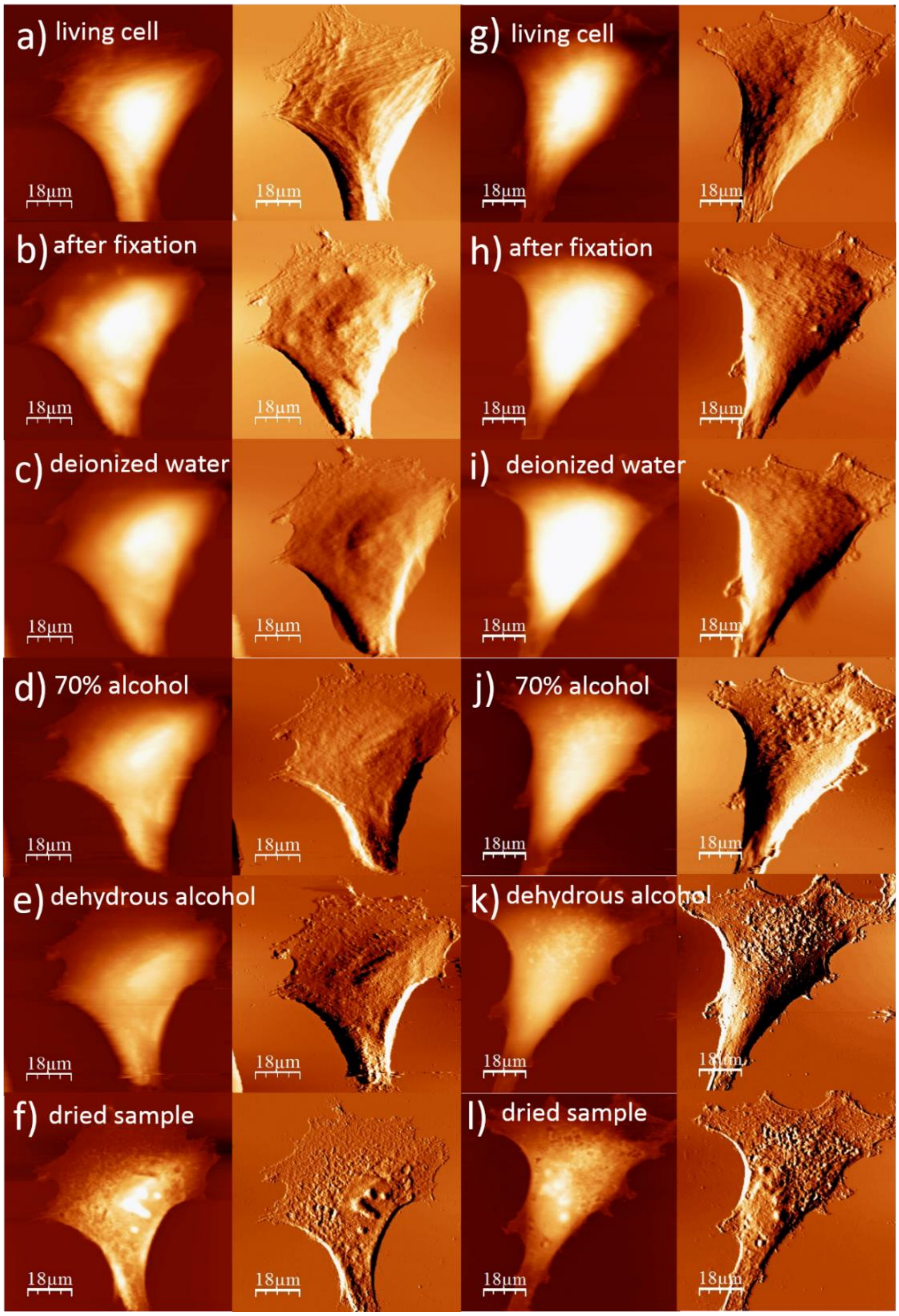

Figure 3.2. *The surface topography and deflection images recorded for WM115 (a-f) and WM266-4 (g-l) melanoma cells: (a&g) living cell, (b&h) fixed cell with paraformaldehyde, (c&i) cell in the deionized water, (d&j) dehydration step with 70 % ethyl alcohol solution, (e&k) dehydration step with anhydrous alcohol, and (f&l) dried sample in air (images adapted from Bobrowska et al. Analytical Biochemistry, 2016, doi:10.1016/j.ab.2016.06.011).*

Images of living cell surface topography were collected in the culture medium (Figure 3.2 a&g). Next, changes of cellular surfaces were visualized after fixation with paraformaldehyde in PBS buffer (Figure 3.2 b&h). The effect of subsequent salt removal was measured for samples immersed in deionized water (Figure 3.2 c&i, for WM115 and WM266-4 cells, respectively). Dehydration effect on cell surface is visualized at two steps i.e. after immersing samples in 70% ethanol solution (Figure 3.2 d&j) and after treatment of the cells with anhydrous ethyl alcohol (Figure 3.2 e&k). Finally, the surface of dried cells (after 15 minutes) was imaged in ambient conditions (Figure 3.2 f&l).

Shapes of melanoma cells remain unchanged independently of the step of the preparation protocol at which the images of the cells were recorded. However, the cellular surface was altered depending on the undergoing preparation step. The largest changes were observed between living cell and fixed cell surfaces. The paraformaldehyde fixation manifested in the less clear image of cell surface. Actin filaments visible previously were less clear but the position of cell nucleus remained stable (the highest fragment of the cell). Such types of images seemed to be characteristic untill the moment when dehydration stage was applied. At these steps, cell membranes collapsed and the localization of cell nucleus began to be clearly visible. Drying of a sample did not changed the resulting cellular surface significantly. To roughly quantify these changes, the height of the cells was measured. Initially, the height of living cells was in the range from 3.5 μm to 4.0 μm. It increases after the paraformaldehyde fixation and deionized water washing, followed by the decrease during dehydration steps. Drying of the sample resulted in the decrease of a cell height below 1 μm (Figure 3.3 a&b, for WM115 and WM266-4 cells, respectively).

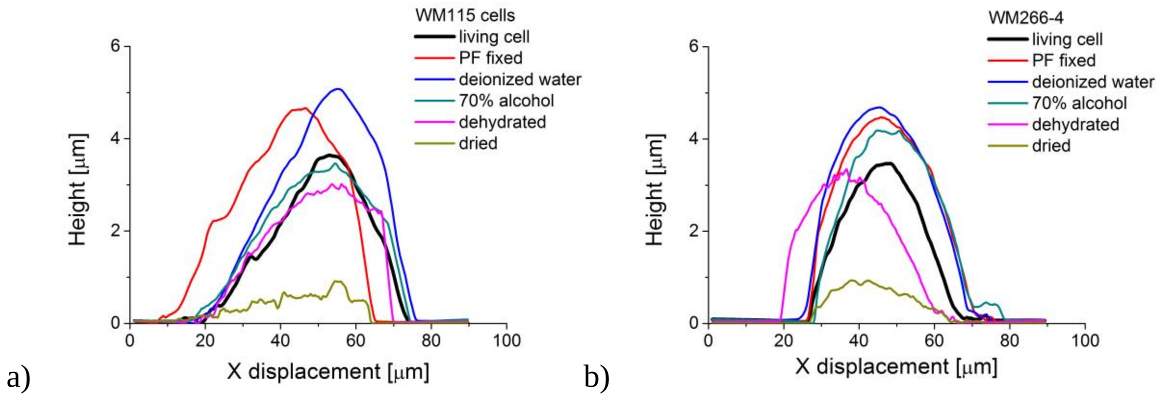

Figure 3.3. *The comparison of cross-sections for WM115 (a) and WM266-4 (b) cells (images adapted from Bobrowska et al. Analytical Biochemistry, 2016, doi:10.1016/j.ab.2016.06.011).*

The highest points in Figure 3.3 a & b indicate the location above cell nucleus, however, its exact structure is hidden by the cell membrane. After fixation with paraformaldehyde, the height of cells increases from 3.5 ÷ 4.0 μm to about 4.0 ÷ 4.5 μm. Interestingly, after salt removal and washing with deionized water, the height of WM115 cells increases further to ~5 μm while for WM266-4 cells it remains comparable to cells fixed with paraformaldehyde. The proposed way of water molecules removal with ethyl alcohol dilutions followed by rinsing the cells with anhydrous alcohol resulted in their height comparable with that observed for living cells. As it was expected, drying of cells leads to significant drop of cells' height, being now of the order of 0.5 ÷ 1.0 μm.

The samples with cells, cultured on silicon substrates and prepared using abovementioned protocol, were used for ToF SIMS experiments. In this technique, the ion bombardment may induce changes to cellular surface that could result in hidden image of surface chemical properties in cells. To verify whether the applied ion beam damages the cellular surface, its visualization was performed by means of scanning electron microscopy (SEM) working in low vacuum conditions under 100 Pa water pressure. In such a way, it was possible to obtain high spatial resolution images of single melanoma cells without any coatings (Figure 3.4 a-f).

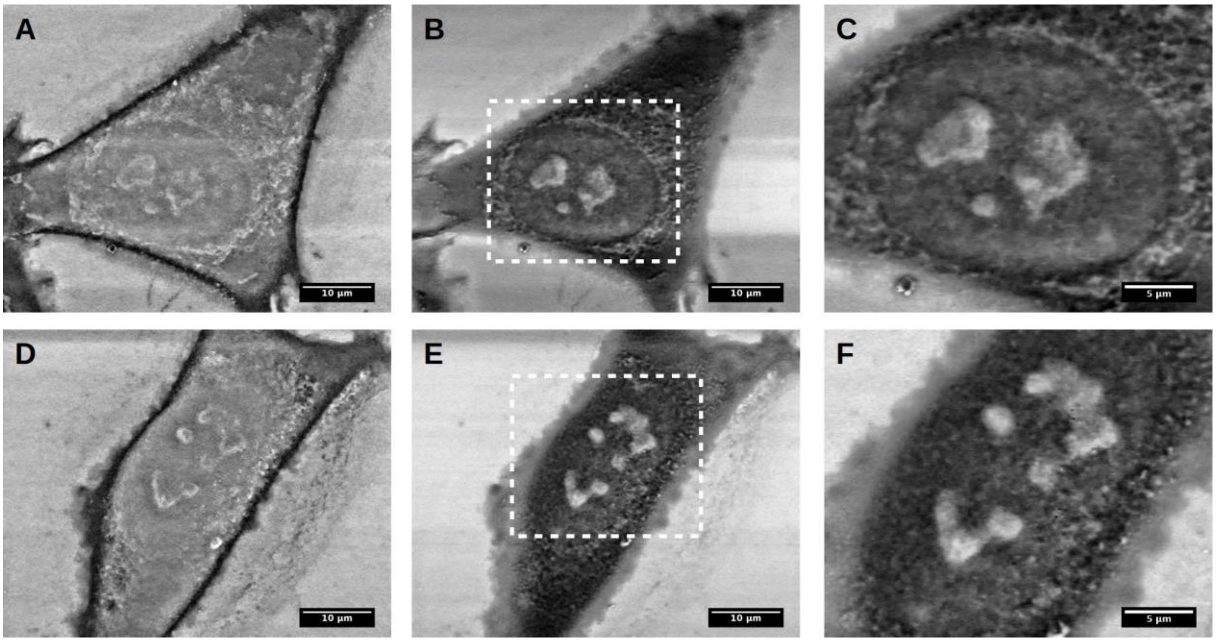

Figure 3.4. *SEM images of WM115 (a, b and c) and WM266-4 (d, e and f) melanoma cells cultured on bare silicon surface, recorded at 2kV (a, d) and 5 kV (b, c, e and f). Images adapted from Bobrowska et al. Analytical Biochemistry, 2016, doi:10.1016/j.ab.2016.06.011.*

SEM images were recorded at two values of electron accelerating voltage, namely, 2 kV and 5 kV. This enabled to image either cell surface (i.e. cell membrane) or deeper parts of a cell (cell nucleus). The former images show corrugations on cell surfaces that veil underlying cell nucleus (Figure 3.4 b&e). Higher accelerating voltage allows to visualize cell nucleus with nucleoli accompanied by numerous mitochondria (Figure 3.4 c&f).

The images recorded by AFM and SEM validated the proposed protocol for single cells preparation methodology. Cellular morphological and structural characteristics can be preserved in the protocol involving fixation, dehydration and drying steps. In parallel, these results demonstrate the complementarity of various microscopic techniques (as AFM and SEM) applied to visualized morphological and structural characteristics of cells. The results show that the proposed methodology of sample preparation for single cells is suitable to study biological samples without using freezing based methods and it can be used in spectroscopic and microscopic techniques operating in vacuum conditions.

3.3.4 Effect of the various media composition

The medium composition is usually cell type specific since it has to provide various constituents required for proper growth of cells. Thus, the surface chemical properties measured using ToF SIMS on dry samples can be influenced by the constituents of culture media attached to cell surface. To verify the effect of culture media composition, in the presented studies, the silicon surfaces were exposed to three different compositions of culture media corresponding to those in human bladder cell cultures, i.e. to EMEM (used in HT1376 cells culture), to RPMI 1640 (used for HCV29 and T24 cells growth), and to RPMI 1640 supplemented with HEPES and sodium pyruvate (applied in the culture of HTB-9 cells). Silicon surfaces were kept in the corresponding culture media for 24 h at 37 °C in an CO_2 incubator. Afterwards, they underwent the steps of ToF SIMS specific sample preparation protocol followed by ToF SIMS measurements. The collected mass spectra were analysed in the same way as mass spectra recorded for bladder cells (as described in the *Methods*). The exemplary mass spectrum of the silicon surface exposed to RPMI 1640 culture medium is shown in Figure 3.5.

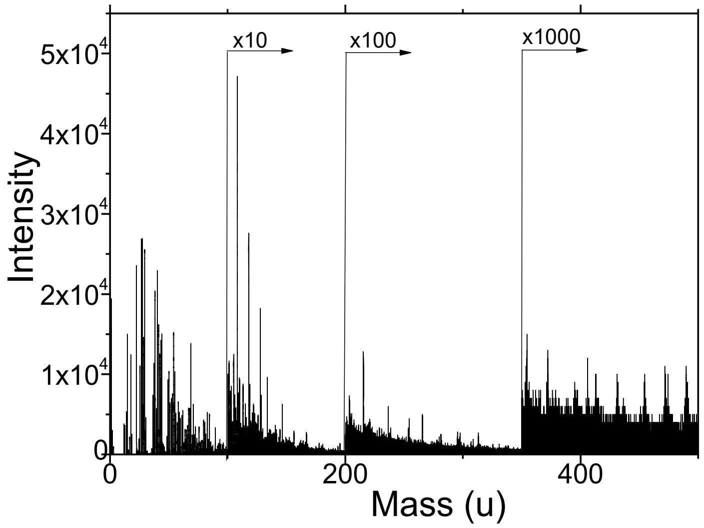

Figure 3.5. *The exemplary positive mass spectrum of the silicon substrate exposed to the RPMI 1640 cell's culture medium.*

The effect of culture medium is negligible in the case when all cell lines are grown in the same culture medium, but it could be considerable for cells cultured in various media. The types of melanoma cells chosen for these studies were grown in the culture medium composed of RPMI 1640 medium supplemented with 10% fetal bovine serum. Thus, the effect of culture media compositions in this case is negligible. Only melanocytes (normal HEMa-LP cells) required a special, dedicated medium. For bladder cells, three distinct culture media were applied since their composition is optimized for the best conditions for cellular growth.

The ToF SIMS positive mass spectrum of bare silicon surface, treated in a similar way as silicon with cells, possesses the organic compounds on its surface, which are resulting from the deposition of medium components. Independently of the culture medium type, analogous complex spectra are observed. Thus, to visualize the effect of the culture media compositions, the PCA was applied according to description in *Methods*. Autoscaling was used as a pre-processing method (Figure 3.6).

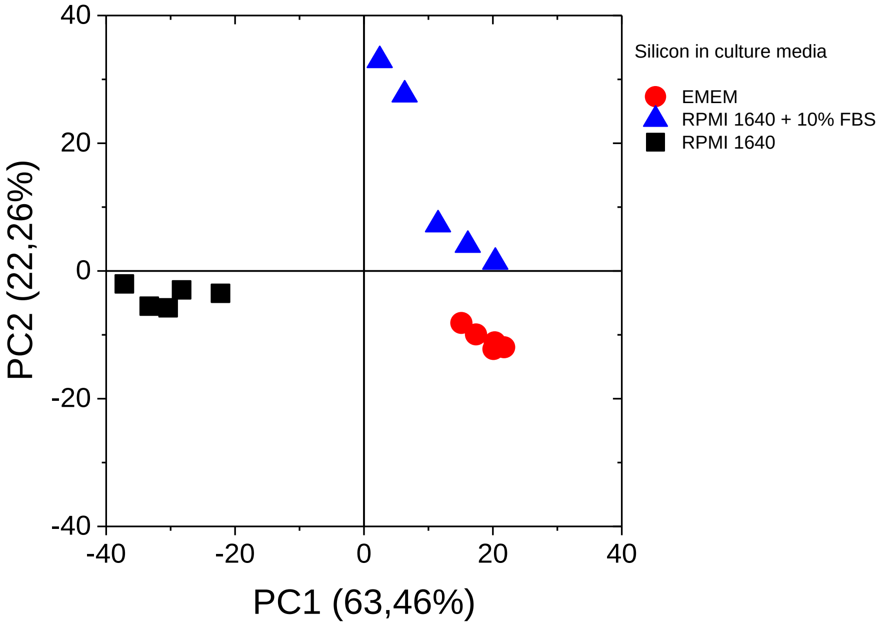

Figure 3.6. *Scores plot of the 2nd principal component (PC2) versus the 1st principal component (PC1). Three different culture media were studied: RPMI 1640, RPMI 1640 supplemented with 10% foetal bovine serum, and EMEM.*

The results of PCA show that mass spectra of silicon surfaces are grouped depending on the culture medium composition. These findings demonstrate that ToF SIMS technique is very sensitive and, simultaneously, they indicate the importance of measuring the reference sample during ToF SIMS experiments, especially, if this technique is applied to study single cells.

3.6 Summary

The use of various experimental techniques to analyse cell structure involves the application of distinct sample preparation protocols. Some of them, such as cell cultures, are conventional, but very often some protocols have to be optimized for a specific type of measurement. The SIMS measurements frequently employed a relatively complicated preparation method that involves freezing in liquid nitrogen in various ways. Namely, the sample preparation for SIMS involves either freeze fraction of single cells or frozen tissue slices. In the presented thesis, two questions were addressed. First, whether it is possible to develop a fixative-based sample preparation protocol and, second, whether it allows one to distinguish between cells originating from various stages of cancer progression. In this research, the functionality of the TOF-SIMS technique to study biological samples without using freezing based methodology for sample preparation is demonstrated.

4. Experimental methods

4.1 Atomic Force Microscopy – basic principles

Atomic force microscopy (AFM) is one of the scanning probe based techniques that enables imaging of surfaces with a sub-nanometric resolution. In the AFM, a flat spring (i.e. cantilever with a probing tip mounted at its free end) is used to scan surface of the sample (Figure 4.1).

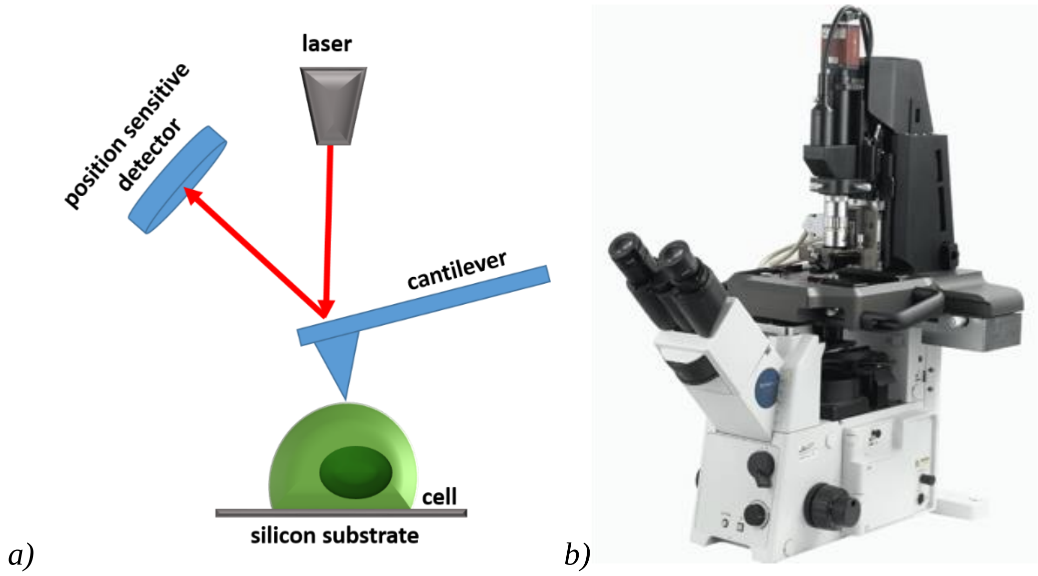

Figure 4.1. *(a) Atomic Force microscope - working principle. (b) An image of the AFM apparatus from Park Systems – a model Xe120 integrated with inverted optical microscope equipped with fluorescence functionality.*

The tip curvature radius of the probing tip varies between few to tens of nanometres. When probing tip is placed in a close proximity to the investigated surface, forces acting between its end and material’s surface deflect the cantilever. The deflection is measured by an optical system consisting of a laser and a position sensitive detector (usually by a photodiode). A precise movement of the sample is realised by a piezo-scanner. All measurements presented in this thesis were carried out using a commercially available atomic force microscope model XE120 manufactured by Park Systems (Korea). This device is integrated with an inverted optical microscope Olympus IX71 used to localize place of interest for the AFM measurements, as well as to collect fluorescence images.

4.1.1 Surface topography measurements.

The surface topography measurements were carried out for both living and dried cells using AFM working in contact mode. Two types of V-shaped silicon nitride cantilevers were applied: (1) PNP-TR-customized (Nanoworld) characterized by a nominal spring constant of 0.03 N/m, and (2) MLCT (Bruker) characterized by nominal spring constants of 0.01 N/m (microlevel type C) and 0.03 N/m (microlever type D). The set point range varied between 0.2 nN and 0.8 nN (adjusted during the surface topography acquisition), while the scan rate range was set between 0.3-1 Hz, depending on the scan size. During the AFM measurements of living cells, glass coverslips with cells immersed in a Petri dish, were mounted on the piezoelectric scanner. Cells were imaged in the RPMI-1640 culture media supplemented with 1% HEPES to stabilize pH during the measurements. AFM images were analysed by means of XEI – software provided by a manufacturer, dedicated to XE 120 set-up and WSxM 5.0 software [93].

4.1.2 Force-distance curves.

The elasticity measurements are realized using AFM working in force spectroscopy mode. Here, cantilever is moving towards to and backwards from the sample surface. During this movement cycle, the deflection of the cantilever is registered as a function of relative scanner position (Figure 4.2). Such relation is later on converted into force versus tip-sample distance curve called shortly *force-distance curve*. Each force-distance curve consists of an approach curve and a retract curve. These curves consist of characteristic regions:

- *base line* that is the deflection of the cantilever recorded when AFM probing tip is far away from the investigated surface. At this distance the interaction forces are negligible,
- *contact point* that is the a point when the AFM probing tip touches the sample surface,
- a region when cantilever is deflected due to interaction forces acting between the probing tip and the sample surface. For stiff substrates, only cantilever deflection is measured. For soft samples, the recorded deflection contains contribution from sample surface deformation. During approach, the deflection

of the probing cantilever increases up to given maximum force value (red line in the Figure 4.2) followed by the deflection decrease observed during the AFM probe withdrawal (blue line in the Figure 4.2), reaching again the level of the base line.

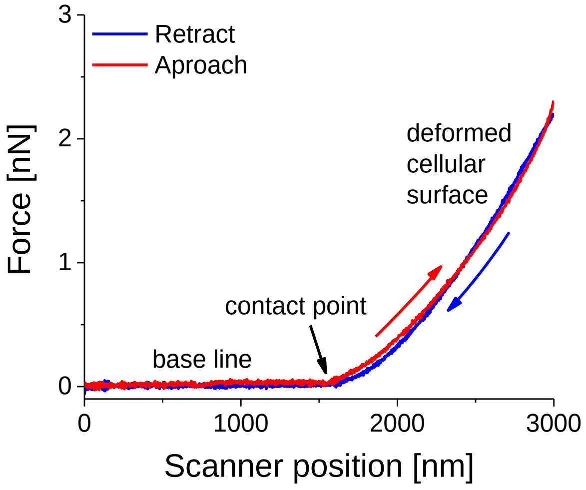

Figure 4.2. *Force-distance curve recorded on a single melanoma cell (WM115). Cantilever deflection (converted into force) reveals non-linear relation when plotted versus scanner (sample) position indicating deformed cellular surface.*

Figure 4.2 presents the force curve recorded on a single WM115 melanoma cell resulting only from cell indentation. There was not any adhesion force occurring between the AFM probing tip and cell's surface.

In the elasticity measurements realized using AFM, an important step is the calibration, i.e. conversion of the cantilever deflection measured in volts into the force value. This is described by the following equation that assumes the knowledge of the cantilever spring constant *k* and photodetector sensitivity *PSD*:

$$F\ [\mathrm{nN}] = deflection\ [\mathrm{V}] \cdot\ k \left[\frac{\mathrm{N}}{\mathrm{m}}\right] \cdot PSD[\frac{\mathrm{nm}}{\mathrm{V}}] \qquad (4.1)$$

4.1.3 AFM-based elasticity measurements

Elasticity measurements were carried out for living cells in a following manner. The force curves were recorded over a scan area varying from 5 x 5 μm^2 up to 10 × 10 μm^2. A grid of 8 × 8 or 7 × 7 or 6 × 6 points was set over the scanned region. On average, 36 – 64 force curves for each single cell were automatically recorded at the approach and retract velocity of 8 μm/s. The total number of measured cells for each studied cell line varied around 50 cells. The measurements were repeated several times with fresh culture cells, medium, and new AFM cantilevers to avoid any kind of systematic error.

4.1.4 The Young's modulus determination

To quantify the indentation depth in the AFM-based elasticity measurements, in parallel to the measured sample, force-distant curves are recorded on stiff, non-deformable reference surface like glass or silicon. In such a case, the deflection of the cantilever registered after the probing tip touches the surface is linear, since the deformation caused by the AFM tip does not occur. By subtracting the reference force-distance curve from that recorded on sample surface, the force-indentation curves can be determined.

The analysis of the force-indentation curves using the Hertz-Sneddon model leads to the determination of the Young's modulus (i.e. elasticity modulus). Based on the Hertz contact mechanics, Sneddon derived a model assuming a rigid, axisymmetric probe indenting a soft, elastic, flat surface. As the AFM tip is frequently a four-sided pyramid, its shape is often assumed to be a cone. In such a case, the Hertz-Sneddon model delivers the following relation between applied load force F and indentation depth δ:

$$F(\delta) = \frac{2\tan\alpha}{\pi} E'\delta^2 \qquad (4.2)$$

Where α is the open angle of the cone [^{0}], E' is the reduced Young's modulus that depends on elastic properties of the cantilever and the sample, as described by the following equation:

$$\frac{1}{E'} = \frac{1-\mu_{cantilever}^2}{E_{cantilever}} + \frac{1-\mu_{sample}^2}{E_{sample}} \qquad (4.3)$$

where $\mu_{cantilever}$ and μ_{sample} represent the Poisson ratios of the cantilever and a sample. In the case of living cells, $E_{cell} << E_{cantilever}$, and thus the reduced Young's modulus can be re-written as:

$$E' = \frac{E_{cell}}{1-\mu_{cell}^2} \qquad (4.4)$$

It is difficult to determine the exact value of μ_{cell}, thus it is often assumed to be 0.5, bearing in mind that a cell which is mainly composed of water, which is an incompressible material.

Finally, the relation between applied load force F and indentation depth δ can be written as follows:

$$F = \frac{2\tan\alpha}{\pi}\frac{E_{cell}}{1-\mu_{cell}^2}\delta^2 \qquad (4.5)$$

Using this equation, the Young's modulus for all studied cells was calculated. Force curves were analysed with the aim to determine the Young's modulus using Origin 8.0 and software developed at the Department of Biophysical Microstructures IFJ PAN [43,94].

4.2 Fluorescence microscopy

All fluorescence images were recorded using optical microscope Olympus XI71 equipped with a X-Cite Series 120Q Lumen Dynamics lamp (uniformly illuminating the whole sample area), U-MWIG2 filter (λ_{exit} = 530-550 nm, λ_{emit} = 590 nm) used for actin filaments visualization, and U-MNB2 one (λ_{exit} = 470-490 nm, λ_{emit} = 520 nm) for fluorescent detection of cell nucleus. For image recording purposes, the XC10 digital camera was used. It provides a 1376 × 1038 pixel image. Images were recorded using the CellSense Dimensions (Olympus). The images were recorded with the objectives 20× and 40× (Universal Plan Fluorite objectives), i.e. magnification of 200 and 400, respectively.

4.3 Scanning electron microscopy (SEM)

The morphology analysis of dried cells, that were previously cultured on silicon substrates, was performed using environmental scanning electron microscope (ESEM) using Quanta 3D FEG (FEI) apparatus. The measurements were carried out under 100 Pa water vapor pressure (to avoid charging) using GSED detector. Electron accelerating voltage during acquisition of secondary electron images was set to 2 keV and 5 keV. The set-up used is available at the Department of Solid State Physics at the Institute of Physics, Jagiellonian University. The measurements were carried out due to the courtesy of prof. Franciszek Krok and dr Benedykt R. Jany.

4.4 Time-of-flight secondary ion mass spectrometry (ToF SIMS)

4.4.1 ToF SIMS – basic principles

Time-of-flight secondary ion mass spectrometry (ToF SIMS) is a mass spectrometric technique used for chemical analysis of various materials. In this method, a high energy primary ion beam bombards a surface of a sample causing transfer of the particle energy to the atoms of the solid by a collision-cascade process (Figure 4.3).

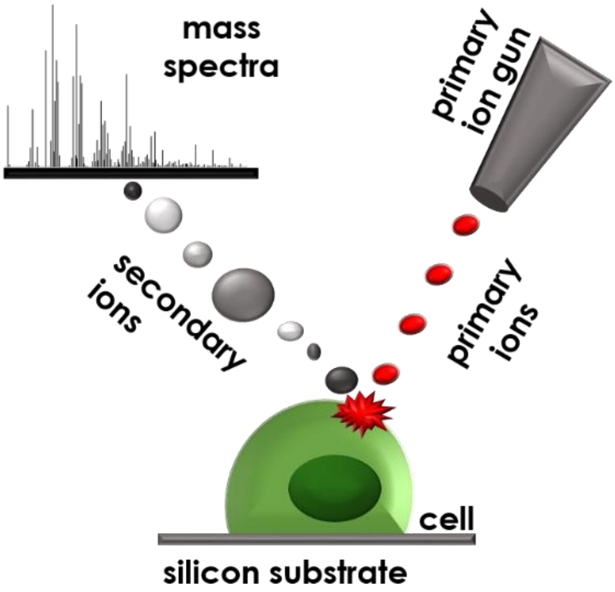

Figure 4.3. *Secondary Ion Mass Spectrometer – the idea of the measurement.*

Then, fast collisions occur between atoms in the sputtered material. Some of them return to the surface resulting in the emission of particles. Those sputtered secondary particles could be electrons, atoms, molecules, atomic and cluster ions. They are detected by a mass spectrometer based on their mass to charge ratio. In this manner a mass spectrum is obtained that enables a chemical analysis of a studied sample.

4.4.2 ToF SIMS – experimental details

The TOF SIMS 5 (ION-TOF, GmbH, Munster) equipped with a 30 keV bismuth liquid ion gun was used to collect mass spectra of dried cells, previously cultured on a silicon substrate. High-resolution m/z mass spectra of secondary ions, emerging from samples bombarded with the Bi_3^+ primary ion beam, were acquired with a time-of-flight mass spectrometer.

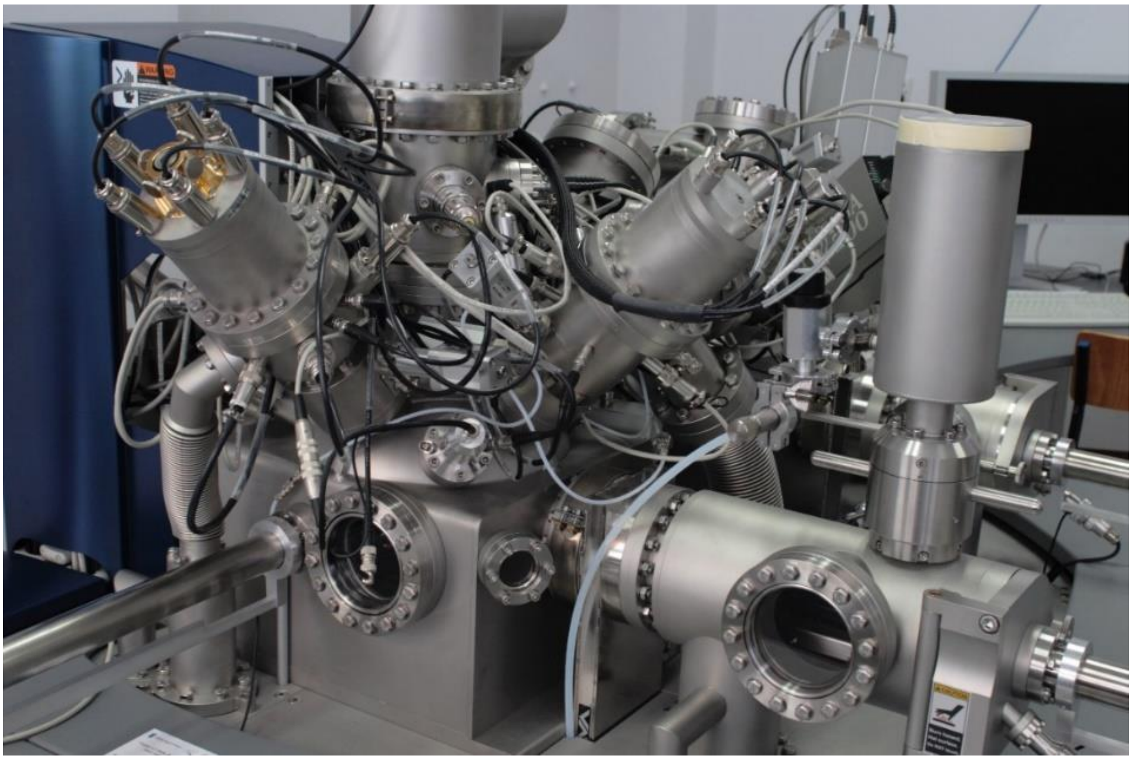

Figure 4.4. *A photography presenting the ToF SIMS system used in the experiments. This system is working at the Department of Advanced Materials Engineering at the Institute of Physics UJ.*

For ToF SIMS measurements, cells on silicon wafers were fixed and dried in the laminar flow chamber (NuAire) and transferred into the lock-in chamber of SIMS apparatus in a dedicated vacuum vessel to maintain sterile conditions. In principle, for ToF SIMS experiments, two types of samples were measured, namely, silicon surfaces without cells (reference samples) and silicon surfaces with cells. To probe single cells, the area of 150 μm × 150 μm was chosen. To maintain the static conditions ($< 10^{12}$ ions/cm^2 for primary ion beam), time of acquisition and primary beam current were adjusted, remaining the sample surface intact. The total dose per one measurement was of the order of 10^8 of primary ions, what yields the dose density of 10^{12}/cm^2. The mass spectra were recorded using Bi_3^+ primary ion beam for positive ions within a mass range from 1 to 800 Da with the resolution $m/\Delta m > 6500$. All samples with cells that were analyzed, and compared together afterwards, were measured in a one experiment batch to avoid any instrumental drift.

4.5 Photothermal Microscopy (PTMS)

4.5.1 PTMS – basic principles

Absorption spectra obtained from photothermal microspectroscopy deliver information about the chemical status of a sample exposed to the infrared (IR) beam modulated by the Michelson interferometer. The IR beam was focused on the sample prepared in a form of "a ball" (as described in Materials and Methods Chapter). The absorption of IR energy causes vibrations and subsequent relaxation of molecular bonds, that release heat detected by a thermal sensing probe, which is further converted into absorption spectra similar to those found in conventional IR spectroscopy. Importantly, no substrate was applied, thus the resulting photothermal response shows stretching and bending of bonds characteristic for specific molecules present in cells only.

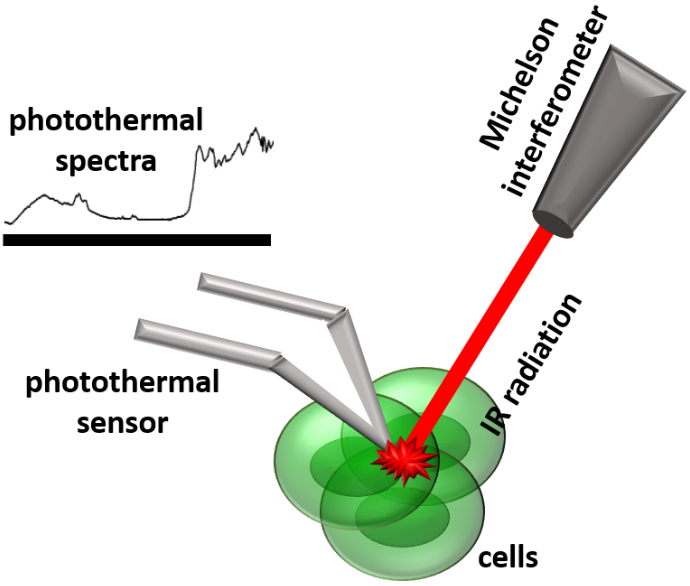

***Figure 4.5**. Principles of PTMS technique.*

The PTMS technique [95] used for acquiring photothermal spectra of melanoma cells is a combination of an atomic force microscope (Explorer, Veeco Instruments, Santa Barbara, USA) with the implemented IFS/66S FT-IR spectrometer (Bruker Optics, Coventry, UK) available at the School of Pharmacy at the East Anglia University in Norwich (UK). In this system, the AFM was equipped with a Wollaston wire thermal probe which is a silver wire characterized by a diameter of 75-µm with a platinum/10% rhodium core of 5 µm in diameter [96]. The probe was used as a localised heat source as well as a temperature sensor. The beam of the spectrometer is directed to the tip of the probe and the temperature change as a function of wavelength is measured due to changes in resistance of the probe. When the probe comes into contact with a sample and the material absorbs light at a specific wavelength, the temperature increases. This is plotted against wavelength to generate a spectrum similar to that found in conventional IR spectroscopy.

4.5.2 Details of PTMS experiments

In the measurements presented in this thesis, samples were measured by isolating material located at the end of the tip. This has the benefit of higher signal-to-noise ratio and eliminates the potential for spectral interference from a supporting substrate [97]. To attach the cells to the tip, cell pellet, taken from Eppendorf tube from PBS solution, was lightly scattered on a clean glass substrate. Next, the tip was dipped into the cellular material and raised. In that manner, a cluster of cells adheres to the tip by physical adsorption, as has been demonstrated previously [98]. Measurements were first carried out without any material to provide a background spectrum, which was used to normalize spectra recorded for cells. Measurements were carried out at a resolution of 8 cm^{-1} for 1000 scans, resulting in acquisition time of approximately 50 minutes. The spectra were recorded within the range of 500 cm^{-1} to 4000 cm^{-1}. The PTMS spectra were acquired for different samples. Each cell cluster was treated as a separate sample. In total, 20-30 spectra were recorded. Measurements were carried out by Dr Jonathan Moffat on samples that were prepared at the IFJ PAN[3].

4.6 Principal Component Analysis – basic principles

PCA is one of the established methods to analyse large data sets [99,100]. The principle of PCA is to reduce the dimensionality of a data set, while retaining as much as possible the variation present in the original predictor variables [101]. In mathematical terms, PCA maximizes the variance of a linear combination of the original predictor variables (Figure 4.6).

---

[3] Measurements were carried out within the frame of EU FP7 project SMW „Single Molecule Workstation“, no. NMP4-SE-2008-213717, financed between 2008 – 2011. Thus, the recorded PTMS spectra are free from any subjective influence of the ToF SIMS experiments. **To perform blind verification of the ToF SIMS results, Justyna Bobrowska re-analysed raw data using the methodology proposed by herself for analysing ToF SIMS mass spectra.**

This transforms original set of variables into a new set of variables called principal components (PCs).

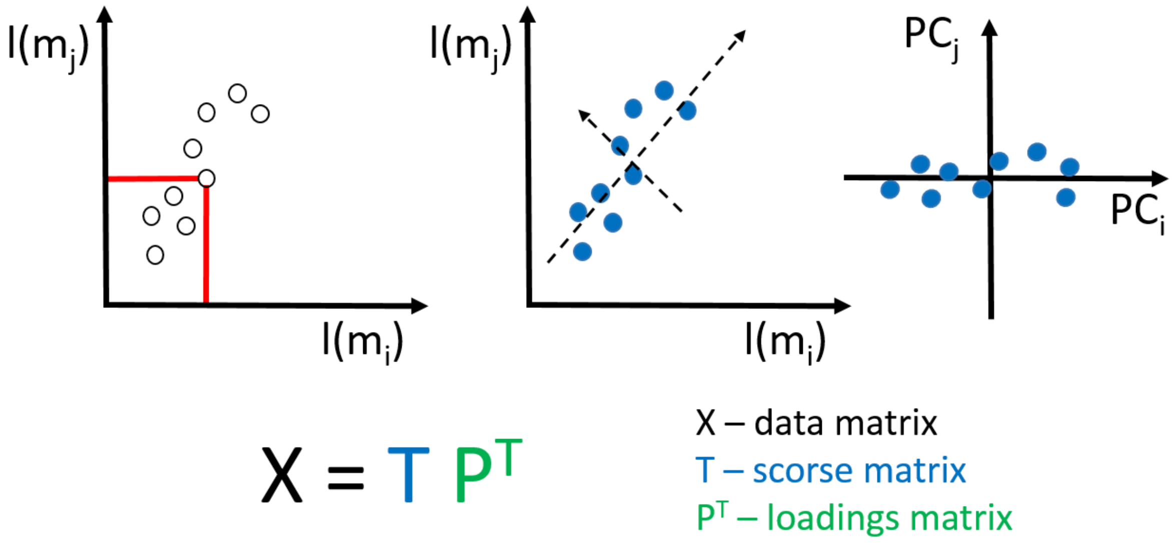

Figure 4.6. *The idea of the principal component analysis (PCA).*

Principal components are orthogonal to each other and are defined in such a way that the first principal component is the direction that describes the highest degree of variance, the 2nd principal component describes the second highest degree of remaining variance, and so on. If we are considering a matrix of spectra, where each spectrum is a vector in a n-dimensional space (n is the number of masses in this case), PCA is basically a matrix rotation into a new set of axes, based on a combination of the original data set, that best describes the spread of the data. The new axes are called *loadings* and they are a measure of the importance of the original variables to the new direction. When a particular peak has high magnitude of a loading then it means that this peak was significant in defining the new direction of maximum difference. The original mass spectrum can be projected on to the new directions of principal components by means of *scores* – the distances along these directions of that spectrum for the particular principal components.

4.6.1 Details of PCA applied to ToF SIMS and PTMS spectra

In the presented thesis, the PCA was applied to analyze spectra recorded by both techniques (PTMS and ToF SIMS). The ToF SIMS spectra were analyzed within the range 0–500 Da, while for PTMS the range from 4000 cm^{-1} to 500 cm^{-1} was used. In the presented approach, the same method of data analysis, without predefining of any particular variables, was applied (Figure 4.7).

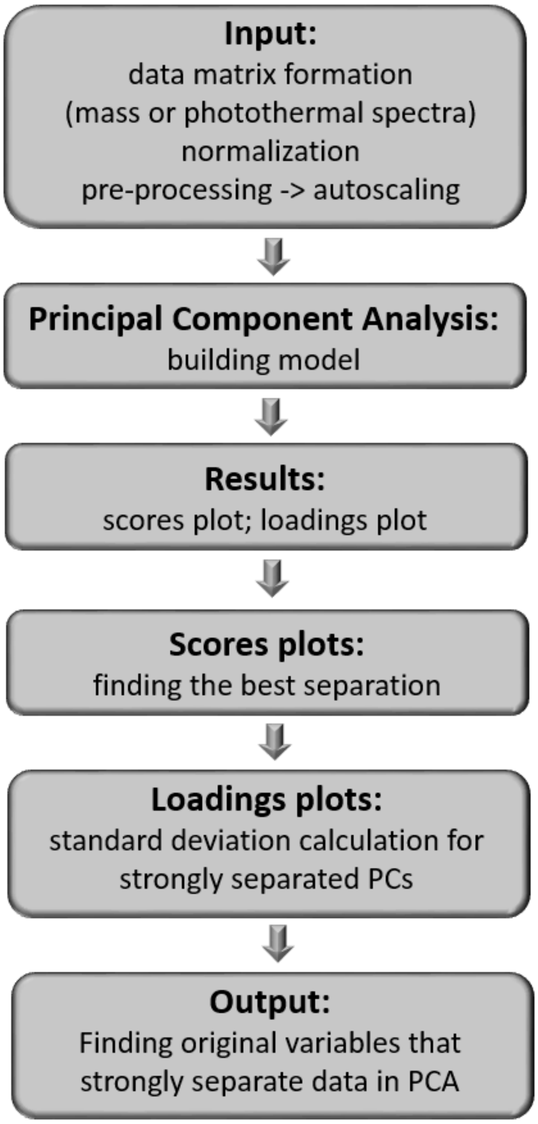

Figure 4.7. *A block diagram showing the proposed method of data analysis.*

Firstly, each recorded spectrum was normalized to the sum of intensities for all peaks. Then, autoscaling was applied as a pre-processing method. In autoscaling, after mean-centering, each variable is divided by the corresponding variable standard deviation. Such a way of pre-processing results in scaling of each variable in a way providing an equal impact on a final result of multivariate analysis. After pre-processing, the PCA was carried out using the PLS Toolbox 7.5.2 (Eigenvector Research, Manson, WA) for MATLAB 8.1.0.604 R2013a (MathWorks, Inc., Natick, MA) software. Original data were analysed with the same weights. The cross-validation algorithm was applied to select the number of components in PCA.

From PCA analyses, both scores and loading plots were obtained. First, the scores plots were reviewed to find the best separated PCs. When it was reached, the standard deviations (SDs) for these components were calculated from the loading plots. The SDs were used as a threshold to find masses or spectral ranges that participate strongly in the separation of PCs, and thereby, they dominate in differentiation between original sets of data.

4.6.2 Pre-processing methods and final PCA results

The complexity of the spectral signatures associated with biological materials is widely known [69,102]. Extracting substantial biological information from the large data sets is one of the major challenges in ToF SIMS research of organic materials. This is one of the reasons why the interpretation can be facilitated by chemometric analysis based on statistical methods, such as principal component analysis (PCA). It is important to remember, that final results of PCA may be strongly influenced by the chosen pre-processing method [101].

For all collected mass spectra recorded for human bladder cancer cells, PCA was implemented and loadings for each original variable were obtained. They are presented in the Figure 4.8 showing, simultaneously, the results of the type of pre-processing method used i.e. either mean centering or autoscaling. Data pre-treatment can be used as a correction for aspects that hamper the biological interpretation of mass spectra. Here, two methods of data pre-processing have been applied and tested, namely, mean centering and autoscaling. Mean centering converts all the intensities to fluctuations around zero instead of around the mean value. In this way it leaves only the relevant variation between the samples for further analysis as it adjusts the differences in the offset between high and low peak intensities [103]. In autoscaling, each variable is divided by standard deviation of this variable for all spectra. As a result of autoscaling, each variable has a mean value equal to zero and a standard deviation of one. In this way, each variable is scaled and, eventually, each variable has an equal impact on the results, what can be crucial for higher masses that have lower intensities in the spectra.

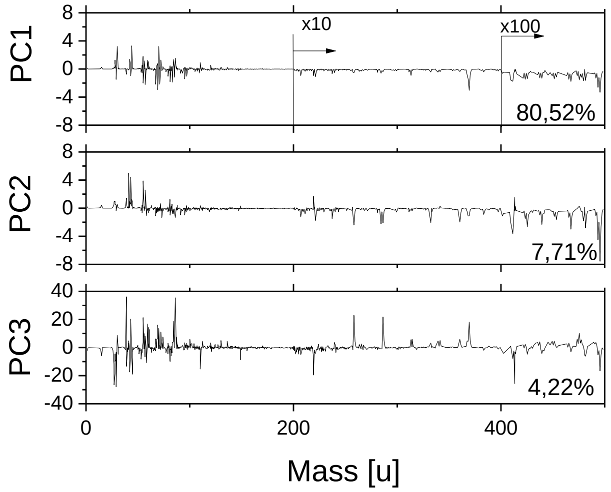

a)

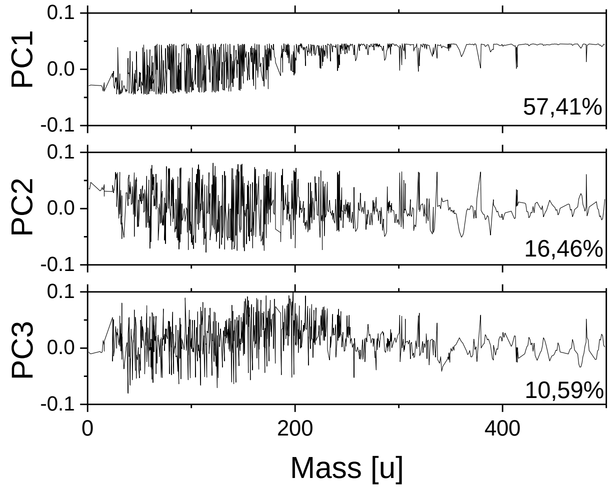

b)

Figure 4.8. *Loadings plot for PC1, PC2 and PC3 components resulted from PCA of ToF SIMS spectra acquired for the studied human bladder cancer cells. Two pre-processing methods were applied i.e. (a) mean centering and (b) autoscaling.*

Depending on the type of pre-processing method applied, the obtained percentages of the total variance are different. The percentage of the total variance can be attributed to variability present within each orthogonal principal component. Mean centering pre-processing delivers values of PC1 = 80.52%; PC2 = 7.71%; PC3 = 4.22%, while after applying of autoscaling, the values of PC1 = 57.41%; PC2 = 16.46%; PC3 = 10.59% were obtained. As it can be seen in the loadings plots, after mean centering initial masses (1-100 Da) have largest amplitudes of loadings (Figure 4.8a). After autoscaling, these values are also significant for higher masses (Figure 4.8b).

Plotting PC components against each other shows the largest separation between the studied human bladder cancer cells for the 3rd principal component (PC3) plotted versus 2nd principal component (PC2). Analogously as for loadings plots, two pre-processing methods were considered (Figures 4.9).

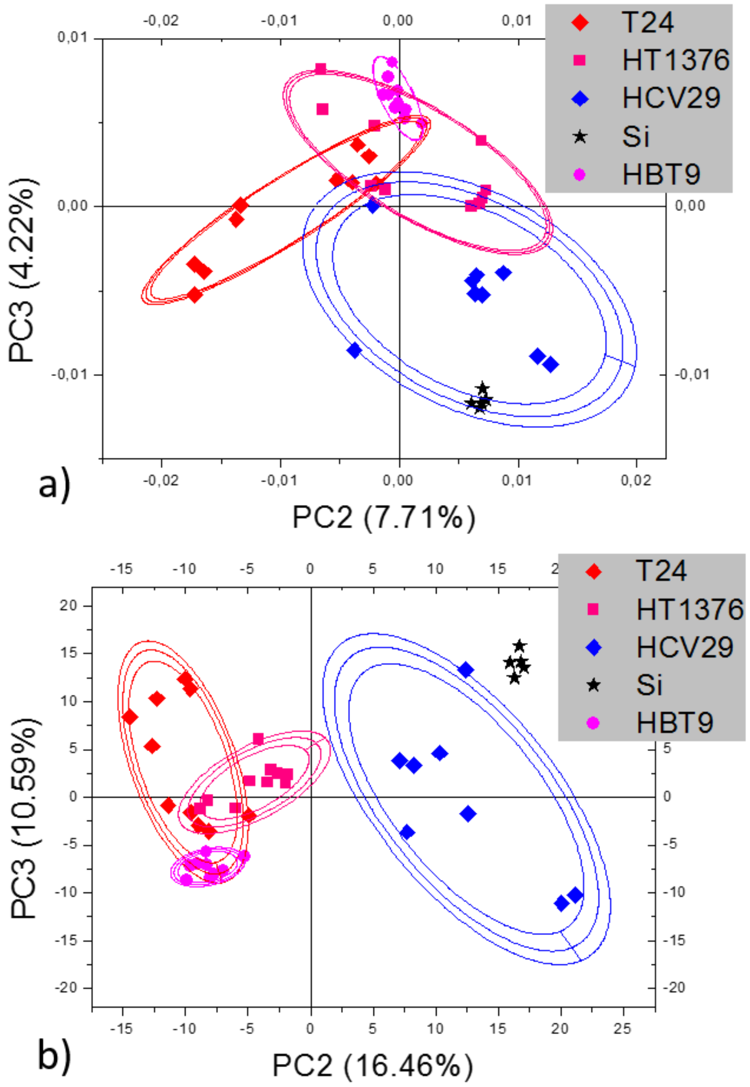

Figure 4.9. *Scores plot for PC3 versus PC2 resulted from PCA of ToF SIMS spectra acquired for the studied human bladder cancer cells. The results were obtained for (a) mean centering and (b) autoscaling pre-processing methods. To each data set confidence ellipses at the confidence levels of the 90%, 95%, and 99% were calculated.*

Each single point, present in the score plots, corresponds to a single mass spectrum presented in the new coordinate system consisting of principal components. They cluster in different parts of coordinate system in a cell-dependent manner. Such separation indicates differences in the chemical compositions of cellular surfaces in human bladder cancer cells.

Clustering occurs also independently of the pre-processing method applied, however, it seems to be more pronounced for autoscaling approach.

4.7 Summary

The realization of the thesis objectives involves the application of several experimental techniques such as *(1)* atomic force microscopy (AFM) used to visualize surface topography and to measure elastic properties of living melanoma cells, *(2)* fluorescent microscopy applied to visualize the organization of actin cytoskeleton, a structure responsible for mechanical resistance of cells, *(3)* time of flight secondary ion mass spectrometry (ToF SIMS) used to study the surface properties of melanoma cells, *(4)* photothermal microspectroscopy (PTMS) used to verify the measurements obtained from ToF SIMS.

To identify the spectral fingerprints of cellular surface in melanoma cells, the principal components analysis (PCA) was applied. In the approach, presented here, the PCA analyses whole mass and photothermal spectra without pre-definition of any particular molecular mass or wavenumbers. Such approach was dictated by a huge complexity of mass spectra and large variability of detected molecular fragments. The proposed methodology of data analysis was verified through PCA of photothermal spectra. In that manner the overall information on surface properties can be obtained.

5. Functionality of ToF SIMS measurements

5.1 Objectives

The main objective of this chapter is to compare surface properties of cancer cells whose deformability is much larger than deformability of reference, non-metastatic cells. By applying the proposed methodology of sample preparation (*Chapter 3*) and data analysis (*Chpater 4*) for single human bladder cells, the functionality of ToF SIMS in detection of cancer alterations has been demonstrated[4].

5.2 Deformability of human bladder cells

Deformability of human bladder cancer cells has been measured at the Department of Biophysical Microstructures (IFJ PAN, Cracow, Poland) several times. The elastic properties of non-malignant HCV29 and cancerous (HTB-9; HT1376, T24) cells were quantified using the Young's modulus. The recently published moduli values are presented in the Table 5.1 (adapted from [104]).

Table 5.1 Deformability of human bladder cells for indentation depth of 500 nm (data taken from Ramos et al. Beilstein J. Nanotechnol. 2014).

Cell lines	*Young's modulus [kPa]*
HCV29, non-malignant cell cancer of ureter (reference cell lines)	10.0 ± 3.0
HTB-9, carcinoma, grade 2	3.8 ± 2.2
HT1376, carcinoma, grade 3	3.9 ± 2.1
T24, transitional cell carcinoma, grade 4	3.6 ± 2.1

The deformability of cancer human bladder cells is much higher as compared to reference HCV29 cells. These alterations are strongly related to the organization, density and

---

[4] Mrs Justyna Bobrowska (first name before marriage Justyna Gostek) carried out all AFM and ToF SIMS measurements and data analysis. The results have been published in the paper Gostek et al. *"Differentiation of human bladder cells using PCA analysis of ToF-SIMS mass spectra*" in *Analytical Chemistry* 88(6) 3195-3201 (2015).

amount of actin which is forming cytoskeleton filaments. The relation between the single cell deformability and actin cytoskeleton has been reported in several other studies [105–109].

5.3 Mass spectra of human bladder cancer cells

The collected mass spectra of samples containing single human bladder cells show large degree of complexity as presented in the Figure 5.1.

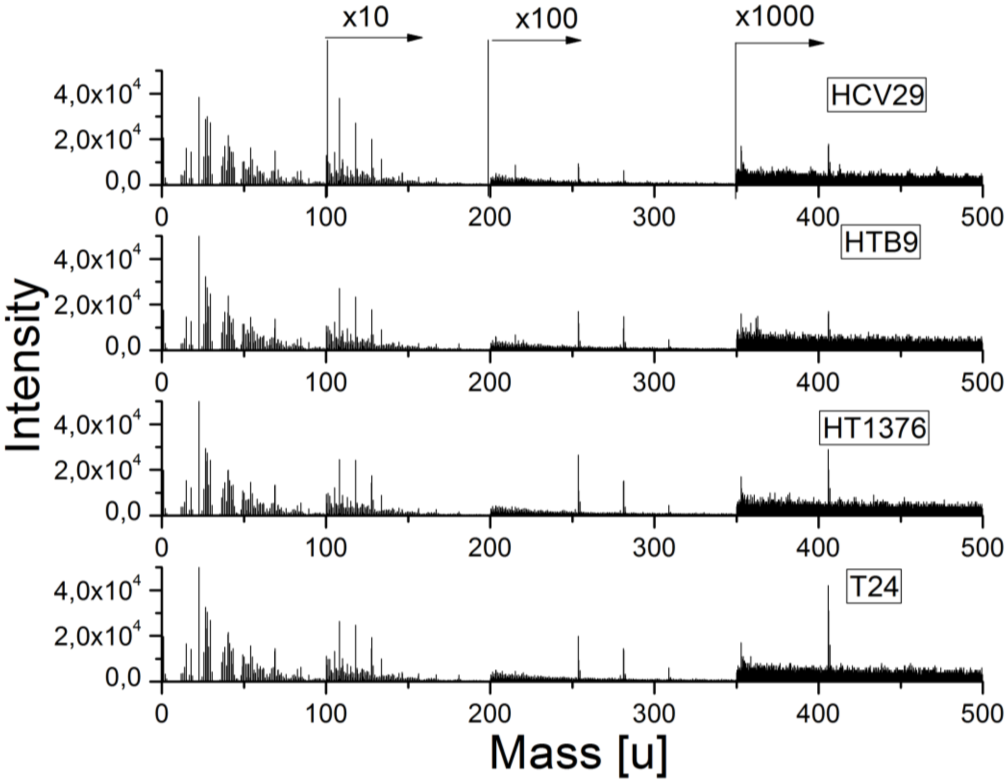

Figure 5.1. *Exemplary positive mass spectra acquired for all studied human bladder cancer cells. The molecular masses were within the range of 0-500 Da, and* Bi_3^+ *primary ion gun was used to induce secondary particles (images adapted from Gostek et al. Analytical Chemistry 88 (2015) 3195 – 3201).*

A large number of peaks characterized by various intensities was observed. It is not possible to define neither a single peak, nor a set of peaks that is specific for only one cell line.

5.4 Surface chemistry based differentiation of human bladder cancer cells

For all collected mass spectra recorded for human bladder cancer cells, PCA was implemented and loadings for each original variable were obtained. They are presented in the Figure 5.2 showing, simultaneously, the PCA results after the use of autoscaling as a pre-processing method.

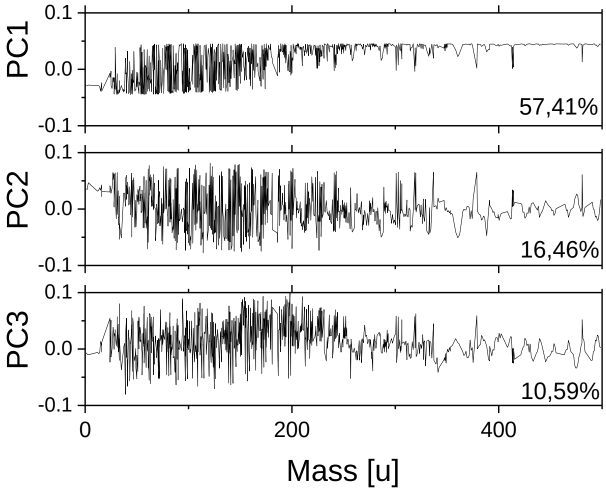

Figure 5.2. *Loadings plot for PC1, PC2 and PC3 components resulted from PCA of ToF SIMS spectra acquired for the studied human bladder cancer cells. As pre-processing method autoscaling was applied. (images adapted from Gostek et al. Analytical Chemistry 88 (2015) 3195 – 3201).*

The percentage of the total variance can be attributed to variability present within each orthogonal principal component. The values of PC1, PC2, PC3 were equal to 57.41%, 16.46%, 10.59%, respectively. Plotting principal components against each other (Figure 5.3) shows the largest separation between the studied human bladder cancer cells for the 3rd principal component (PC3) plotted versus 2nd principal component (PC2).

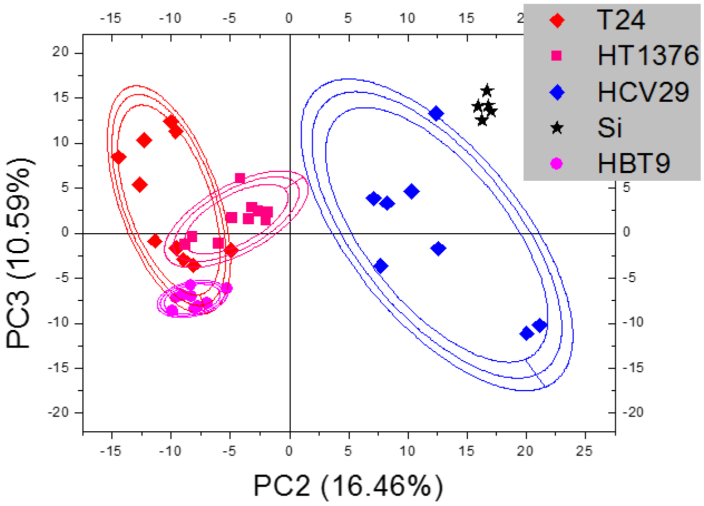

Figure 5.3. *Scores plot for PC3 versus PC2 resulted from PCA of ToF SIMS spectra acquired for the studied human bladder cancer cells. To each data set confidence ellipses at the confidence levels of the 90%, 95%, and 99% were calculated. As pre-processing method autoscaling was applied.*

Each single point, present in the score plot, corresponds to the single mass spectrum presented in the new coordinate system consisting of principal components. They cluster in different parts of coordinate system in a cell-dependent manner. The data points corresponding to mass spectra acquired for HCV29 non-malignant cells can be clearly distinguished from the remaining three cancerous cell lines. Also it can be observed, that the distribution of points for HCV29 cells is the widest. That might indicate that chemical composition of non-malignant human bladder cells is more variable as compared to cancerous cells. Alternately, it can be noticed, that the morphology of the HCV29 cells differs considerably from the remaining three cell lines. It can also influence the obtained separation. The non-malignant cells vary significantly in shape that is rather elongated in comparison to rounded human bladder cancerous cells and denotes a distinct organization of cytoskeleton fibrils, most probably actin filaments [104]. The remaining three cancerous cell lines (HTB-9, HT1376 and T24) have rounded shape and poorly differentiated cytoskeleton [104,110]. The distribution of points corresponding to cancerous cells in the scores plots (Figure 5.3) is much narrower. Thus, it suggests similar chemical composition of those cell lines.

5.5 Molecular masses derived from PCA analysis

As PCA was performed for the whole range of mass spectra, without pre-definition of any particular mass peaks *a priori*, it was possible to choose masses causing strongest differentiation afterwards. In the scores plots shown in Figure 5.4, mass spectra of non-malignant HCV29 cells have a positive values of PC2 while cancerous cell lines have negative values. This observation permits to find these mass peaks that cause the strongest differentiation, based on PCA results. Thus, the average value and standard deviation (*SD*) of the PC2 loadings was calculated. Subsequently, all mass peaks with value of PC2 loading below -*2SD* were chosen, as these were causing the largest differentiation between non-malignant and cancerous cell lines. This constitutes the selection criterion for molecular masses. The results of the selection are presented in the Table 5.2.

Table 5.2. *Masses with PC2 loading values below −2SD (for autoscaling)*

Mass [u]	Determined formula	Assignment	Mass [u]	Determined formula	Assignment
60.09	$C_3H_{10}N^+$	fatty acid−lipid head[a]	141.12	$C_8H_{15}NO^+$	
88.08	$C_3H_{10}N_3^+$		144.08	$C_{10}H_{10}N^+$	
97.07	$C_6H_9O^+$	fatty acid−lipid head[a]	150.10	$C_{10}H_{14}O^+$	α-tocopherol[b]
102.10	$C_4H_{12}N_3^+$	ARG, arginine[a]	151.10	$C_{10}H_{15}O^+$	α-tocopherol[a]
114.14	$C_8H_{18}^+$	fatty acid−lipid tail[b]	159.09	$C_{10}H_{11}N_2^+$	TRP, tryptophan[a]
127.11	$C_5H_{11}N_4^+$	ARG, arginine[a]	170.19	$C_{11}H_8NO^+$	TRP, tryptophan[a]
132.09	$C_{10}H_{12}^+$	fatty acid−lipid tail[b]	200.14	$C_{11}H_{20}O_3^+$	
139.11	$C_9H_{15}O^+$	fatty acid−lipid head[b]	226.16	$C_{13}H_22O_3^+$	

[a] - *Assignment based on literature data* [70,74,77,111,112] [b] - *Proposed assignment*

In the case of autoscaling, selected molecular mass peaks can be attributed to lipids and there are also several signals coming from amino acids, arginine and tryptophan. When autoscaling was used, larger fragments, up to 226.16 Da, became more relevant, coming from not only lipid chains but also amino acids.

5.6 Summary

Assuming that elasticity changes are associated with alterations occurring on a cell surface, the ToF SIMS measurements presented in this chapter were carried out on human bladder cancer HTB-9, HT1375, and T24 cells. These cells are significantly more deformable as compared to reference, non-malignant HCV29 cells [46,104]. The obtained results show that previously measured mechanical properties of human bladder cells are accompanied by distinct surface properties as demonstrated using ToF SIMS.

The applied methodology of PCA to analyse the recorded ToF SIMS mass spectra distinguishes between various types of cancer cells in human bladder. The PCA analysis carried out for the whole range of molecular masses (up to 500 Da) clearly distinguish non-malignant HCV29 cells from the remaining three cancerous cell types (HTB-9, HT1376, T24 cell lines). It is worth to recall that there was no need to choose *a priori* particular masses from mass spectra to discriminate between cell lines. The PCA was sensitive enough to find substantial differences between cells based on analysis of the whole range of acquired spectra. This is a huge advantage in terms of potential applications of the ToF SIMS technique to identify the pathological state of the sample. By analysing the molecular mass range dominating in the separation of non-malignant cells from the cancerous ones, it was possible to select peaks at molecular masses that influenced strongly the obtained separation. Based on literature data the proposed peak assignment pointed out at these masses that are characteristic for lipids and for some amino acids, such as arginine or tryptophan. These findings show that the invasive phenotype of human bladder cancer cells can be correlated with the alterations in chemical compositions of the studied cells.

6. Morphological and mechanical properties of melanoma cells from VGP (WM115) and skin metastasis (WM266-4).

6.1 Objectives

The specific aim of the presented thesis is to find physico-chemical characteristics that enable to differentiate between two closely related melanoma cell lines based on nanomechanical properties obtained by atomic force microscopy. This chapter describes the properties of two melanoma cell types, namely WM115 and WM266-4, derived from the same patient from two different stages of melanoma progression. The WM115 cells were derived from the primary tumour in vertical growth phase (VGP), whereas the WM266-4 cells were established from a metastasis to skin. As a first step, surface morphology and mechanical properties of these melanoma cells were characterized by atomic force and fluorescence microscopes. Part of these studies has been already published in the paper by Gostek et al. "*Nano-characterization of two closely related melanoma cell lines with different metastatic potential*" published in *European Biophysics Journal* 44 49-55 (2015)[5].

6.2 Morphology of melanoma cells in low and high cellular densities

The simplest way applied to analyse the morphology of cells uses either optical or fluorescent microscopes. In particular, by fluorescent staining of actin cytoskeleton, the shape of single cells can be directly visualized. On the other hand, the shape of cells is a result of many factors influencing cellular behaviour during culture. Thus, in the presented case, the organization of F-actin filaments was observed at two cellular densities, i.e. at a single cell level as well as in conditions of semi-confluent monolayer (Figure 6.1). The fluorescent images were recorded for both melanoma cell lines (WM115 and WM266-4) after 3 days of growing in two

---

[5] Mrs Justyna Bobrowska (family name before marriage Justyna Gostek) carried out all atomic force (AFM) and fluorescence microscopy (MF) measurements. These measurements were performed within the frame of the collaborative projects between IFJ PAN and Institute of Biophysics (Johannes Kepler University (JKU, Linz, Austria) entitled (1) „Studies of correlation between surface receptors expression (integrins and cadherins) and mechanical properties of living cells" 2011/2012; number 8507/R11/R12 and (2) "Single molecular characterization of integrin-mediated adhesion to laminin in normal human melanocytes and melanoma cells" 01.05.2013-31.04.2015; number PL 04/2013. All data presented within this chapter were collected by Ms Justyna Gostek using an integrated AFM/MF system working at the IFJ PAN. Mrs Justyna Bobrowska has had the opportunity to measure her samples using an integrated system composed of AFM and fluorescence microscopes working at the JKU Linz (Austria).

distinct densities. To quantify morphological characteristics, surface areas of cells and nuclei were determined. They served as parameters to calculate the *N/C ratio* (a nucleus surface area divided by a cytoplasm surface area) that might be used as a marker to diagnose melanoma similarly to the cervical squamous epithelium [113].

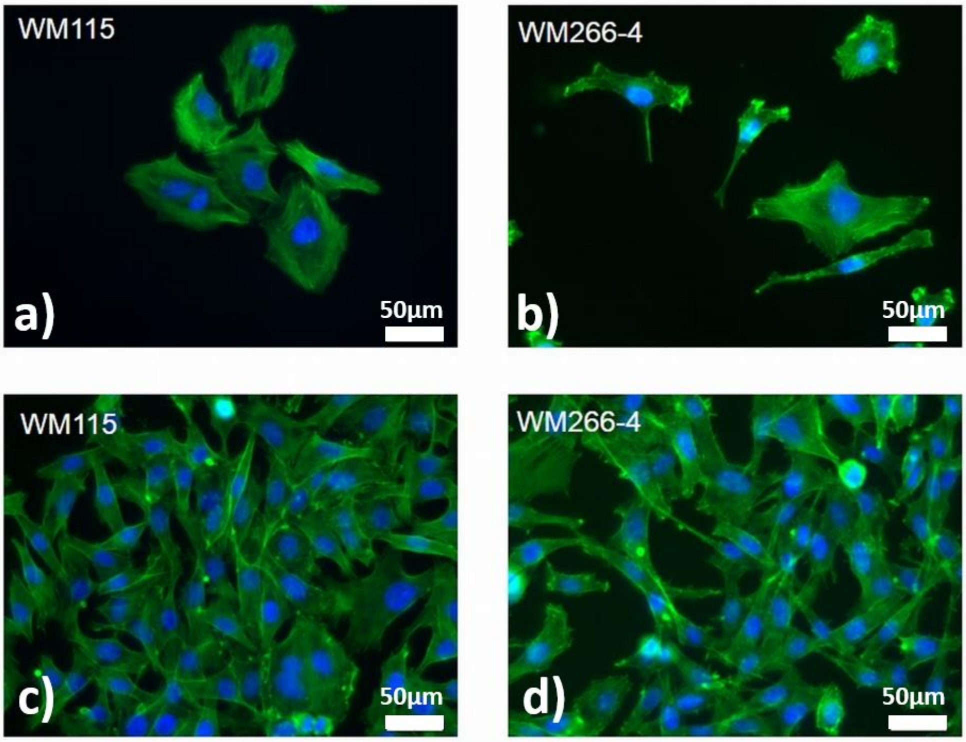

Figure 6.1. *F-actin (green) distribution in the studied melanoma cells cultured both as (a, b) single cells and in conditions of a semi-confluent monolayer (c, d). Blue denotes cell nuclei (image adapted from Gostek et al. European Biophysics Journal 44 (2015) 49-55).*

To quantify the changes in cell shape based on the fluorescently labelled cell nuclei and F-actin filaments, the average size of a nucleus (A_N) and, simultaneously, a cell (A_C) was determined by dividing the coverage area of the corresponding images by the number of cells (as described elsewhere [114]). Then, the ratio between a nucleus and a cytoplasm (*N/C*) was calculated as follows (Table 6.1):

$$N/C = A_N/(A_C-A_N) \tag{6.1}$$

The surface area occupied by single cells (A_C) is larger in the case of WM115 melanoma cells (from VGP progression stage) as compared to WM266-4 cells (skin metastasis). The alterations of nucleus surface area (A_N) are not considerable between these two cell lines. What is worth to highlight, the WM266-4 cells undergo larger changes in surface areas at the cellular and nuclear levels. For both melanoma cell lines, surface area drops significantly as the density of cells increases. The surface of cells grown at higher density constitutes 69 % and 47 % of the surface area of single cells (low density) for WM115 and WM266-4, respectively. The accompanying alterations in cell nucleus surface are 71% (WM115) and 68 % (WM266-4). These changes can be quantified by an *N/C* ratio. Such determined *N/C* ratio might be used to diagnose cancers, like in case of cervical squamous epithelium, showing a potential usefulness in clinical applications as its value increases with increased accumulation of abnormal changes in cervical intraepithelial neoplasia. Smaller value of *N/C* ratio denotes a cell which spread out well on a surface while its value close to one indicates a round cell.

Table 6.1. *The surface derived parameters quantifying morphological changes in melanoma cells. The data are represented as a mean ± standard deviation (SD).*

Cell type, density	A_C [μm^2]	A_N [μm^2]	*N/C*	*Overlap* [%]	*N/C*
WM115 low cellular density	1630 ± 480	280 ± 70	0.21 ± 0.10	0.81	0.21 ± 0.11
WM115 high cellular density	1130 ± 240	200 ± 10	0.22 ± 0.06	8.18	0.20 ± 0.06
WM266-4 low cellular density	1500 ± 350	220 ± 30	0.17 ± 0.05	0.78	0.17 ± 0.07
WM266-4 high cellular density	700 ± 60	150 ± 10	0.27 ± 0.04	13.18	0.23 ± 0.04

The cultures of the melanoma cells at higher cellular density display places where cells overlap (Figure 6.1. c&d). The contribution of overlapping effect is mainly observed at higher cellular density with overall level of around 10%-15%. For such a case, the *N/C* ratio is underestimated. The *N/C* ratio corrected by the overlapping effect shows statistically significant differences between WM266-4 cells cultured at low and high cellular densities (p = 0.0302, calculated based on Students t-test). The absence of statistically significant difference is observed for WM115 cells at low and high cellular densities (p = 0.8036), WM115 and WM266-4 cells cultured at low cellular density (p = 0.3448), and high cellular density (p = 0.2048). For the studied melanoma cells, the obtained *N/C* ratio reaches values close to ~0.2 and it rather describes conditions suitable for cell spreading than the differentiation between melanoma cells from VGP and metastatic stages of melanoma progression.

6.3 Topography of melanoma cell surface

The surface topography of melanoma cells was measured using atomic force microscopy working in contact mode (Xe120, Park Systems). The glass slide with living cells immersed in culture medium was mounted on the AFM piezoelectric scanner. Next, an optical image was collected to find relative positions of a cell to be measured and a probing AFM cantilever (Figure 6.2a). Then images of surface topography were recorded (both height and deflection images were collected, Figure 6.2b and c, respectively).

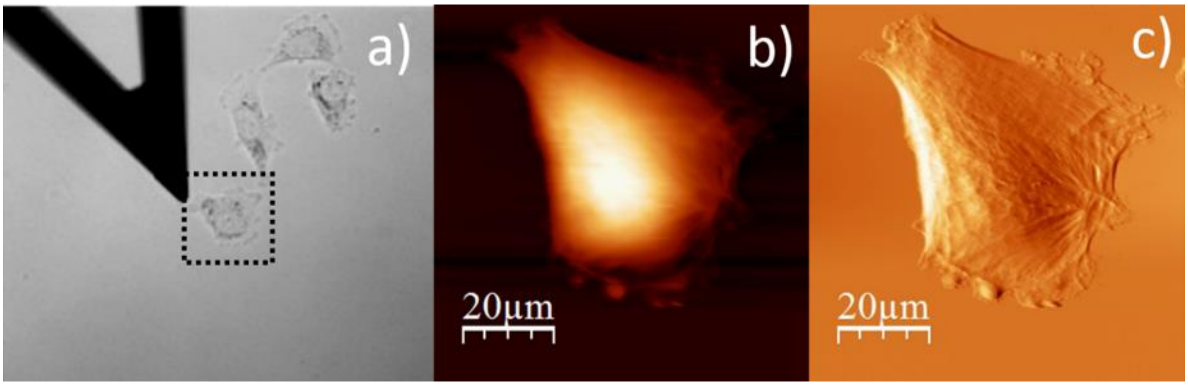

Figure 6.2. *The idea of AFM measurements: a) optical image, b) AFM topography, c) AFM error mode image of single WM115 melanoma cell.*

The surface topography of single melanoma cells was recorded at large scan areas of 90 µm × 90 µm. Measurements were carried out on living cells in conditions provided by the culture medium. The deflection images presented in the Figure 6.3 show triangular shape of single cells that is characteristic for both studied melanoma cell types.

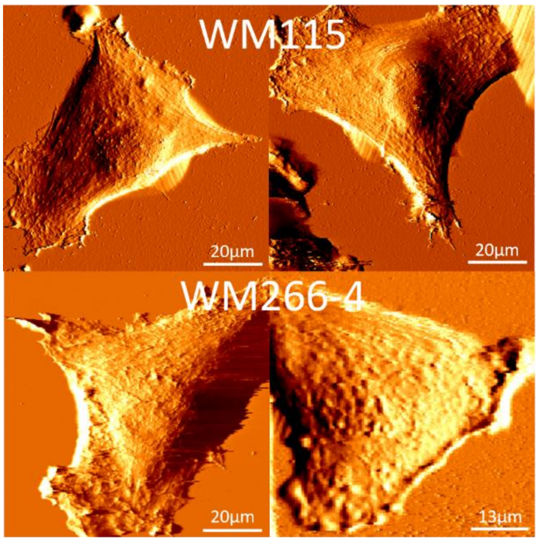

Figure 6.3. *Typical AFM error images of living melanoma WM115 and WM266-4 cells showing characteristic triangular shape of single cells.*

Independently of the studied cell type (WM115 or WM266-4), the observed single cell shape was very similar, often showing a nucleus in a central region of a cell. To investigate the cellular surface at nanoscale, i.e. at the level allowing for the visualization of F-actin filaments organization beneath cell membrane, smaller scan areas of 15 × 15 µm^2 were chosen. The AFM deflection images of cellular surface are presented in the Figure 6.4 (a-c for WM115 and d-f for WM266-4 melanoma cells, respectively).

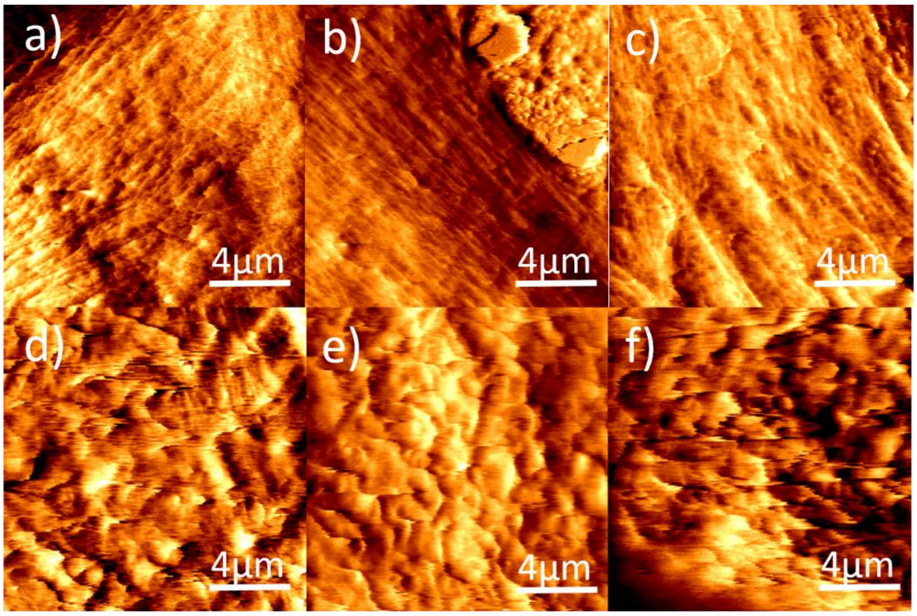

Figure 6.4. *Fragments of cellular surface recorded for WM115 (a–c) and WM266-4 (d–f) living melanoma cells, recorded in liquid condition, i.e. culture medium.*

Deflection images, recorded with high resolution, reveal distinct surface topography of the studied melanoma cell lines. In the case of WM115 cells (Figure 6.4a–c), linearly organized structures are observed. They can be attributed to actin cytoskeleton lying beneath cell membrane. Their organization is characterized by the presence of long bundles of filaments interspersed with much shorter ones. Interestingly, such aligned organization of fibres disappeared for cells derived from WM266-4 culture (Figures 6.4d–f). The surface of these cells was found to be very rough and decorated with numerous dorsal “ruffles” or “ridges”. These ridges appeared to be flexible as they were easy to displace in the direction of scan. Similar structures have also been described for other cells, such as skin fibroblasts and liver endothelial cells [21].

The literature data published so far enables to attribute the observed filamentous structures to F-actin filaments [21, 22]. However, the direct proof of their presence can be derived by using a fluorescence microscope integrated with AFM one. The results of such combination are presented in the Figures 6.5 and 6.6 for WM115 and WM266-4 melanoma cells, correspondingly. To visualize the morphological organization of F-actin filaments and to identify F-actin, the AFM topography images were recorded together with epi-fluorescence ones, using the AFM integrated with inverted optical microscope equipped with fluorescence functionality (available at the JKU, Linz). Here, melanoma cells were stained with rhodamine-phalloidin dye, which specifically binds to actin filaments. First, fluorescent images of F-actin were recorded, followed by AFM surface topography images (Figures 6.5 and 6.6).

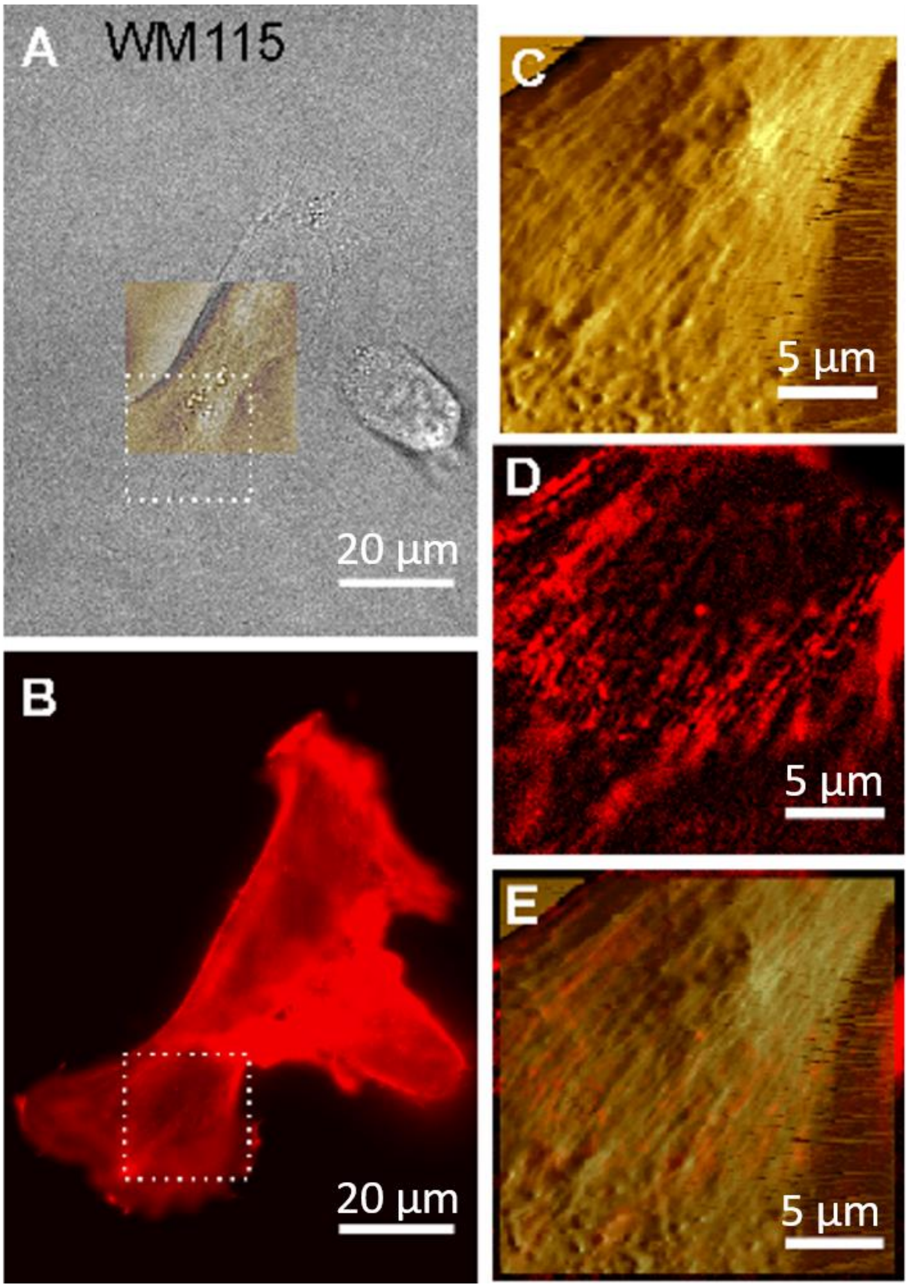

Figure 6.5. *A) Overlay of optical image with AFM image. B) Fluorescent image of fixed WM115 cell C) AFM topography image of WM115 cell in the selected area. D) Fluorescent image in the selected area. E) Overlay of fluorescent image with AFM image. (image adapted from Gostek et al. European Biophysics Journal 44 (2015) 49-55).*

AFM images (Figure 6.5c) and Figure 6.6c') show two distinct organizations of actin in WM115 and WM266-4 cells, respectively. This was verified with fluorescence microscopy showing linear structures composed of F-actin in WM115 cells (Figure 6.5d) and disordered filaments in WM266-4 ones (Figure 6.6d').

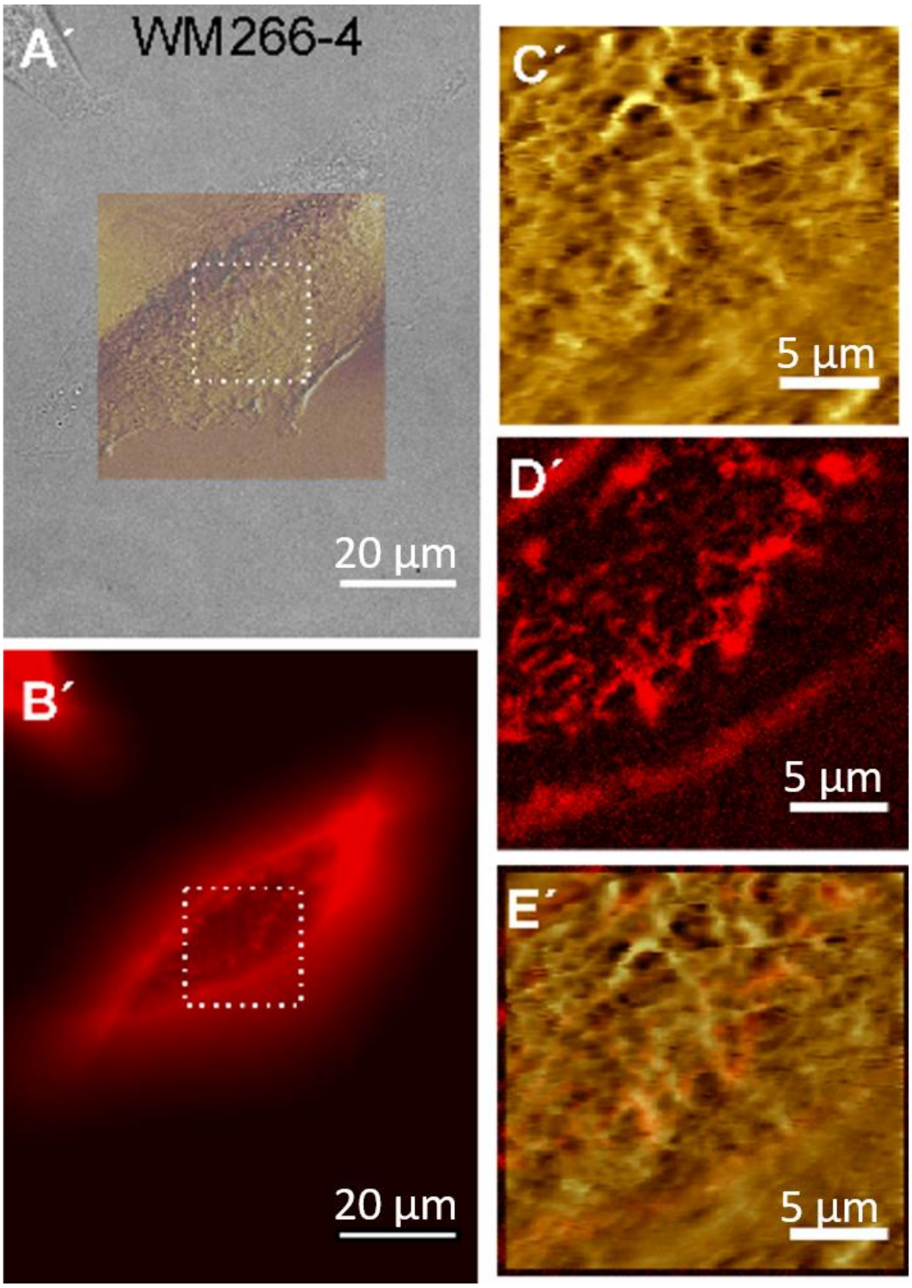

Figure 6.6. *A) Overlay of optical image with AFM image. B) Fluorescent image of fixed WM115 cell C) AFM topography image of WM115 cell in the selected area. D) Fluorescent image in the selected area. E) Overlay of fluorescent image with AFM image. (image adapted from Gostek et al. European Biophysics Journal 44 (2015) 49-55).*

The observed surface structures were properly attributed to the actin filaments and flexible ridges composed of membrane cortex. Based on these results, it has been postulated that distinct organization of F-actin in WM115 and WM266-4 melanoma cells is also reflected in various mechanical properties of these cells.

6.4 Nano-mechanical properties of melanoma cells

The images of surface topography recorded for both studied cell lines have shown different cytoskeletal organization. Knowing from literature [94,115–118] that alterations in cellular elasticity measured by AFM can be directly correlated with actin filament organization within a cell, the nanomechanical characterization of melanoma cells from VGP progression stage and skin metastasis has been performed aiming at quantitative description of the observed cell surface changes through the Young's modulus (detailed methodology is described in the *Methods* chapter). During the indentation into the cell, the AFM tip meets a variety of structures whose mechanical response can be different. Thus, the first structure is a glycocalix attached to the surface of cell membrane on the extracellular side, then, AFM probe indents the cortex built of a network of actin filaments and, finally, feels deeper parts of the cell filled with cytosol and various organelles. Thus, the smaller indentation depths reflect the mechanical response dominated by cell membrane tension and superficial layers of F-actin filaments. Deeper indentations provide information about the contribution of distinct cellular organelles like, for example, cell nucleus. Therefore, the Young's modulus calculated from elasticity measurements is an indentation depth-dependent function [24].

The elastic properties of the studied melanoma cells (WM115 and WM266-4) were calculated for three indentation depths, i.e. 50 nm characterized by dominant role of glycocalix and cell membrane (Figure 6.7), 200 nm revealing strong mechanical response originating from actin cytoskeleton (Figure 6.8), and 500 nm delivering the overall elasticity of a single cell (Figure 6.9).

For the smallest considered indentation depth equal to 50 nm (Figure 6.7), the Young's modulus value shows large variations attributed to the presence of distinct superficial structures present both on external part of cell membrane (like glycocalix) or just beneath cell membrane (like short actin filaments). Thus, the mechanical response to indenting AFM probe represents effective elasticity of all these structures, however, most probably with dominating contribution originating from cell membrane tension. The similar values of the Young's modulus obtained for WM115 and WM266-4 cells are independent of cellular density. These values reflect the properties of the same materials, i.e. mostly cell membrane that is composed of the same types of molecules in both cell lines.

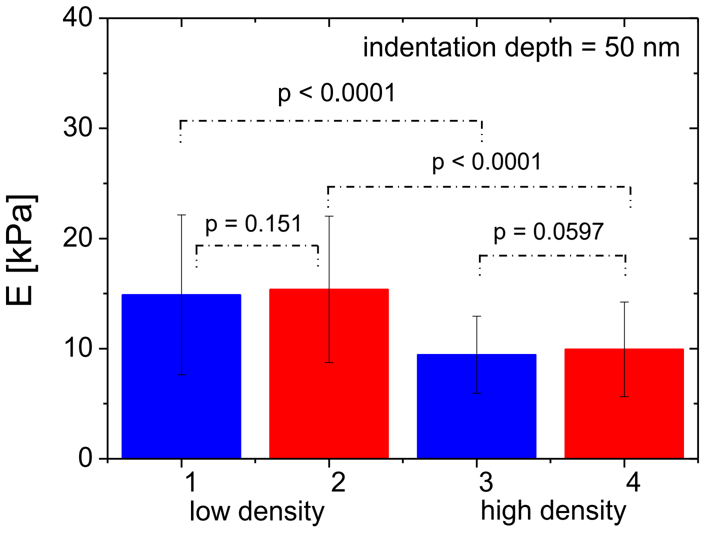

Figure 6.7. *The Young's modulus, presented as a mean ± standard deviation, determined for melanoma cells cultured at low and high cellular density. The modulus was calculated for the indentation depth of 50 nm. WM115 cells – blue bar, WM266-4 cells – red bar. Statistical difference was obtained by using Student's t-test (image adapted from Gostek et al. European Biophysics Journal 44 (2015) 49-55).*

The superficial layer of the cell has also a small contribution of F-actin filaments that in both studied cell types also have similar mechanical properties. The significant difference was observed between cells cultured at low and high density. The corresponding fluorescent images are presented in Figure 6.1. One could expect, that in such a case the modulus value should increase as density of cells increases, especially, as single cell spreading area decreases denoting larger cellular packing. This could be a case for cells with highly developed cytoskeleton with thick and clearly visible actin stress fibres. However, in the studied melanoma cells, the actin cytoskeleton is poorly differentiated, thus, dense packing exposes soft cell membrane to exterior. The indenting AFM probe, most probably, meets the accumulation of soft cell membrane. Lower elastic modulus observed for high density cultures indicates that such an accumulation of soft cellular membrane is not negligible in mechanical response, independently of the indentation depths.

For larger indentation depth of 200 nm, significant differences in cellular deformability are observed for melanoma cells cultured at low cellular density, while denser growth manifests in the same modulus values for both studied melanoma cells (Figures 6.8).

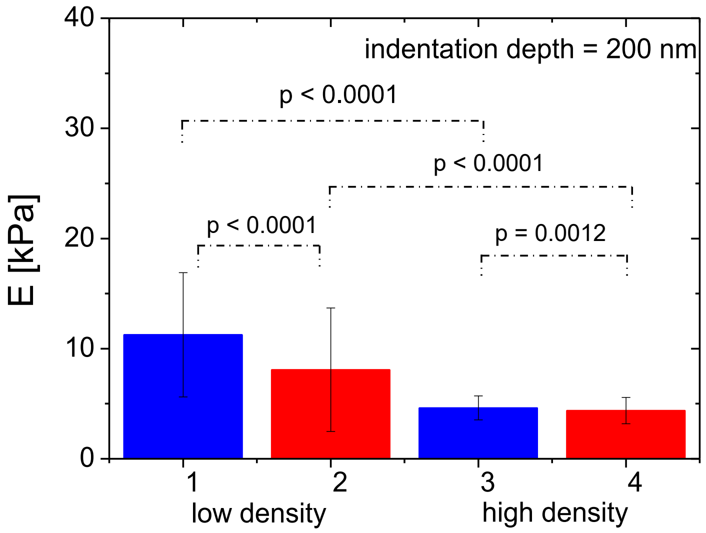

Figure 6.8. *The Young's modulus values, presented as a mean ± standard deviation of the cell population, obtained for living melanoma cells grown at low and high density. WM115 cells – blue bar, WM266-4 cells – red bar. Results for indentation depth of 200 nm. Statistical difference tested using Student's t-test (image adapted from Gostek et al. European Biophysics Journal 44 (2015) 49-55).*

The cellular elasticity at the indentation depths of 200 nm contains mainly contribution from actin cytoskeleton. The differences observed in cellular morphology and organization of actin filaments (Figure 6.1 a&b) agree with elasticity measurements (Figure 6.8), when single cells are studied. Increase in the cellular density manifests in a drop of the difference between WM115 and WM266-4 cells what was attributed to the presence of neighbouring cells. Further increase of the indentation depth delivers the mechanical response originating from various cellular structures inside the cell (Figure 6.9).

The obtained results of Young modulus at the indentation depth of 500 nm showed that WM115 cells were more rigid ($p < 0.0001$) as compared to WM266-4 cells regardless of cellular density. These values can be assigned to the overall elasticity of a cell. This agrees with already reported results showing larger deformability of cancerous cells in, for example, breast or prostate cancers [94]. The presence of flexible ridges in WM266-4 melanoma cells prevents the long actin filaments to be squeezed by the indenting AFM probe, resulting in lower value of Young's modulus. Smoother surface of WM115 cells allows easier access to F-actin filaments for the indenting AFM probe. Thus, at the same indentation depth and same cellular density, the WM155 cells appeared to be more rigid than WM266-4 ones.

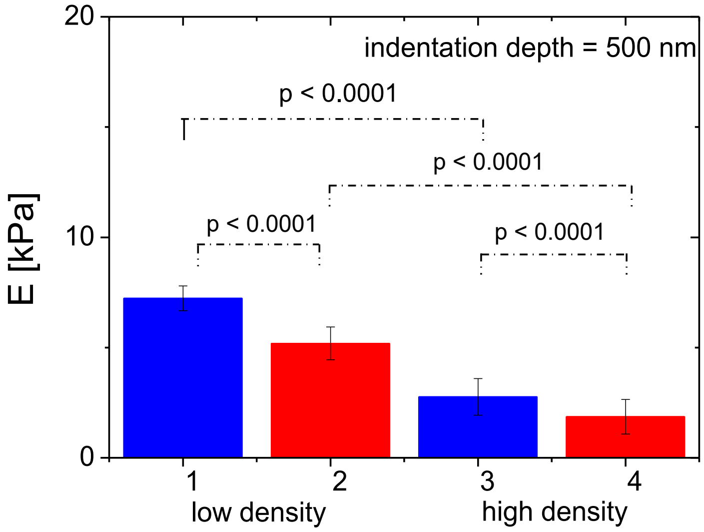

Figure 6.9. *The Young's modulus values, presented as a mean ± standard deviation of the cell population, obtained for living melanoma cells grown at low and high density. WM115 cells – blue bar, WM266-4 cells – red bar. Results for indentation depth of 500 nm. Statistical difference tested using Student's t-test (image adapted from Gostek et al. European Biophysics Journal 44 (2015) 49-55).*

The elasticity measurements, carried out for melanoma cells at low (Figure 6.1 a&b) and high (Figure 6.1 c&d) cellular densities, show systematically larger deformability of cells cultured in the presence of neighbouring cells (Figures 6.7 - 6.9) regardless of the indentation depth chosen for the analysis (50 nm, 200 nm or 500 nm). Most probably, this is linked with observed overlapping of cells as it has been shown in the Figure 6.1.

6.5 Summary

The analysis of cellular properties using data recorded by atomic force and fluorescence microscopes delivers the characteristics that enable to differentiate between various cell types. Such approach applied here to characterize two types of melanoma cells (WM115 cells from VGP progression stage and WM266-4 ones from skin metastasis) shows similar morphological characteristics for both studied cell types. They have spindle-like shape visible independently of the cellular density (Figure 6.1) as observed in fluorescent images. The surface topography recorded by AFM shows well organized actin filaments in VGP WM115 melanoma cells and their disorganization in WM266-4 cells from skin metastasis. The surface area occupied by single cells is larger in the case of WM115 melanoma cells as compared to WM266-4 cells. The alterations of nucleus surface area are not significant between these two cell lines (Table 6.1). For the studied melanoma cells, the obtained N/C ratio reaches values close to ~0.2 and it rather describes conditions suitable for cell spreading than the differentiation between melanoma cells from VGP and metastatic stages of melanoma progression. The considerable differences between WM115 and WM266-4 cells are accompanied by differences observed using AFM. The surface topography images show that the cytoskeletal network of WM115 cells is better organized, showing cortical filamentous structure (Figure 6.3) whereas WM266-4 cells are rougher with the presence of characteristic flexible ridges or ruffles (Figure 6.3). The obtained results show also that larger deformability of metastatic WM266-4 melanoma cells correlates with the presence of flexible ridges. Because the ridges (or ruffles) were constantly detected only in WM266-4 cells, it can be assumed that their presence might be associated with the melanoma progression. The elasticity measurements show larger deformability of metastatic WM266-4 melanoma cells that correlates with the presence of flexible ridges.

The combination of fluorescent and atomic force microscopes allows to characterize the surface properties of melanoma cells originating from two stages of cancer progression i.e. vertical growth phase and metastasis to skin. Single melanoma cells can be clearly identified by both, namely, detailed images of their surface at nm scale and by their nano-mechanical properties. The alterations observed on cell surface suggest strongly altered patterns of surface molecules that can be translated into distinct surface chemistry.

7. Surface chemistry in melanoma cells from VGP (WM115) and skin metastasis (WM266-4).

7.1 Objectives

The WM115 and WM266-4 melanoma cells have similar morphology observed under an optical microscope but, as it was reported in the *Chapter 6*, they slightly differ in mechanical properties and cellular surface characteristics at the nanoscale level. Thus, the main objective of these studies was to verify whether the observed morphological and mechanical changes are accompanied by distinct surface chemistry. To investigate the surface chemical properties of WM115 and WM266-4 melanoma cells, time-of-flight secondary ion mass spectrometry (ToF SIMS) and photothermal microspectroscopy (PTMS) were employed. Simultaneously, since both techniques deliver information on chemical composition of the sample surface, analogous results can be treated as a verification of the proposed methodology of sample preparation and data analysis procedure. The strong complexity of recorded mass and photothermal spectra requires the principal component analysis (PCA) to be applied to detect spectral signatures that can be used further for the cells' differentiation.

7.2 PCA of mass spectra recorded for WM115 and WM266-4 melanoma cells

Mass spectra of melanoma cells (WM115 and WM266-4) and accompanying reference sample (i.e. a silicon substrate) were acquired as described in the *Methods* chapter. Spectra were collected in the mass range 0-500 Da using Bi_3^+ primary ion beam. Typical mass spectra of positive ions recorded for melanoma cells and reference silicon surface are presented in Figure 7.1.

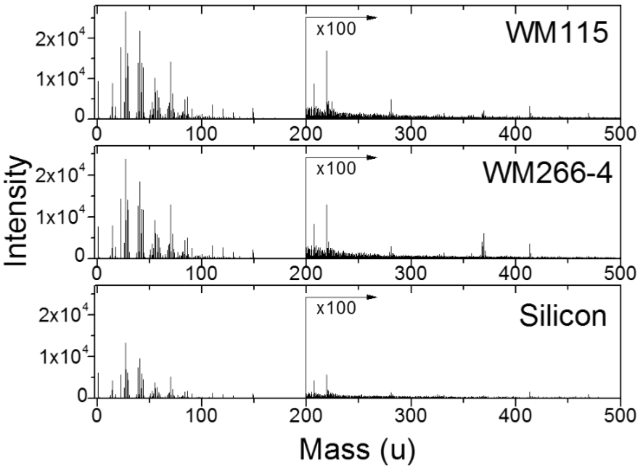

Figure 7.1. *Exemplary positive mass spectra acquired for melanoma cells and silicon substrate reference, in the range 0-500 Da, using* Bi_3^+ *primary ion beam.*

Within the recorded mass range of 1–500 Da, the mass spectra reveal a large degree of complexity manifested in a large number of peaks with various intensities. Since cells are built up from the same components, the only expected difference lies in changes in intensities of the detected molecular masses. As the bombarding primary ions hit the superficial layers of the cell surface, they most probably cause fragmentation of lipids from the cell membrane together with embedded proteins and glycans i.e. carbohydrate moieties covalently attached either to proteins or to lipids. Since the bombarded cell surface area is smaller than the overall bombarded surface area, one can also expect molecular fragments originating from culture medium components deposited on silicon surface. Thus, the measurements of cells were recorded together with the reference sample, i.e. a silicon surface that was used as a substrate for cells. This silicon substrate (without cells) underwent the same treatment as silicon substrates with growing cells, i.e. they were incubated in the RPMI-1640 medium for the 48 hours and followed the same dehydrating and drying protocol as described in the *Materials*.

To resolve whether it is possible to detect differences between the studied melanoma cell lines (WM115 versus WM266-4 ones), PCA was used to analyse mass spectra (according to the protocol presented in *Methods*; autoscaling was applied as a pre-processing method). The percentages of the total variance, accounting for the variability explained by each orthogonal principal component, are as follows: PC1 = 43.12%, PC2 = 25.17%, and PC3 = 9.30%. The relation between principal components and an original variable (mass of secondary ions) is presented in the loadings plot (Figure 7.2).

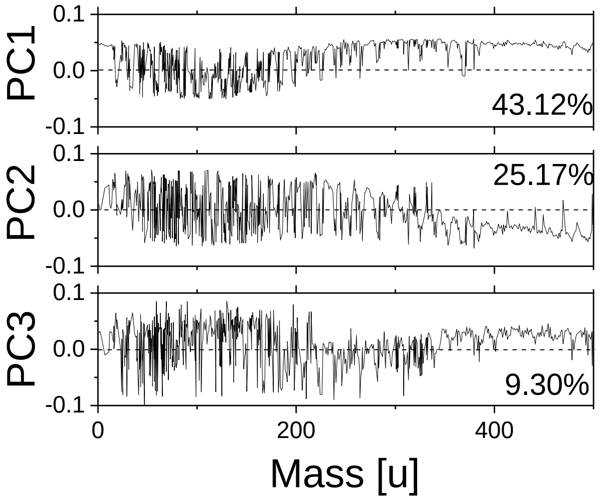

***Figure 7.2.** Loadings plot for PC1, PC2 and PC3 components resulted from PCA of ToF SIMS spectra acquired for the studied melanoma cells, autoscaling was used as a pre-processing method.*

Despite the large variance percentage for PC1 (43.12%), the PCA shows the strongest differentiation between VGP (WM115) and metastatic (WM266-4) melanoma cells for PC3 and PC2 components (Figure 7.3). In Figure 7.3, each dot corresponds to one mass spectrum recorded for each sample type. To statistically quantify the separation between data sets obtained for melanoma cells, confidence ellipses are calculated at the confidence levels of the 90%, 95%, and 99%.

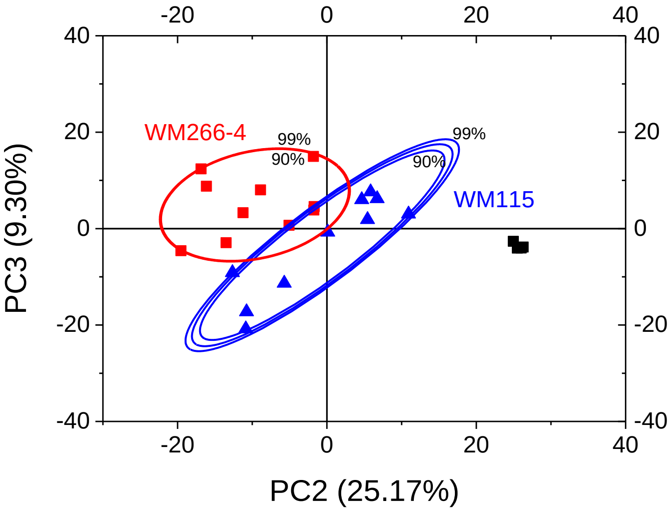

***Figure 7.3.** Scores plot for PC3 versus PC2 resulted from PCA of ToF SIMS spectra acquired for the studied melanoma cells together with confidence ellipses calculated at the 90%, 95%, and 99% confidence levels.*

From the figure 7.3, one can see that for WM115 melanoma cells (VGP cells), the PC3 component has revealed both, positive or negative values, present in almost equal contributions (5/10 versus 4/10, respectively). The negative PC2 values are accompanied by negative PC3, while positive PC2 corresponded to positive PC3. For cells derived from skin metastasis (WM266-4), positive PC3 values are observed in excess (8/10) and they are accompanied by negative PC2 values. To find which molecular masses are responsible for the separation between the WM115 and WM266-4 melanoma cells, standard deviations (*SD*) of PC2 and PC3 components were calculated using loadings plots (Figure 7.2). The obtained values were SD_{PC2} = 0.03758 and SD_{PC3} = 0.03612 for PC2 and PC3, respectively. Combining standard deviations with PC2–PC3 scores plot the selection criteria are defined in a following manner (Figure 7.4).

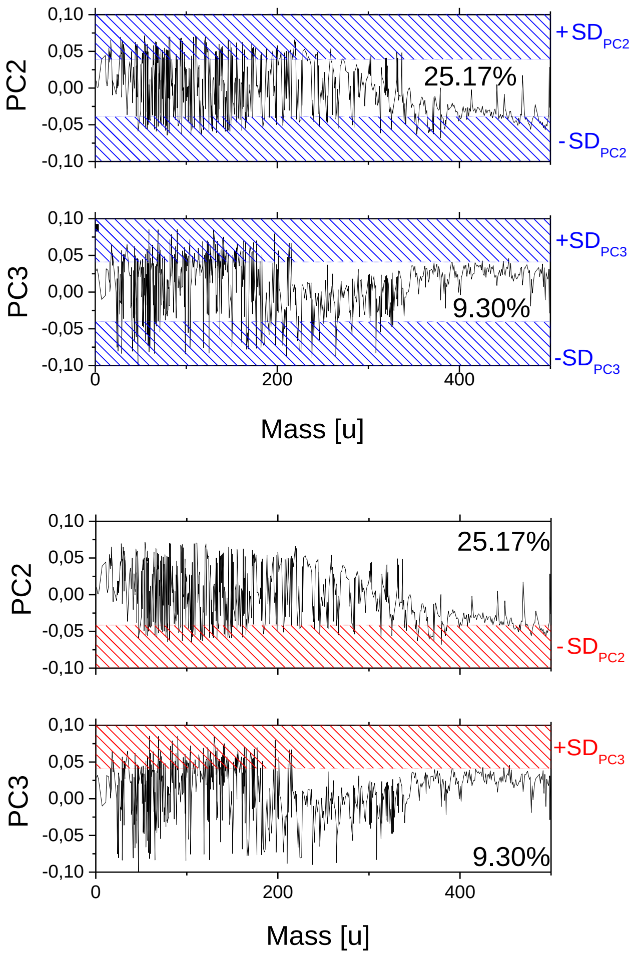

a)

b)

Figure 7.4. *Graphical representation of selection criteria based on standard deviations of PC2 and PC3 used to determine molecular masses that contribute strongly to the separation of melanoma cells present in the recorded mass spectra of a) VGP WM115 cells (blue area), and b) WM266-4 cells (metastasis to skin, red area).*

The mass spectra recorded for VGP WM115 melanoma cells are placed either in the 1st quadrant (both PCs values positive) or in 3rd quadrant (both PCs values negative). To select the masses present on a surface of WM115 cells that contribute strongly to data separation, all molecular masses fulfilling simultaneously the following conditions were chosen (Figure 7.4a):

$$PC3 > +SD_{PC3} \quad \text{and} \quad PC2 > +SD_{PC2}$$

$$\text{or } PC3 < -SD_{PC3} \quad \text{and} \quad PC2 < -SD_{PC2}$$

Mass spectra of cells originating from skin metastasis (WM266-4 cells) are mainly located in the 4th quarter of the PC3–PC2 plot (Figure 7.3). Most of PC3 values were positive whereas PC2 ones were negative. Thus, to select masses present on a surface of WM266-4 cells dominating in melanoma cell selection, the following criteria were defined (Figure 7.4b):

$$PC3 > +SD_{PC3} \quad \text{and} \quad PC2 < -SD_{PC2}$$

The fulfilment of the above defined criteria indicates the masses that most strongly affect melanoma cell separation in PCA (Table 7.1).

Table 7.1. *Summary of molecular masses that separate the studied melanoma cells, observed in the PC3–PC2 plot, found using the selection criteria defined based on the analysis of PCs standard deviations.*

Mass [Da]	Chemical formula	Proposed structure	Mass [Da]	Chemical formula	Proposed structure
16,02	NH_2^+		123,06	$C_6H_7N_2O^+$	
17,03	NH_3^+		125,00	$Si_3C_3H_5N_2^+$	Si substrate
18,04	NH_4^+		126,09	$C_7H_{12}NO^+$	
30,04	CH_4N^+	Glycine	135,07	$C_5H_{11}O_4^+$	
31,04	CH_5N^+		137,07	$C_2H_{11}SN_5^+$	
32,05	CH_6N^+		142,94	$Na_2SO_4H^+$	**adsorbed medium**
40,02	$C_2H_2N^+$		146,06	$C_7H_6N_4^+$	
44,01	$C_2H_6N^+$	Alanine	150,08	$C_5H_{13}NPO_2^+$	Phosphocholine
46,03	CH_4NO^+		155,09	$C_{12}H_{11}^+$	Fatty acid-lipid tail
52,02	CH_3NNa^+		155,15	$C_{10}H_{19}O^+$	Fatty acid-lipid head
53,04	$C_4H_5^+$		157,08	$C_{11}H_{19}O^+$	Fatty acid-lipid head
55,02	$C_3H_3O^+$		159,10	$C_{10}H_{11}N_2^+$	Tryptophan
55,05	$C_4H_7^+$		164,92	$Na_3SO_4^+$	**adsorbed medium**
57,02	$SiC_2H_5^+$	Si substrate	166,08	$C_5H_{13}NPO_3^+$	Phosphocholine

Table 7.1 cd. *Summary of molecular masses that separate the studied melanoma cells, observed in the PC3–PC2 plot, found using the selection criteria defined based on the analysis of PCs standard deviations.*

Mass [Da]	Chemical formula	Proposed structure	Mass [Da]	Chemical formula	Proposed structure
57,05	$C_3H_7N^+$		168,08	$C_{12}H_{10}N^+$	
57,07	$C_4H_9^+$		172,08	$C_{12}H_{12}O^+$	Fatty acid-lipid head
58,03	$C_2H_4NO^+$		173,10	$C_{12}H_{13}O^+$	Fatty acid-lipid head
58,06	$C_3H_8N^+$	Phosphocholine	174,10	$C_{12}H_{14}O^+$	Fatty acid-lipid head
59,07	$C_3H_9N^+$	Phosphocholine	184,10	$C_5H_{15}NPO_4^+$	Phosphocholine
60,08	$C_3H_{10}N^+$	Phosphocholine	185,10	$C_{13}H_{13}O^+$	Fatty acid-lipid head
61,01	$C_2H_5S^+$	Methionine	186,09	$C_9H_{14}O_4^+$	
65,04	$C_5H_5^+$		195,10	$C_{13}H_{11}N_2^+$	
66,04	$C_5H_6^+$		198,10	$C_6H_{17}NPO_4^+$	Phosphocholine
67,04	$C_4H_5N^+$		199,11	$C_{14}H_{15}O^+$	Fatty acid-lipid head
67,05	$C_5H_7^+$		206,09	$C_5H_{14}NPO_4Na^+$	Phosphocholine
69,07	$C_4H_5O^+$	Threonine	215,12	$C_{11}H_{19}O_4^+$	
71,01	$C_3H_3O_2^+$	Serine	224,11	$C_8H_{19}NPO_4^+$	Phosphocholine
71,98	$CSN2^+$		225,12	$C_{12}H_{17}O_4^+$	
77,00	C_5HO^+		226,11	$C_{12}H_{18}O_4^+$	
87,95	$FeNOH_2$		240,13	$C_{19}H_{12}^+$	Fatty acid-lipid tail
87,97	$SiN_2O_2^+$	Si substrate	246,11	$C_8H_{18}NPONa^+$	Phosphocholine
90,04	$C_3H_8SN^+$		255,13	$C_{13}H_{19}O_5^+$	
98,02	$C_4H_4NO^+$	Asparagine	264,26	$C_{19}H_{36}^+$	Fatty acid-lipid tail
98,98	C_3HSNO^+		281,10	$C_{12}H_{18}O_6Na^+$	**adsorbed medium**
102,09	$C_5H_{12}NO^+$		282,14	$C_{21}H_{30}^+$	Fatty acid-lipid tail
104,11	$C_5H_{14}N^+$	Phosphocholine	313,27	$C_{19}H_{37}O_3^+$	phospholipid
107,05	$C_7H_7O^+$	Tyrosine	410,21	$C_{19}H_{31}O_8Na^+$	**adsorbed medium**
108,94	$Si_3C_2H^+$	Si substrate	448,22	$C_{26}H_{49}O_3K^+$	**adsorbed medium**
120,08	$C_8H_{10}N^+$	Phenyloalanine	454,22	$C_{21}H_{35}O_9Na^+$	**adsorbed medium**
122,06	$C_3H_8NO_2S^+$	cysteine	474,23	$C_{29}H_{46}O_5^+$	

As mass spectra were collected from squared regions with single cells inside, the secondary ions originate mainly from two sources:

(1) silicon surface covered with deposited culture medium components and also cellular debris, and

(2) from cell surface.

The presence of fragments such as $Si_3C_2H^+$ at 57.02 Da; $SiN_2O_2^+$ at 87.97 Da; $Si_3C_2H^+$ at 108.94 Da; $Si_3C_2H^+$ at 108.94 Da and $Si_3C_3H_5N_2^+$ at 125.00 Da are strongly linked with the deposition of small cellular debris and culture medium components. The thickness of the layer is small enough to emit silicon-contained fragment from the underlying substrate. Fragments containing sodium ions detected at molecular masses of 142.94 Da, 164.92 Da, 206.09 Da, 246.11 Da, 281.10 Da, 410.21 Da, 448.22 Da, and 454.22 Da probably indicate the sodium atoms deposited from the medium on a cell surface. They can be attached, for example, specifically to proteins forming sodium channels or non-specifically through electrostatic interactions to various components of cell membrane. These molecules can be also both, protonated and sodiated [119]. These sodium containing molecular masses were also observed in the mass spectra of the reference silicon sample. However, the substrate effect seems to be negligible since the mass spectra recorded for reference silicon surface treated in the same way as silicon substrates with cells, have much smaller intensity and also they are grouped in one place (Figure 7.3). The distribution of the data is very narrow indicating homogenous surface properties, thereby denoting uniform deposition of culture media components. That is why it can be assumed, that the observed data separation originates from intrinsic properties of two studied melanoma cell lines. The detected secondary ions can be most probably attributed to molecules present on a cell surface, like lipids or proteins, as ToF SIMS working in the static conditions provides the information from the outermost layers. Molecular masses of some ions have been already identified based on literature data [71–76,120]. Part of them can be assigned to amino acids coming from proteins anchored or deposited on a surface of cell membrane. Many observed intensity maxima correspond to fragments composed of hydrocarbon chains present in lipids forming the bilayer. Several masses can be attributed to phosphocholine, based on literature data [119,121]. Phosphocholine is a head group of phosphatidylcholine or a part of sphingomyelin, both constituting the lipid fraction of cellular membranes.

7.3 Differentiation of melanoma cell lines based on photothermal spectra (PTMS)

Photothermal microspectroscopy[6] absorption spectra deliver information about the chemical status of a sample exposed to the infrared (IR) beam modulated by the Michelson

---

[6] The photothermal microspectroscopy experiments were performed using a PTMS device located at the School of Pharmacy at the East Anglia University in Norwich (UK). Measurements were carried out by Dr Jonathan Moffat on samples that were prepared at the IFJ PAN. Measurements were carried out within the frame of EU FP7 project SMW „Single

interferometer. The absorption of IR energy causes vibrations and subsequent relaxation of molecular bonds that release heat detected by a thermal sensing probe, which is further converted into absorption spectra similar to those found in conventional IR spectroscopy (Figure 7.5). The photothermal spectra can be used to verify the results obtained based on ToF SIMS experiments. To minimize the effect of the substrate, the IR beam was focused on the sample prepared in a form of "a ball" (as described in *Materials and Methods*). Importantly, no substrate was applied in the whole experiments, thus, the resulting photothermal response shows stretching and bending of bonds characteristic for specific molecules present in cells only. As it was expected, the photothermal absorption spectra recorded by PTMS revealed complex characteristics, showing very similar shape but varying by the intensities of the absorption maxima (Figure 7.5). The spectra were recorded within the range of 500 cm^{-1} to 4000 cm^{-1}, encompassing the range characteristic for lipids (2800 – 3000 cm^{-1}), DNA/RNA (1000 cm^{-1} –1250 cm^{-1}) and proteins (1600 – 1700 cm^{-1}; 1500 – 1560 cm^{-1}; amide I and amide II regions, respectively).

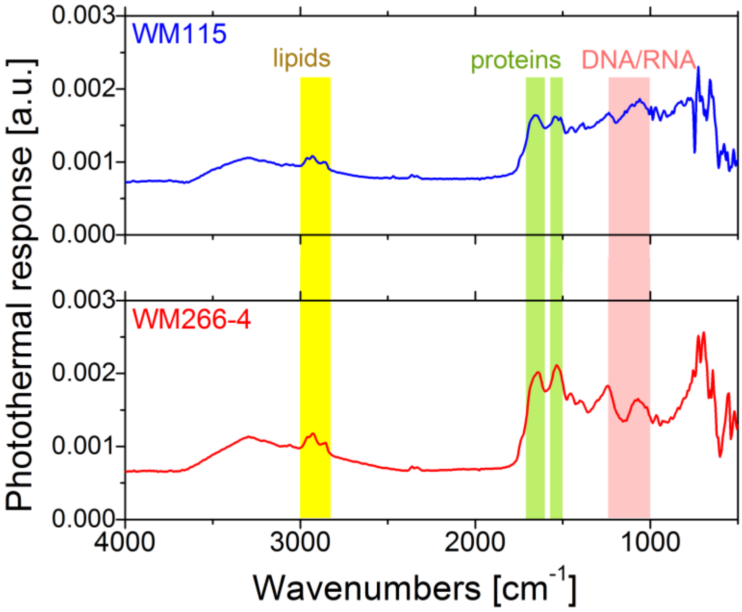

Figure 7.5. *Typical photothermal spectra recorded for WM115 (vertical growth phase) and WM266-4 (metastasis of WM115 to skin) melanoma cell lines.*

Molecule Workstation", no NMP4-SE-2008-213717, financed between 2008 – 2011. Thus, the recorded PTMS spectra are free from any subjective influence of the ToF SIMS experiments. **To performed blind verification of the ToF SIMS results, Justyna Bobrowska re-analysed raw data using the methodology proposed by her for analysing ToF SIMS mass spectra.**

To perform blind verification of the ToF SIMS results, raw PTMS spectra were analyzed using the approach proposed within the presented thesis, without *a priori* knowledge of the characteristic spectral ranges for both studied melanoma cell lines. The PCA calculations were the same as those applied for ToF SIMS mass spectra, as described in *Materials and Methods*. The percentages of the total variance, accounting for the variability explained by each orthogonal principal component, are as follows: PC1 = 53.65%, PC2 = 24.31%, and PC3 = 14.33%. The results of the PCA show analogous separation between PC2 and PC3 components (Figure 7.6).

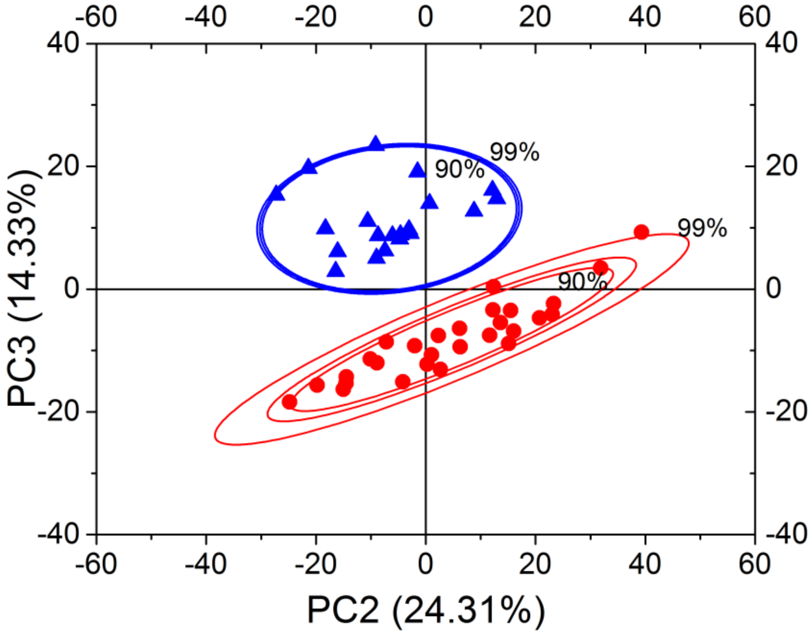

Figure 7.6. *PC3–PC2 scores plot obtained for PCA applied to photothermal spectra recorded for melanoma cells, plotted together with confidence ellipses calculated at 90%, 95%, and 99% confidence levels.*

The confidence ellipses calculated at 90%, 95%, and 99% confidence levels confirmed separation between the studied data sets for melanoma cells. This indicates that WM115 and WM266-4 melanoma cells have distinct chemical properties that can be attributed to melanoma progression. For VGP melanoma cells (WM115), the PC3 shows positive values only while for cells derived from skin metastasis (WM266-4) negative PC3 values are observed in excess (24/27). Similarly, as for ToF SIMS mass spectra, the criteria for the selection of spectral ranges contributing mostly to the melanoma cells separation are defined based on standard deviations for PC2 and PC3 using loadings plots (Figure 7.7).

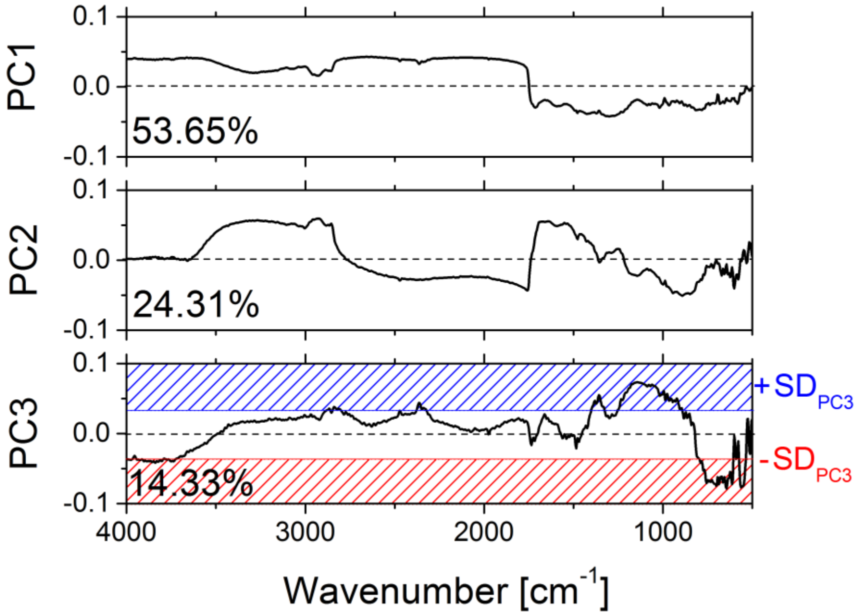

Figure 7.7. *Loadings values obtained for PC1, PC2, and PC3 in relation to the wavenumber, together with marked selection criteria used to find the spectral regions contributing mostly to melanoma cells separation on PC3-PC2 scores plot.*

The selection criteria are as follows:

$$PC3 > +SD_{PC3}$$

$$\text{or} \qquad PC3 < -SD_{PC3}$$

Spectral regions with values of PC3 loadings higher than $+SD_{PC3}$ (Figure 7.6, marked in blue) indicate stretching and bending of molecular bonds, characteristic for specific molecules present on a surface of WM115 melanoma cells. The spectral range where PC3 loadings is lower than $–SD_{PC3}$ (Figure 7.6, marked in red) corresponds to WM266-4 cells from skin metastasis. A summary is presented in Table 7.2.

Table 7.2. Summary of spectral range that separates the studied melanoma cells, observed in the PC3–PC2 plot, found using the selection criteria defined based on the analysis of PCs standard deviations.

Wavenumber region [cm^{-1}]	Vibrational mode types present in the detected spectral range
4000-3700	broad O–H and N–H stretching
2780–2890	2874 cm^{-1} – symmetric C–H stretching vibrations of CH_3 (lipids)
	2850 cm^{-1} – symmetric C–H stretching vibrations of CH_2 (lipids, choline, phospholipids)
2300–2380	CH stretch combinations
1320–1410	1397 cm^{-1} – symmetric stretching of COO^-
	1379 cm^{-1} – symmetric bending of CH_3 (proteins, lipids)
890–1260	1230 cm^{-1} – 1245 cm^{-1} – antisymmetric stretching of PO_2^- (DNA, RNA, phospholipids, phosphorylated proteins)
	1237 cm^{-1} – antisymmetric stretching of PO_2^- (phospholipids, proteins)
	1173 cm^{-1} – antisymmetric stretching of –CO–O–C (esters)
	1160 cm^{-1} – 1120 cm^{-1} – stretching of C–O (RNA ribose)
	1150 cm^{-1} – C–O stretching, C–O–H bending (carbohydrates, mucin)
	1083 cm^{-1} – symmetric stretching of PO_2^- (proteins, phospholipids, DNA)
	1078 cm^{-1} – symmetric stretching of C–C (glycogen)
	1063 cm^{-1} – symmetric stretching of –CO–O–C (phospholipids and cholesterol esters)
	1050 cm^{-1}; 1060 cm^{-1}; 1015 cm^{-1} – symmetric stretching of C–O (carbohydrates, mucin, DNA, RNA ribose)
	1050 cm^{-1} – stretching of C–O–P (phosphate ester)
	1028 cm^{-1} – deflection C–H–O (glycogen)
	968 cm^{-1} – stretching of C–O (DNA, phospholipids)
	950 cm^{-1} – stretching of P–O (phosphorylated proteins)
	920 cm^{-1} – stretching of C–O–P (phosphorylated proteins)
610–805	'*Fingerprint region*'
	730 cm^{-1}; 720 cm^{-1}; 718 cm^{-1} – CH_2 rocking (lipids)
	725 cm^{-1}– bending of N–H bending (amide bands of proteins)
	627 cm^{-1}– bending of O=C–N bending (amide bands of proteins)
	600 cm^{-1} – bending of C=O (amide bands of proteins)
530–570	'*Fingerprint region*'

Spectral ranges characteristic for each melanoma cell types, either WM115 or WM266-4 cells, are within the range of 530–570 cm^{-1}, 610–805 cm^{-1}, 890–1260 cm^{-1}, 1320–1410 cm^{-1}, 2300–2380 cm^{-1}, 2780–2890 cm^{-1} and 3700–4000 cm^{-1}. Most of the bands present within the selected ranges indicate phospholipids vibrations [122–129] to be dominating in PCA separation of melanoma cells (such as 1230 cm^{-1} – 1245 cm^{-1} – antisymmetric stretching of PO_2^-; 1237 cm^{-1} – antisymmetric stretching of PO_2^-; 1083 cm^{-1} – symmetric stretching of PO_2^- ; 1063 cm^{-1} – symmetric stretching of –CO–O–C; 968 cm^{-1} – stretching of C–O) [122,128,129]). Surprisingly, the proposed methodology of PCA indicated mostly the dominant alterations for lipids, not for proteins (there is no indication towards amide I or amide II regions), which is consistent with ToF SIMS data. It should be highlighted that in the photothermal measurements, a probing tip was immersed into a group composed of few tens, fixed but still wet, cells. In such a case, the response originated from lipids seemed to dominate due to lack of damage in cell membrane observed during sample drying.

7.4 Summary

Since the ToF SIMS data recorded for complex biological samples are difficult to be interpreted due to fragmentation phenomenon of large biomolecules [130], it is desirable to accompany such measurements with other experimental methods that also probe surface chemistry. One of such techniques is photothermal microspectroscopy that was employed to analyse chemical properties of the studied melanoma cell lines. PTMS combines the advantages of conventional FTIR with the high resolution of near-field sensors [96,131]. In comparison to conventional FTIR spectroscopy, the sample preparation in PTMS is less strict [132], thus, it seems to be good to compare results obtained at single cell level.

A huge complexity of mass and photothermal spectra observed for cells (Figures 7.1 & 7.5) disables the direct analysis and the exact value of a particular mass or wavelength is difficult to be determined. Thus, the PCA used for data reduction enhances the existing differences in original datasets of the investigated samples. In the presented thesis, a whole range of spectra, recorded for two melanoma cell lines (WM115 and WM266-4 ones) were analysed. These cells come from relatively close stages of cancer progression. The proposed methodology of PCA data treatment enabled to treat both types of spectra (mass and photothermal) in a blind way i.e. without choosing particular mass or wavelength in advance. In the PCA results presented in Figure 7.3 and Figure 7.6, the majority of spectra recorded for WM266-4 melanoma cells, originated from metastasis to skin, are grouped in the different quadrants of the coordinate system, using PC2 vs PC3 scores, as compared to spectra grouping for WM115 melanoma cells from vertical growth phase. The distribution of points in the PCA scores plots is not very homogenous, what can be influenced by different phases of the cell cycle, as these cells were not synchronized. Nevertheless, a distinct separation between primary melanoma and skin metastasis cell lines can be observed.

Based on PCA loadings plots (Figure 7.4 and Figure 7.7), the objective criteria for cellular data separation were defined and used to identify masses and wavelengths regions that differentiate these cells. By applying these criteria based on a variation of standard deviation (SD), maxima with the corresponding values of loadings were found in both types of spectra recorded for cells. In that manner, molecular masses and wavenumbers regions causing the strongest differentiation between the studied melanoma cell lines were identified.

Some of the molecular masses found can be attributed to surface presence of such amino acids as glycine, alanine, methionine, threonine, serine, asparagine and tryptophan. Furthermore, many masses can be assigned to fragments of phosphocholine being a structural component of both phospholipids and sphingomyelin in cellular membranes [119]. Such assignment seems to be highly probable and was confirmed by studies showing altered phospholipid composition in cancer cells [133]. Abnormal choline metabolism, overexpression of the choline kinase and phosphocholine accumulation are reported to be a common feature of breast, ovarian, lung and prostate cancers [134–136]. Also, sphingomyelin (having phosphocholine in its chemical structure) is differently expressed between cancerous and normal regions in the colon cancer liver metastasis [137]. The identified spectral ranges in photothermal spectra pointed to perturbations in DNA/RNA and lipids composition, surprisingly, not for proteins, despite the fact that closer analysis of amide I and amide II regions shows differences in the photothermal spectra. This suggests that alterations induced during cancer progression in proteins are less dominant as compared to those observed for lipids.

8. Physico-chemical properties of melanoma cells from various stages of cancer progression

8.1 Objectives

The main objective of the study was to evaluate whether there is a correlation between cellular deformability and the surface chemical properties in the studied melanoma cells. Thus, the main aim of the studies presented here is to demonstrate that combination of two techniques, atomic force microscopy (AFM) and time of flight secondary ions mass spectrometry (ToF SIMS) deliver complementary sets of data. To realize it, the mechanical and surface chemical properties of melanoma cell lines originating from various stages of melanoma progression were evaluated. The studied populations of cells originated from: *(i)* primary tumour sites WM35 (originally isolated from a patient's skin diagnosed with radial growth phase (RGP)), WM115 (derived from a 55 year old female skin melanoma at a vertical growth phase (VGP)) and WM793 (established from the vertical growth phase (VGP)); *(ii)* skin metastasis WM266-4 (established from a cutaneous skin metastasis detected in the same patient as WM115 cells) and WM239 (derived from a cutaneous skin metastasis); and *(iii)* lung metastasis 1205Lu (originated from a lung metastasis diagnosed in the same patient as WM793 cells) and A375P (derived from a solid malignant tumour located in the lung). The results were compared with those obtained for human melanocytes (HEMa-LP primary cell line).

8.2 Elasticity of melanoma cells

Analogously to studies performed for WM115 and WM266-4 melanoma cells presented in *Chapter 6,* as a first step, the mechanical properties of all melanoma cells were characterized using AFM. The elasticity of living cells was quantified by the Young's modulus value (Figure 8).

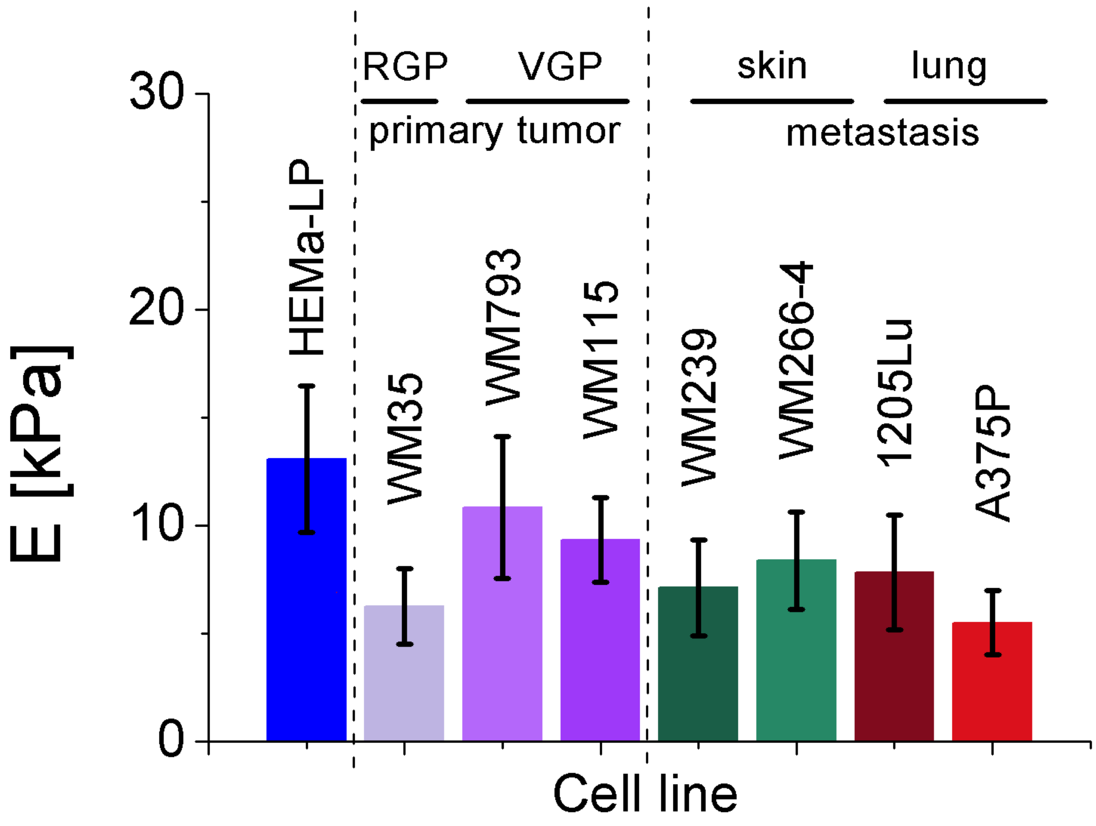

Figure 8.1. *The Young's modulus of melanocytes and melanoma cells, presented as a mean ± standard deviation calculated from more than 50 cells measured for each melanoma cell line*[7] *(RGP/VGP – radial/vertical growth phase).*

To compare elasticity values between cells, the Young's modulus was calculated for the indentation depth of 600 nm. The modulus determined for such a depth denotes the overall elastic properties of cells [138]. The obtained elasticity results showed that melanocytes (E = 13.08 ± 3.39 kPa) were more rigid, as compared to all melanoma cell lines, what agrees with the already reported results on cancer cells deformability [94,105,107,108]. Interestingly, melanoma WM35 cells, originated from radial growth phase (melanoma progression stage when cells do not form metastasis), were characterized by low elastic modulus, placing them in a deformability scale just before A375P cells, originating from lung metastasis. These RGP cells were more deformable, compared to cells originating from the vertical growth phase (next stage of melanoma progression), i.e. WM115 VGP and WM793 VGP ones. The moduli reached

---

[7] The AFM elasticity measurements were carried out as described in *Methods.* Statistics: for each melanoma cell lines more than 50 cells were measured. For each single cell one force curves map has been collected containing 36 to 64 force curves. This gives approximately 2000 force curves per each cell line to be analyzed.

values of 6.26 ± 1.76 kPa, 9.33 ± 1.96 kPa and 10.84 ± 3.30 kPa, for the A375P, WM115 and WM793 cell lines, respectively. Melanoma cells derived from the skin metastasis (i.e. WM266-4 and WM239, 8.38 ± 2.26 kPa and 7.12 ± 2.22 kPa, correspondingly) are characterized by lower values of the Young's modulus in comparison to the VGP melanomas, whereas those derived from lung metastasis were comparable or even more deformable (7.83 ± 2.67 kPa and 5.50 ± 1.50 kPa, for 1205Lu and A375P cells, respectively).

The statistical significance of the Young's modulus determined for the studied melanoma cells was verified by applying Student t-test. The test was performed at the significance of $\alpha = 0.05$ (Table 8.1).

Table 8.1. Student t-test comparison of the results present in the Figure 8.1 showing the Young's modulus of melanoma cells.

Cell type	HEMa-LP	WM35	WM793	WM115	WM239	WM266-4	1205Lu	A375P
HEMa-LP	ns	****	***	****	****	****	****	****
WM35		ns	****	****	*	****	***	*
WM793			ns	**	****	****	****	****
WM115				ns	****	*	**	****
WM239					ns	**	ns	****
WM266-4						ns	ns	****
1205Lu							ns	****
A375P								ns

**** $p < 0.0001$
*** $0.0001 < p < 0.001$
** $0.001 < p < 0.01$
* $0.01 < p < 0.1$
ns – not significant difference between cells' population

It is worth to highlight that among the studied cell lines, there are two pairs of cells that are derived from the same patients i.e. WM266-4 cells are the metastasis of WM115 cells to skin and 1205Lu are the metastasis of WM793 to lung. However, the Young's modulus of WM115 cells was not significantly different from WM266-4, whereas its value for WM793 cells was significantly different from the one for 1205Lu cells. This is linked with distinct structure of actin cytoskeleton responsible for cellular mechanical properties of these cells (Figure 8.2).

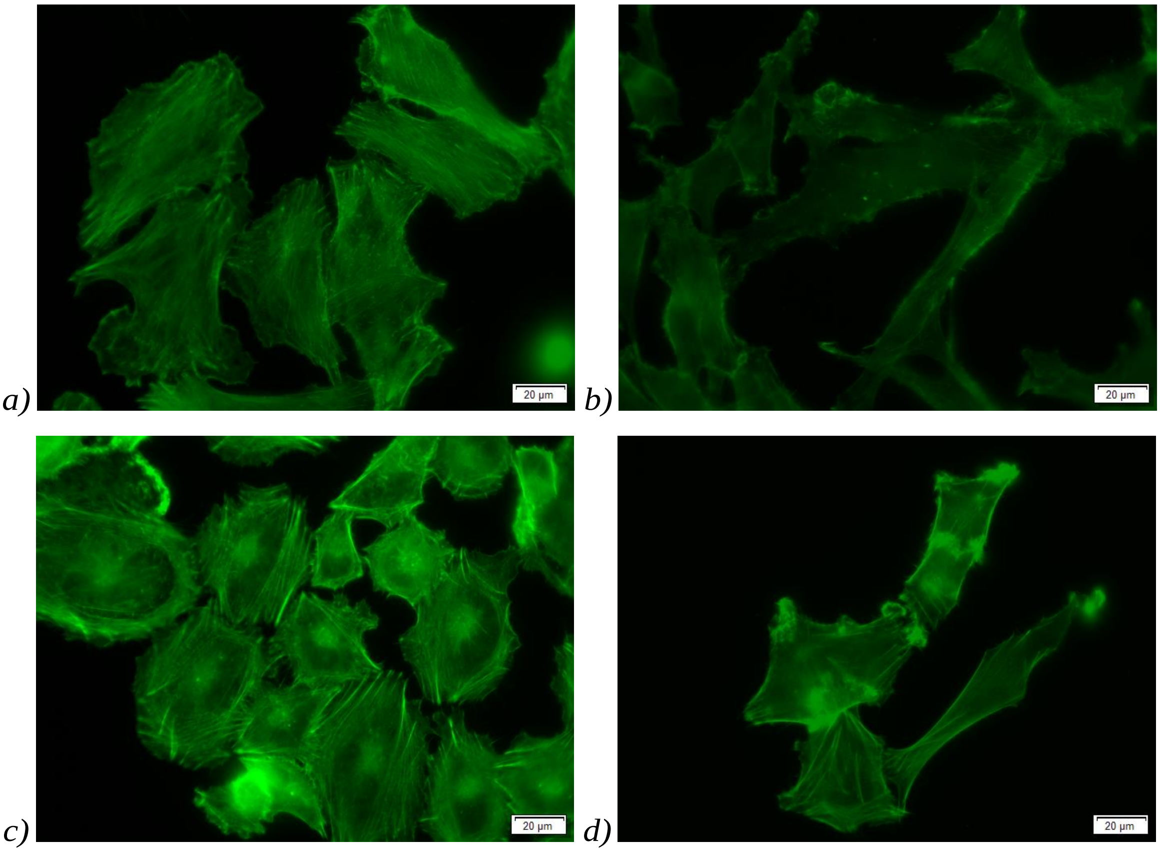

Figure 8.2. *The organization of actin cytoskeleton in two pairs of melanoma cell lines derived from the same patient: a) WM115, b) WM266-4, c) WM793 and d) 1205Lu.*

Distinct deformability of melanoma cells, measured within the indentation depths of 600 nm, indicated that changes related to melanoma progression can be linked with alterations in the structure of cellular surface. This has been already reported in studies showing distinct expression level of various surface receptors [139]. Thus, it is highly probable that the application of such techniques as ToF SIMS will enable to identify the chemical surface properties.

8.3 PCA of mass spectra for melanoma cells

Analogously as for WM115 and WM266-4 cells described in the *Chapter 7*, ToF SIMS mass spectra were recorded and analysed by applying PCA with autoscaling as the pre-processing method. The PCA analysis of all spectra together delivered the percentage of the total variance, accounting for the variability explained by each orthogonal principal component, are as follows: PC1 = 36.98%, PC2 = 20.29%, and PC3 = 11.59%. Despite the large variance percentage for PC1 (36.98%), the PCA shows the largest differentiation between melanoma cells for PC3 and PC2 components, similarly as for measurements carried out only for WM115 and WM266-4 cells (data included in earlier chapters of the thesis). Thus, similarly to previous studies, the PC scores plot of PC3 and PC2 components was considered here (Figure 8.3). In Figure 8.3, each dot corresponds to one mass spectrum recorded for each sample type.

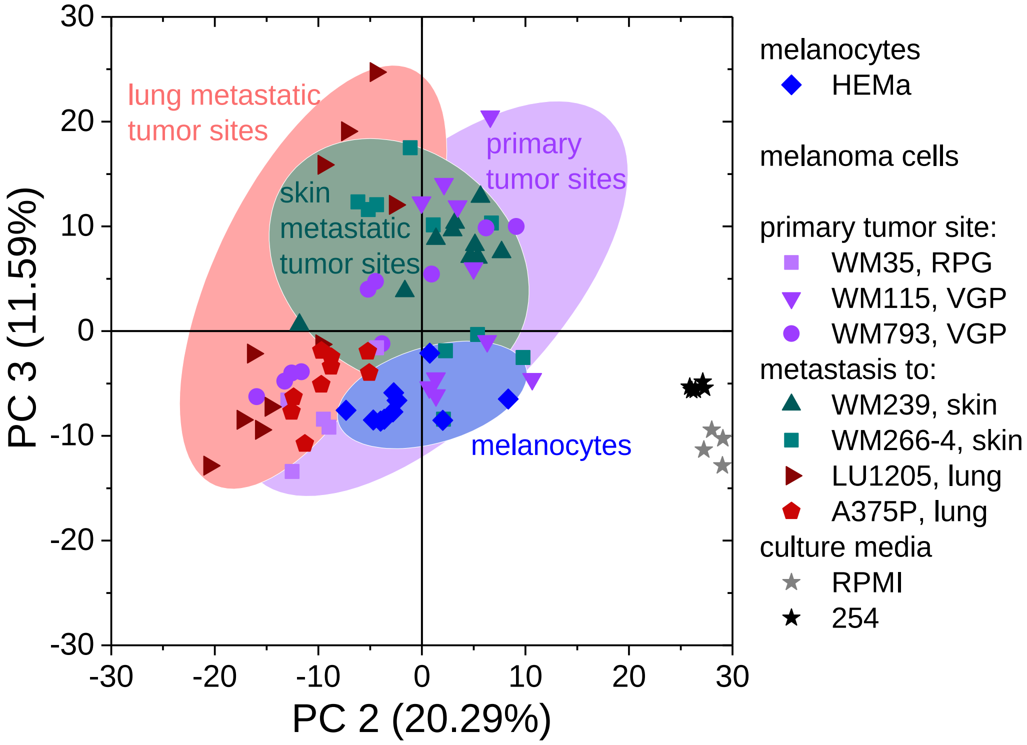

__Figure 8.3.__ Scores plot for PC3 versus PC2 resulted from PCA of ToF SIMS spectra acquired for all measured melanoma cells, melanocytes and reference silicon substrates treated with RPMI or 254 culture media.

For all studied melanoma cells, the data points in PC scores plot overlap, thus, the separation between the specific cell lines is not clearly visible. However, one can see a few general relations. The first one is that reference samples are grouped in significantly distinct place on the PCs scores plot (grey and black starts, for silicon surface in RPMI 1640 and 254 culture media, respectively) and that all recorded mass spectra form very narrow distributions, indicating similarities in emitted fragments of culture media components. The other relation is that melanoma cells originating from the similar stage of cancer progression group around similar types of cells. And thus, cells from skin metastasis form a separate group than cells from lung metastasis, while cells from primary tumour site span over a whole area in PCs score plot. Melanocytes form a separate group that can be relatively clearly distinguished from other cells. Simultaneously, the Figure 8.3 shows that in case of so many spectra, the analysis of the score plots is not an easy task. Thus, to resolve whether there are differences within the studied melanoma cells, the data were re-analysed according to their origin.

The melanoma pair of WM115 and WM266-4 ones, described in previous chapters, originates from the same patient. WM115 are the cells from VGP phase, while the WM266-4 are metastasis to skin. Among the studied melanoma cells, there is also another pair of cell lines that originates from one patient i.e. WM793 (VGP) and 1205Lu (metastasis to lung). The PCA of mass spectra acquired for the latter pair of melanoma cell lines and a reference silicon substrate delivers values of PC1 = 44.34%; PC2 = 30.55% and PC3 = 15.22% of total variance (Figure 8.4a). The scores plot obtained for this pair of cell lines delivered analogous separation between cells from VGP and metastatic sites as that observed for WM115 and WM266-4 pair (Figure 8.4b&d).

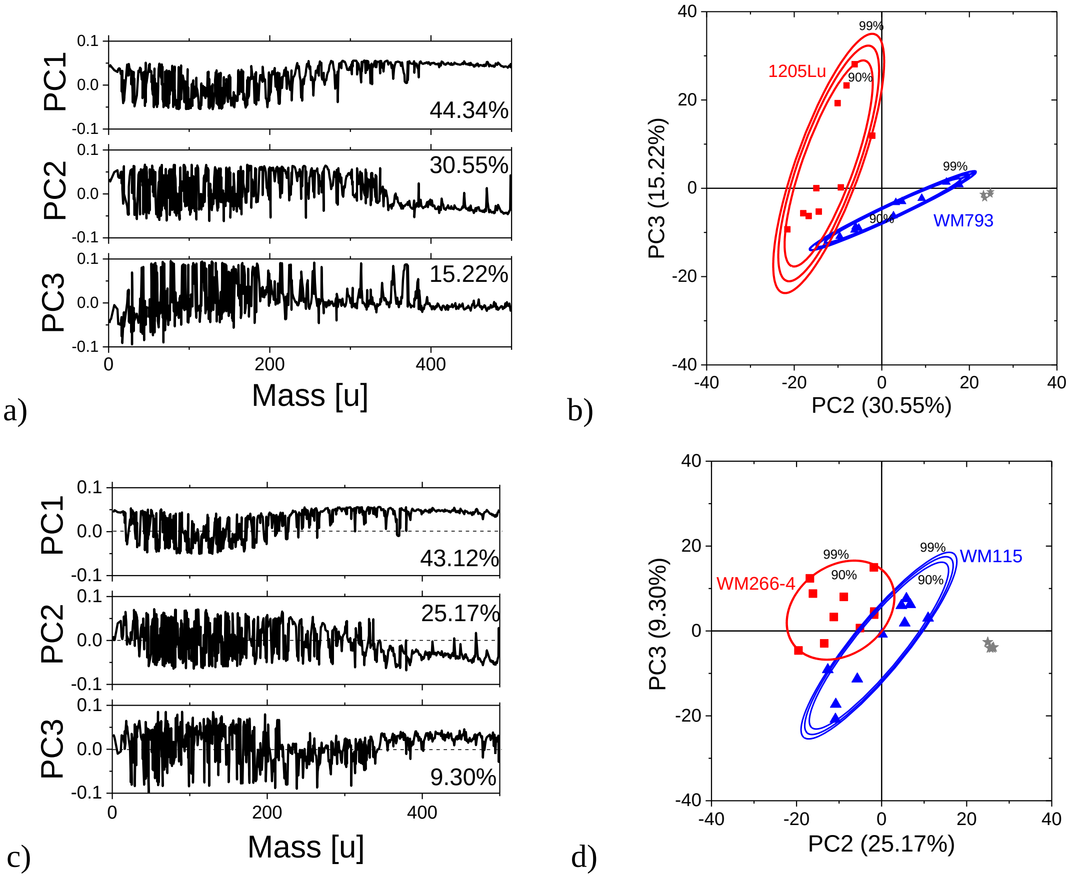

__Figure 8.4.__ Comparison of WM793 and 1205Lu melanoma cells. (a) Loadings plot for PC1, PC2 and PC3 components resulted from PCA of ToF SIMS spectra. (b) The corresponding scores plot for PC3 versus PC2. Black stars denote measurements carried out on reference silicon surface with deposited component of RPMI160 culture medium. The results are plotted together with confidence ellipses calculated at 90%, 95%, and 99% confidence levels. Analogous results obtained for similar melanoma cell pairs i.e. WM115 and WM266-4 ones (c&d, re-plotted loadings and scores plot from Chapter 7).

To quantify the separation between data sets for melanoma cells, confidence ellipses were calculated at the confidence levels of 90%, 95%, and 99%. The separation between PCA results observed for both pairs of melanoma cells was accompanied by differences in melanoma cell elasticity. For WM793 and 1205Lu better separation in scores plot corresponds to larger difference in the Young's modulus (10.84 ± 3.3 kPa versus 7.83 ± 2.67 kPa for WM793 and 1205Lu, respectively; $p < 0.0001$), while for WM115 and WM266-4 cells the difference in cellular deformability was much smaller (9.33 ± 1.96 kPa versus 8.38 ± 2.26 kPa, correspondingly; $p < 0.1$). These results may be correlated with the fact, that the metastasis to skin introduces lower alterations on cellular surface, compared to invasion to lung. Such a separation confirms that proposed approach using a whole mass spectra in PCA can distinguish between various cell populations.

The elasticity measurements show large differences between VGP cells (WM115 and WM793) and lung metastasis (1205Lu and A375P) at the level of $p < 0.0001$ (Table 8.1). To assess whether the PCA will result in data separation, mass spectra recorded for all these cell lines were analysed. The PCA outcome is presented in the Figure 8.5, showing loadings (Figure 8.5a) and PCs scores plot (Figure 8.5b). The confidence ellipses were calculated at the confidence levels of 90%, 95%, and 99%.

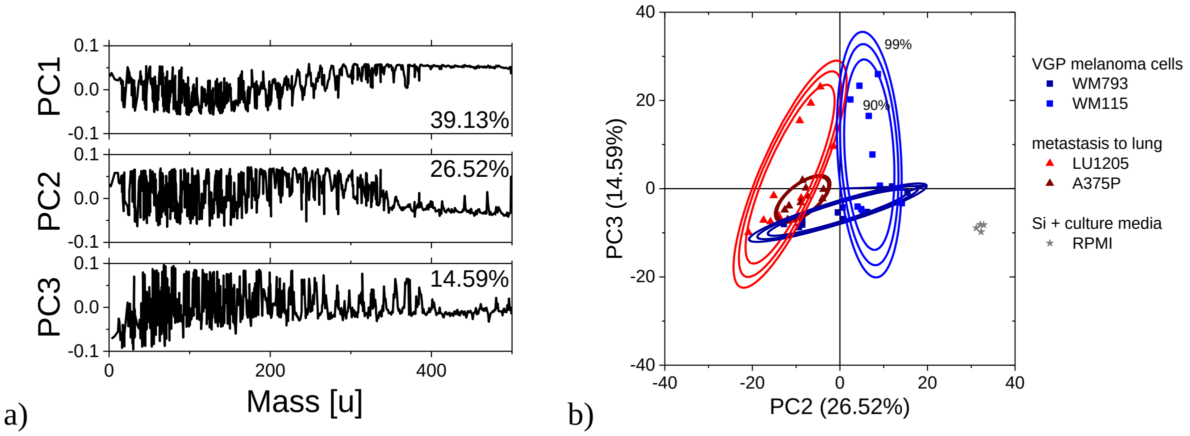

Figure 8.5. *Comparison of melanoma cells from VGP and metastatic sites in lung. (a) Loadings plot for PC1, PC2 and PC3 components resulted from PCA of ToF SIMS spectra. (b) The corresponding scores plot for PC3 versus PC2. Grey stars denote measurements carried out on reference silicon surface with deposited component of RPMI160 culture medium. The results are plotted together with confidence ellipses calculated at 90%, 95%, and 99% confidence levels.*

The percentage of the total variance for these four cell lines was as follows: PC1 = 39.13%; PC2 = 26.52% and PC3 = 14.59%. The scores plot shows clearly that VGP melanoma cells are clearly separated from the cells derived from the lung metastasis, what correlates with elasticity measurements.

Next, the comparison of VGP cells with those originated from skin metastasis was performed (Figure 8.6). In this case, the elasticity measurements show the large difference ($p < 0.0001$) between VGP WM793 and WM239 (skin metastasis) cells and small, although still significant ($p < 0.1$), difference between the VGP WM115 and WM266-4 ones. The determined loadings and PCs scores plots are presented in Figure 8.6a and Figure 8.6b, respectively. The obtained percentage of the total variance for each principal component was PC1 = 46.73%; PC2 = 19.37% and PC3 = 8.68%.

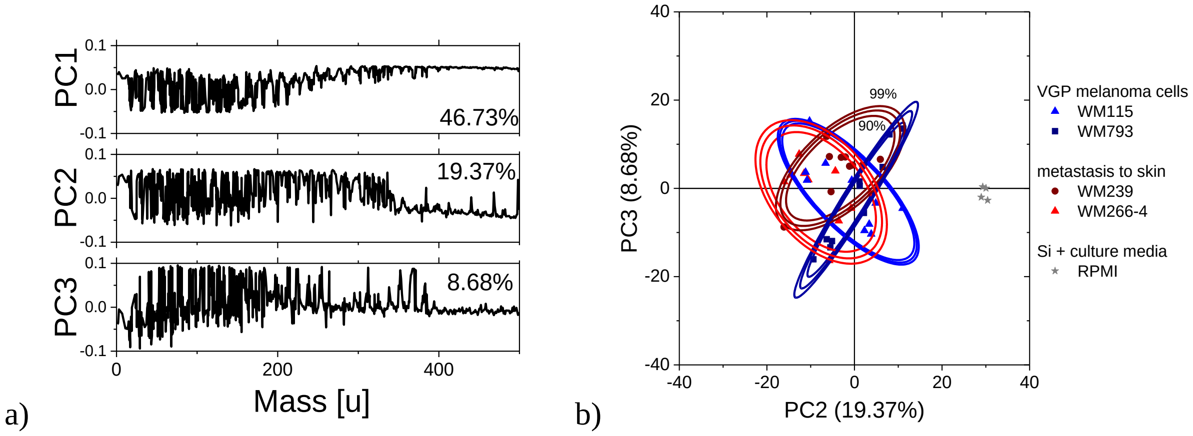

Figure 8.6. *Comparison of melanoma cells from VGP and metastatic sites in skin. (a) Loadings plot for PC1, PC2 and PC3 components resulted from PCA of ToF SIMS spectra. (b) The corresponding scores plot for PC3 versus PC2. Grey stars denotes measurements carried out on reference silicon surface with deposited component of RPMI160 culture medium. The results are plotted together with confidence ellipses calculated at 90%, 95%, and 99% confidence levels.*

The PC scores plot shows that in case of cells with large elasticity difference i.e. WM793 and WM239, it is still possible to observe the PCA data separation, while for a pair of cells with smaller elasticity difference the presence of other datasets influences the data separation. When only two cell lines are compared, as in case of WM115 and WM266-4 cells (Figure 8.4), the alterations in surface chemical properties of cells are strong enough to be observable.

Summarising the PCA outcome, the overall conclusion can be made, that, apparently, PCA is more sensitive when analysing smaller data sets. With large data sets, such as ten different samples (eight cell lines and two references) only the strongest differences in surface chemical composition can be observed, like in this case, between melanocytes and the rest of melanoma cell lines.

8.4 Summary

The results gathered in this chapter show an attempt to find a correlation between cellular deformability, surface chemistry and stage of melanoma progression by combining the results based on AFM and ToF SIMS measurements. When all eight cell types are considered together, the PCA outcome results in the following conclusions (Figure 8.3):

a) melanocytes overlap with VGP (WM115 & WM793) cells what denotes similarities in the overall surface composition of these cells. Also, these cells are characterized by similar Young's moduli of 13.08 ± 3.39 kPa, 9.33 ± 1.96 kPa, 10.84 ± 3.30 kPa, respectively.

b) melanocytes separate clearly from cells originating from lung metastasis (1205Lu & A375P) indicating distinct overall chemical surface properties of cellular surface, and simultaneously, melanocytes are of about 50%–60% more rigid.

c) melanocytes separate also from cells derived from skin metastasis (i.e. they have distinct overall chemical properties of cellular surface) and they are of about 35–40 % more rigid.

d) VGP cells overlap with cells derived from skin metastasis indicating similarities in surface composition. The mechanical properties of these cells varied from 7–8 kPa (skin metastasis) to 9–11 kPa (VGP).

e) cells originated form skin metastasis overlap with cells established from lung metastatic sites and primary tumour sites (RGP and VGP stages). Such PCA outcome suggests strongly the variability of cells forming various types of secondary tumour sites in skin. The elasticity of these cells lies within the stiffness range with two border limits 5–6 kPa (lung metastasis) and 9–11 kPa (VGP cells).

Additionally to overall PCA for all studied melanoma cells, it is possible to calculate PCs scores for specific pairs of the studied cells. The most significant results were obtained for two pairs of melanoma cells derived from two patients. The first pair is WM793 and 1205Lu being the representatives of VGP and lung metastasis, respectively. The mechanical properties of these cells are significantly different. The VGP cells are of about 27% more rigid as compared to 1205Lu cells. These cells are characterized by clear separation in the PCs scores plot indicating large variability in the surface chemical composition. The other pair of melanoma cells, namely, WM115 and WM266-4 ones represents cells that originate from VGP and skin metastasis. When analysed together, the elasticity measurements delivered only a small difference in elastic modulus, of the order of 10%, while PCA of mass spectra shows clear separation between these cell lines (Figure 8.4). The similar PCA and elasticity results obtained for analogous melanoma cell lines confirm the observed relation between cellular deformability and surface chemical properties. Comparing the surface chemistry of VGP cells (WM793 and WM115) with that of cells originated from lung metastasis (1205Lu and A375P) based on PCA of mass spectra, one can see two groups of data (Figure 8.5). The former belongs to VGP cells, while the latter to cells originated from lung metastasis. This relation vanishes when VGP cells are compared with those derived from skin metastasis (Figure 8.6). The PCA outcomes correlate with the elasticity measurements, showing the decrease of cells deformability according to melanoma progression stage, i.e. VGP cells (less deformable) > cells from skin metastasis > cells from lung metastasis (large deformability).

9. Summarizing biomechanical and biochemical characteristics in melanoma cells

The main aim of the presented thesis was to find whether alterations observed in cellular deformability are accompanied or correlated with the surface composition of melanoma cells. By means of two high resolution techniques, originally used to characterize surface properties, namely, atomic force microscopy (AFM) and time of flight secondary ions mass spectrometry (ToF SIMS), characteristic quantitative or semi-quantitative parameters were obtained. The studies were focused mainly on melanoma cells involving distinct groups of cells coming from various stages of melanoma progression. They can be divided into three main groups, i.e., cells from *(i)* radial/vertical growth phase, *(ii)* metastasis to skin, and *(iii)* metastasis to lung. The results are compared to melanocytes – cells of the origin of malignant melanoma.

Various studies carried out so far with the use of AFM constitute that increased cellular deformability is a general feature of most cancer types [140]. Melanoma cells follow this direction; all studied melanoma cell lines, independently of the cancer progression stage, are significantly more deformable as compared to melanocytes. The explanation for that is the alteration in actin cytoskeleton, as shown in the comparison of F-actin in the pair of melanoma cells delivered from the same patient (WM115 & WM266-4).

To identify the spectral fingerprints of cellular surface in melanoma cells, the principal components analysis (PCA) was applied. In the approach, presented in this thesis, the PCA was calculated for the whole mass (or photothermal) spectrum, without the pre-definition of any particular molecular masses or wavenumbers. This approach enables the identification of the molecular masses that dominate in the data separation. As a proof of concept, human bladder cancer cell lines were chosen for the ToF SIMS measurements. They are non-malignant HCV29 cancer cells of ureter, resembling morphology of normal epithelial cells, bladder carcinoma of distinct grades i.e. HTB-9 (grade I) and HT1376 (grade IV) and T24 transitional cell carcinoma. Their choice was dictated by two reasons. The first one is that cancerous HTB-9, HT1376, and T24 cells, as it has been shown in the earlier studies, are characterized by large deformability as compared to non-malignant HCV29 ones [104]. Moreover, they become soft at early stages of cancer progression. That is why, one could expect that their surface properties are distinct enough to cause the ToF SIMS data separation in PCs scores plots. The PCA was carried out for the whole range of molecular masses (up to 500 Da), clearly distinguishing non-malignant HCV29 cells from the remaining three cancerous cell types (HTB-9, HT1376, T24 cell lines).

It is worth to highlight that there was no need to choose *a priori* particular masses from mass spectra to discriminate between cell lines. The PCA was sensitive enough to find substantial differences between cells based on analysis of the whole range of acquired spectra. The PCA carried out on ToF SIMS spectra recorded for human bladder cancer cells has been shown to clearly discriminate between non-malignant and cancerous bladder cell lines, but it was impossible to correlate the separation degree with bladder malignancy. For cells originated from close stages of cancer progression, the mass spectra were very similar and basically differed by the maxima intensity, not, as one could expect, due to the presence of a unique mass that would be characteristic for only one cell type. These measurements confirmed that changes in biomechanics of bladder cells can be linked with alterations of their surface, however, there was no clear separation between cancerous cells. This could be linked with the fact that cancer-related changes, like softening of single cells, occur at early stages of cancer progression.

The more challenging approach is to find biomechanical and biophysical features that can differentiate between cancerous cells, in particular, in cases when they originate from very close stages of cancer progression. The example of such a case is a melanoma cell pair of WM115 and WM266-4 cells that comes from the same patient and WM266-4 cells are the metastasis to skin of the WM115 ones. The analysis of cellular properties by atomic force and fluorescence microscopes has delivered characteristics that enable to differentiate between these cell lines. Images of cells recorded by inverted optical and fluorescence microscope show similar morphological characteristics. Both studied cell types (VGP WM115 melanoma cells and WM266-4 ones from skin metastasis) have spindle-like shape, visible independently of the cellular density. Also, the recorded fluorescent and AFM images show nicely organized actin filaments in WM115 melanoma cells (Figure 6.4a-c) while their organization undergoes disordering in WM266-4 cells from skin metastasis (Figure 6.4d-f). The surface area occupied by single cells (AC) is larger in the case of WM115 melanoma cells (from VGP progression stage), as compared to WM266-4 cells (skin metastasis). The alterations of nucleus surface area (AN) are not significant between these two cell lines. For the studied melanoma cells, the obtained N/C ratio reaches values closed to ~0.2 and it rather describes conditions suitable for cell spreading than the differentiation between melanoma cells from VGP and metastatic stages of melanoma progression. The considerable differences between WM115 and WM266-4 cells are accompanied by differences observed using AFM.

The analysis of AFM topographical images revealed considerable differences between WM115 and WM266-4 cells that were not visible under optical microscope due to its low resolution, ~200–300 nm, as compared to the AFM (several nm). The cytoskeletal network of

WM115 cells was better organized (cortical filamentous structure), whereas WM266-4 cells were rougher with the presence of characteristic flexible ridges (or ruffles). Because the ridges (or ruffles) were constantly detected only on WM266-4 cells, it can be assumed that their presence might be associated with the melanoma progression. In this thesis, it was demonstrated, that the combination of non-optical atomic force microscopy and optical fluorescence microscopy enables the identification of cellular structures and nano-mechanical properties of melanoma cells. The obtained results show that larger deformability of metastatic WM266-4 melanoma cells correlates well with the presence of flexible ridges. Single melanoma cells can be clearly identified by detailed images of their surface at nm scale and by their nano-mechanical properties. Recent studies revealed significant differences in the nano-mechanical properties of benign and cancerous cells that were attributed to alterations in F-actin filaments organization. However, the larger deformability of cancer cells is not always caused by the reorganization of actin cytoskeleton. Here, it was demonstrated that the elasticity of melanoma cells could be correlated with the presence of F-actin-based flexible ridges, typical only for metastatic melanoma cells. These results may help to understand the role of nano-mechanical properties in melanoma development.

Due to extensive research carried out over the last few decades, the knowledge about organic compounds emitted from cells or tissue surfaces upon primary ion bombardments is still expanding. So far, mass spectra of amino acids [71–73] and lipids [74–76,120] were established to study protein and lipid contents on cell or tissue surfaces. However, despite that, ToF SIMS data recorded for complex biological samples are still difficult to be interpreted due to fragmentation phenomenon of large biomolecules [130]. There is no possibility to identify the sample only by looking at the ToF SIMS spectrum [141]. That is the reason, why multivariate analysis is widely applied to find spectral differences between biological samples [69]. In the presented thesis, PCA was used to discriminate between two closely related melanoma cell lines (WM115 and WM266-4) based on the recorded ToF SIMS spectra. To confirm the obtained results, another technique, namely photothermal microspectroscopy, was employed to analyse chemical properties of the studied melanoma cell lines. PTMS is a spectroscopic technique that combines the advantages of conventional FTIR with the high resolution of near-field sensors [96,131]. In comparison to conventional FTIR spectroscopy, the sample preparation in PTMS is less strict [132], thus, it seems to be good to compare results obtained at single cell level. Therefore, to verify the applied PCA methodology, photothermal spectra were analysed within the entire range of 500–4000 cm^{-1}. The FTIR-based spectroscopy has been already shown to be applied in diagnosis of cancer [122,127].

A huge complexity of mass and photothermal spectra observed for WM115 and WM266-4 cells (Figures 7.1 & 7.5) disables the direct analysis and the exact value of a particular mass or wavelength is difficult to be determined. The use of PCA for data reduction enhances the existing differences in original datasets of the investigated samples. In the presented work, it is postulated that a whole range of spectra, recorded for two melanoma cell lines that come from relatively close stages of cancer progression, contains sufficient, encoded information to differentiate between these cancer progression stages. The proposed methodology of PCA data treatment enabled to treat both spectra types (mass or photothermal) with the blind eye i.e. without choosing particular mass or wavelength. The advantage of the proposed approach lies in objective criteria for the cellular data separation. In the PCA results presented in Figure 7.3 and Figure 7.6, the majority of spectra recorded for WM266-4 melanoma cells, originated from metastasis to skin, are grouped in the different quadrants of the coordinate system using PC2 vs PC3 scores, as compared to the way of spectra grouping from WM115 melanoma cells from vertical growth phase. The distribution of points in the PCA scores plots is not very homogenous, what can be influenced by different phases of the cell cycle, as these cells were not synchronized. Nevertheless, a distinct separation between primary melanoma and skin metastasis cell lines can be observed. By applying the criteria based on a standard deviation (SD) of loadings, maxima with the corresponding values of loadings were found in both spectra types recorded for cells. Based on that, molecular masses and wavenumbers regions causing the strongest differentiation between the studied melanoma cell lines were obtained. Some of the molecular masses found can be attributed to surface presence of such amino acids as glycine, alanine, methionine, threonine, serine, asparagine and tryptophan. Furthermore, many masses can be assigned to fragments of phosphocholine, being a structural component of both phospholipids and sphingomyelin in cellular membranes [119]. Such assignment seems to be highly probable and was confirmed by studies showing altered phospholipid composition in cancer cells [133]. Abnormal choline metabolism, overexpression of the choline kinase and phosphocholine accumulation are reported to be a common feature of breast, ovarian, lung and prostate cancers [134–136]. Also, sphingomyelin (having phosphocholine in its chemical structure) is differentially expressed between cancerous and normal regions in the colon cancer liver metastasis [137].

Analogously, as for the ToF SIMS experiment, the spectral regions causing largest differentiation between the studied melanoma cell lines have been chosen. The largest perturbations, influencing PCA-based separation, were obtained for DNA and lipids. It should be noted that chemical fixation influences the collected spectra, especially, that IR peaks in the spectrum of glutaraldehyde may overlap with those characteristic for lipids, amide I and other biomolecules [141]. However, because it is assured that both cell lines were treated with the same fixation procedure within one batch of the preparation experiment to avoid any potential drifts, the obtained differentiation between melanoma cell lines is not caused by the glutaraldehyde residues. This supports the PCA results of ToF SIMS spectra, indicating also that phosphocholine is responsible for data sets separation of melanoma cells. This is also supported by the results presented in the previous chapter, showing that the surface of WM266-4 melanoma cells was more rough with the presence of characteristic cell membrane flexible ridges (or ruffles), composed mainly of phospholipids filled with actin filaments.

In the final chapter of the presented thesis, the results of the investigation of seven melanoma cell lines and melanocytes are presented. So far, there are not many data in the literature describing ToF SIMS experiments carried out for more than four cell lines in one study. In 2006, Kulp et al., in a very interesting study, examined the differentiation between three human breast cancer cell types: MCF-7 and T47D - estrogen receptor positive (ER+) and MDA-MB-231 - estrogen receptor negative (ER-) [142]. In 2007, Baker et al. have investigated three prostate cancer cell lines: LNCaP (prostate cancer cells derived from lymph node metastasis), non-malignant PNT2 (transfected normal prostate epithelial cells with genome of SV40 virus) and PC-3 (prostate cancer cells derived from bone metastasis) [143]. What is more, with the development of the SIMS apparatuses, novel sample preparation procedures and statistical methods of the data analysis, the ToF SIMS technique has become the powerful tool in the studies of large data sets of mass spectra acquired for several cell lines. Recently, Robinson et al. have used ToF-SIMS in combination with multivariate analysis (MVA) to investigate the complex lipid-related metabolite variations from eight breast cancer cell lines. Mass spectra were collected from four triple negative classified cell lines (ER-, PR-, and HER-), three ER and PR receptor-positive lines (ERþ and PRþ), and one line that was ER, PR, and also HER2 positive (ERþ, PRþ, and HERþ) [144]. Thus, the comparison of biomechanical and biophysical properties of melanoma cells is in fact, one of the first attempts to find the correlation between them. The obtained results (*Chapter 8*) confirmed the hypothesis, that cancer progression causes alterations in the morphological and mechanical properties of cancerous cells and these differences are connected with overall biochemical changes in the cellular surface composition.

10. References

[1] P.B. Chapman, A. Hauschild, C. Robert, J.B. Haanen, P. Ascierto, J. Larkin, et al., Improved survival with vemurafenib in melanoma with BRAF V600E mutation., N. Engl. J. Med. 364 (2011) 2507–2516. doi:10.1056/NEJMoa1103782.

[2] M. Demierre, M.S. Sabel, K.A. Margolin, State of the Science 60th, (2008) 1728–1743. doi:10.1002/cncr.23643.

[3] V. Bevelacqua, Y. Bevelacqua, S. Candido, A. Amoroso, C. Guarneri, A. Strazzanti, et al., Nectin like-5 overexpression correlates with the malignant phenotype in cutaneous melanoma ABSTRACT :, 3 (2012) 882–892.

[4] J.M. Koomen, K.S.M. Smalley, Using quantitative proteomic analysis to understand genotype specific intrinsic drug resistance in melanoma Abstract :, 2 (2011) 329–335.

[5] J.K. Soo, A.D. Mackenzie Ross, D.M. Kallenberg, C. Milagre, W. Heung Chong, J. Chow, et al., Malignancy without immortality? Cellular immortalization as a possible late event in melanoma progression, Pigment Cell Melanoma Res. 24 (2011) 490–503. doi:10.1111/j.1755-148X.2011.00850.x.

[6] A.N. Houghton, D. Polsky, Focus on melanoma, 2 (2002) 275–278.

[7] M. Patarroyo, K. Tryggvason, I. Virtanen, Laminin isoforms in tumor invasion, angiogenesis and metastasis, Semin. Cancer Biol. 12 (2002) 197–207. doi:10.1016/S1044-579X(02)00023-8.

[8] J.H. Miner, P.D. Yurchenco, Laminin functions in tissue morphogenesis., Annu. Rev. Cell Dev. Biol. 20 (2004) 255–84. doi:10.1146/annurev.cellbio.20.010403.094555.

[9] S. Schéele, A. Nyström, M. Durbeej, J.F. Talts, M. Ekblom, P. Ekblom, Laminin isoforms in development and disease, J. Mol. Med. 85 (2007) 825–836. doi:10.1007/s00109-007-0182-5.

[10] R.O. Hynes, Integrins: versatility, modulation, and signaling in cell adhesion., Cell. 69 (1992) 11–25. doi:10.1016/0092-8674(92)90115-S.

[11] R.O. Hynes, The emergence of integrins: A personal and historical perspective, Matrix Biol. 23 (2004) 333–340. doi:10.1016/j.matbio.2004.08.001.

[12] C. Zhu, G. Bao, N. Wang, Mechanical Response, Cell Adhesion, and Molecular

Deformation, (2000) 189–226.

[13] D.A. Fletcher, R.D. Mullins, Cell mechanics and the cytoskeleton, 463 (2010) 485–492. doi:10.1038/nature08908.

[14] a. Santiago-Walker, L. Li, N.K. Haass, M. Herlyn, Melanocytes: From morphology to application, Skin Pharmacol. Physiol. 22 (2009) 114–121. doi:10.1159/000178870.

[15] C. Wellbrock, S. Rana, H. Paterson, H. Pickersgill, T. Brummelkamp, Oncogenic BRAF Regulates Melanoma Proliferation through the Lineage Specific Factor MITF, 3 (2008). doi:10.1371/journal.pone.0002734.

[16] L.N. Kwong, J.C. Costello, H. Liu, S. Jiang, T.L. Helms, A.E. Langsdorf, et al., Oncogenic NRAS signaling differentially regulates survival and proliferation in melanoma, Nat Med. 18 (2012) 1503–1510. http://dx.doi.org/10.1038/nm.2941.

[17] J. Nikkola, P. Vihinen, T. Vlaykova, M. Hahka-Kemppinen, J. Heino, S. Pyrhonen, Integrin chains beta1 and alphav as prognostic factors in human metastatic melanoma., Melanoma Res. 14 (2004) 29–37. doi:10.1097/00008390-200402000-00005.

[18] V.D. Criscione, M. a Weinstock, Melanoma thickness trends in the United States, 1988-2006., J. Investig. Dermatologyinvestigative Dermatology. 130 (2010) 793–797. doi:10.1038/jid.2009.328.

[19] R. King, P.B. Googe, M.C. Mihm, Thin melanomas., Clin. Lab. Med. 20 (2000) 713–29. http://www.ncbi.nlm.nih.gov/pubmed/11221511.

[20] T. Ochalek, F.J. Nordt, K. Tullberg, M.M. Burger, Correlation between cell deformability and metastatic potential in B16-F1 melanoma cell variants, Cancer Res. 48 (1988) 5124–5128.

[21] Z.H. Stachurski, Mechanical behavior of materials, 2009. doi:10.1016/S1369-7021(09)70086-0.

[22] M.F. Ashby, Physical modelling of materials problems, Mater. Sci. Technol. 8 (1992) 102–111. doi:10.1179/026708392790170351.

[23] M.A. Meyers, P.-Y. Chen, A.Y.-M. Lin, Y. Seki, Biological materials: Structure and mechanical properties, Prog. Mater. Sci. 53 (2008) 1–206. doi:10.1016/j.pmatsci.2007.05.002.

[24] C.T. Lim, E.H. Zhou, S.T. Quek, Mechanical models for living cells - A review, J.

Biomech. 39 (2006) 195–216. doi:10.1016/j.jbiomech.2004.12.008.

[25] G. Du, A. Ravetto, Q. Fang, J.M.J. Den Toonder, Cell types can be distinguished by measuring their viscoelastic recovery times using a micro-fluidic device, Biomed. Microdevices. 13 (2011) 29–40. doi:10.1007/s10544-010-9468-4.

[26] M.N. Starodubtseva, Mechanical properties of cells and ageing, Ageing Res. Rev. 10 (2011) 16–25. doi:10.1016/j.arr.2009.10.005.

[27] E. Moeendarbary, A.R. Harris, Cell mechanics: Principles, practices, and prospects, Wiley Interdiscip. Rev. Syst. Biol. Med. 6 (2014) 371–388. doi:10.1002/wsbm.1275.

[28] L. Wolff, P. Fernandez, K. Kroy, Inelastic mechanics of sticky biopolymer networks, New J. Phys. 12 (2010). doi:10.1088/1367-2630/12/5/053024.

[29] C. Verdier, J. Etienne, A. Duperray, L. Preziosi, Review: Rheological properties of biological materials, Comptes Rendus Phys. 10 (2009) 790–811. doi:10.1016/j.crhy.2009.10.003.

[30] M. Radmacher, M. Fritz, C.M. Kacher, J.P. Cleveland, P.K. Hansma, Measuring the viscoelastic properties of human platelets with the atomic force microscope., Biophys. J. 70 (1996) 556–67. doi:10.1016/S0006-3495(96)79602-9.

[31] J. Alcaraz, L. Buscemi, M. Grabulosa, X. Trepat, B. Fabry, R. Farré, et al., Microrheology of human lung epithelial cells measured by atomic force microscopy., Biophys. J. 84 (2003) 2071–9. doi:10.1016/S0006-3495(03)75014-0.

[32] S. Suresh, Biomechanics and biophysics of cancer cells., Acta Biomater. 3 (2007) 413–438. doi:10.1016/j.actbio.2007.04.002.

[33] S. Suresh, Connections between single-cell biomechanics and human disease states : gastrointestinal cancer and malaria, 1 (2005) 15–30. doi:10.1016/j.actbio.2004.09.001.

[34] M. Perez-moreno, C. Jamora, E. Fuchs, Sticky Business : Orchestrating Cellular Signals at Adherens Junctions, 112 (2003) 535–548.

[35] M.R.K. Mofrad, Rheology of the Cytoskeleton, Annu. Rev. Fluid Mech. 41 (2009) 433–453. doi:10.1146/annurev.fluid.010908.165236.

[36] P.A. Pullarkat, P.A. Fernández, A. Ott, Rheological properties of the Eukaryotic cell cytoskeleton, Phys. Rep. 449 (2007) 29–53. doi:10.1016/j.physrep.2007.03.002.

[37] A.D. Bershadsky, N.Q. Balaban, B. Geiger, Adhesion-dependent cell

mechanosensitivity., Annu. Rev. Cell Dev. Biol. 19 (2003) 677–95. doi:10.1146/annurev.cellbio.19.111301.153011.

[38] A. Hall, The cytoskeleton and cancer, Cancer Metastasis Rev. 28 (2009) 5–14. doi:10.1007/s10555-008-9166-3.

[39] M.A. Jordan, L. Wilson, Microtubules and actin filaments: Dynamic targets for cancer chemotherapy, Curr. Opin. Cell Biol. 10 (1998) 123–130. doi:10.1016/S0955-0674(98)80095-1.

[40] M. Makale, Cellular mechanobiology and cancer metastasis, Birth Defects Res. Part C - Embryo Today Rev. 81 (2007) 329–343. doi:10.1002/bdrc.20110.

[41] P. Hinterdorfer, Y.F. Dufrêne, Detection and localization of single molecular recognition events using atomic force microscopy., Nat. Methods. 3 (2006) 347–355. doi:10.1038/nmeth871.

[42] Y. Seo, W. Jhe, Atomic force microscopy and spectroscopy, Reports Prog. Phys. 71 (2008) 016101. doi:10.1088/0034-4885/71/1/016101.

[43] M. Lekka, D. Gil, K. Pogoda, J. Dulińska-Litewka, R. Jach, J. Gostek, et al., Cancer cell detection in tissue sections using AFM., Arch. Biochem. Biophys. 518 (2012) 151–6. doi:10.1016/j.abb.2011.12.013.

[44] W. Xu, R. Mezencev, B. Kim, L. Wang, J. McDonald, T. Sulchek, Cell Stiffness Is a Biomarker of the Metastatic Potential of Ovarian Cancer Cells, PLoS One. 7 (2012). doi:10.1371/journal.pone.0046609.

[45] C. Brunner, A. Niendorf, J.A. Kas, Passive and active single-cell biomechanics: a new perspective in cancer diagnosis, Soft Matter. 5 (2009) 2171–2178. doi:10.1039/B807545J.

[46] M. Lekka, P. Laidler, D. Gil, J. Lekki, Z. Stachura, a Z. Hrynkiewicz, Elasticity of normal and cancerous human bladder cells studied by scanning force microscopy., Eur. Biophys. J. EBJ. 28 (1999) 312–316. http://www.ncbi.nlm.nih.gov/pubmed/10394623.

[47] M. Radmacher, Measuring the elastic properties of biological samples with the AFM, IEEE Eng Med Biol Mag. 16 (1997) 47–57. http://www.ncbi.nlm.nih.gov/pubmed/9086372.

[48] A.N. Ketene, E.M. Schmelz, P.C. Roberts, M. Agah, The effects of cancer progression

on the viscoelasticity of ovarian cell cytoskeleton structures., Nanomedicine. 8 (2012) 93–102. doi:10.1016/j.nano.2011.05.012.

[49] M. Lekka, P. Laidler, M. Łabe, Specific Detection of Glycans on a Plasma Membrane of Living Cells with Atomic Force Microscopy, (2006) 505–512. doi:10.1016/j.chembiol.2006.03.006.

[50] S. Kumar, V.M. Weaver, Mechanics, malignancy, and metastasis: the force journey of a tumor cell., Cancer Metastasis Rev. 28 (2009) 113–127. doi:10.1007/s10555-008-9173-4.

[51] D. Hanahan, R.A. Weinberg, Hallmarks of cancer: the next generation., Cell. 144 (2011) 646–674. doi:10.1016/j.yane.2012.02.046.

[52] S. Chandra, D.R. Lorey, SIMS ion microscopy in cancer research: single cell isotopic imaging for chemical composition, cytotoxicity and cell cycle recognition., Cell. Mol. Biol. 47 (2001) 503–518.

[53] R. Aebersold, M. Mann, Mass spectrometry-based proteomics., Nature. 422 (2003) 198–207. doi:10.1038/nature01511.

[54] Norman Sheppard, The Historical Development of Experimental Techniques in Vibrational Spectroscopy, in: Handb. Vib. Spectrosc., 2002.

[55] J. Schmitt, H.-C. Flemming, FTIR-spectroscopy in microbial and material analysis, Int. Biodeterior. Biodegradation. 41 (1998) 1–11. doi:10.1016/S0964-8305(98)80002-4.

[56] P. Williams, Secondary Ion Mass Spectrometry, Appl. At. Collis. Spectrosc. 182 (1983) 327 – 377. doi:10.1016/B978-0-12-409547-2.05228-8.

[57] J. Schwieters, H.G. Cramer, T. Heller, U. Jürgens, E. Niehuis, J. Zehnpfenning, et al., High mass resolution surface imaging with a time-of-flight secondary ion mass spectroscopy scanning microprobe, J Vac. Sci. Technol. 9 (1991) 2864–2871. doi:10.1116/1.577145.

[58] A. Benninghoven, E. Niehuis, U. Munster, Probing Real =World Samples, 65 (1993).

[59] J.J. Thomson, Rays of Positive Electricity, Nature. 79 (1908) 52–56. doi:10.1038/079052a0.

[60] A. Benninghoven, Surface investigation of solids by the statical method of secondary ion mass spectroscopy (SIMS), Surf. Sci. 35 (1973) 427–457. doi:10.1016/0039-

6028(73)90232-X.

[61] P. Galle, Sur une nouvelle méthode d'analyse cellulaire utilisant le phénomène d'émission ionique secondaire, Ann Phys Biol Med., (1970) 42: 83–94.

[62] E.J. Lanni, S.S. Rubakhin, J. V Sweedler, Mass spectrometry imaging and profiling of single cells, J. Proteomics. 75 (2012) 1–16. http://linkinghub.elsevier.com/retrieve/pii/S1874391912001509.

[63] A. Benninghoven, E. Loebach, Tandem mass spectrometer for secondary ion studies, Rev. Sci. Instrum. 42 (1971) 49–52. doi:10.1063/1.1684875.

[64] B.T. Chait, K.G. Standing, A time-of-flight mass spectrometer for measurement of secondary ion mass spectra, Int. J. Mass Spectrom. Ion Phys. 40 (1981) 185–193. doi:10.1016/0020-7381(81)80041-1.

[65] D. Breitenstein, C.E. Rommel, R. Möllers, J. Wegener, B. Hagenhoff, The chemical composition of animal cells and their intracellular compartments reconstructed from 3D mass spectrometry, Angew. Chemie - Int. Ed. 46 (2007) 5332–5335. doi:10.1002/anie.200604468.

[66] S. Chandra, G.H. Morrison, Sample preparation of animal tissues and cell cultures for secondary ion mass spectrometry (SIMS) microscopy., Biol. Cell. 74 (1992) 31–42.

[67] J. Malm, D. Giannaras, M.O. Riehle, N. Gadegaard, P. Sjövall, Fixation and drying protocols for the preparation of cell samples for time-of-flight secondary ion mass spectrometry analysis, Anal. Chem. 81 (2009) 7197–7205. doi:10.1021/ac900636v.

[68] S. Parameswaran, R.S. Verma, Scanning electron microscopy preparation protocol for differentiated stem cells, Anal. Biochem. 416 (2011) 186–190. doi:10.1016/j.ab.2011.05.032.

[69] E.S.F. Berman, L. Wu, S.L. Fortson, K.S. Kulp, D.O. Nelson, K.J. Wu, Chemometric and statistical analyses of ToF-SIMS spectra of increasingly complex biological samples, Surf. Interface Anal. 41 (2009) 97–104. doi:10.1002/sia.2953.

[70] T. Leefmann, C. Heim, S. Siljeström, M. Blumenberg, P. Sjövall, V. Thiel, Spectral characterization of ten cyclic lipids using time-of-flight secondary ion mass spectrometry., Rapid Commun. Mass Spectrom. 27 (2013) 565–81. doi:10.1002/rcm.6483.

[71] J.B. Lhoest, M.S. Wagner, C.D. Tidwell, D.G. Castner, Characterization of adsorbed protein films by time of flight secondary ion mass spectrometry, J. Biomed. Mater. Res. 57 (2001) 432–440. doi:10.1002/1097-4636(20011205)57:3<432::aid-jbm1186>3.0.co;2-g.

[72] M.S. Wagner, D.G. Castner, Characterization of Adsorbed Protein Films by Time-of-Flight Secondary Ion Mass Spectrometry with Principal Component Analysis, Langmuir. 17 (2001) 4649–4660. doi:10.1021/la001209t.

[73] C.D. Tidwell, D.G. Castner, S.L. Golledge, B.D. Ratner, K. Meyer, B. Hagenhoff, et al., Static time-of-flight secondary ion mass spectrometry and x-ray photoelectron spectroscopy characterization of adsorbed albumin and fibronectin films, Surf. Interface Anal. 31 (2001) 724–733. doi:10.1002/sia.1101.

[74] M.K. Passarelli, N. Winograd, Lipid imaging with time-of-flight secondary ion mass spectrometry (ToF-SIMS)., Biochim. Biophys. Acta. 1811 (2011) 976–90. doi:10.1016/j.bbalip.2011.05.007.

[75] H. Nygren, K. Börner, B. Hagenhoff, P. Malmberg, J.-E. Månsson, Localization of cholesterol, phosphocholine and galactosylceramide in rat cerebellar cortex with imaging TOF-SIMS equipped with a bismuth cluster ion source., Biochim. Biophys. Acta. 1737 (2005) 102–10. doi:10.1016/j.bbalip.2005.10.004.

[76] Y.K. Magnusson, P. Friberg, P. Sjövall, J. Malm, Y. Chen, TOF-SIMS analysis of lipid accumulation in the skeletal muscle of ob/ob mice., Obesity (Silver Spring). 16 (2008) 2745–2753. doi:10.1038/oby.2008.424.

[77] C.R. Anderton, B. Vaezian, K. Lou, J.F. Frisz, M.L. Kraft, Identification of a lipid-related peak set to enhance the interpretation of TOF-SIMS data from model and cellular membranes, Surf. Interface Anal. 44 (2012) 322–333. doi:10.1002/sia.3806.

[78] K.S. Kulp, E.S.F. Berman, M.G. Knize, D.L. Shattuck, E.J. Nelson, L. Wu, et al., Chemical and biological differentiation of three human breast cancer cell types using time-of-flight secondary ion mass spectrometry., Anal. Chem. 78 (2006) 3651–3658. http://www.embase.com/search/results?subaction=viewrecord&from=export&id=L43848958.

[79] M. Fartmann, C. Kriegeskotte, S. Dambach, A. Wittig, W. Sauerwein, H. Arlinghaus, Quantitative imaging of atomic and molecular species in cancer cultures with TOF-

SIMS and Laser-SNMS, Appl. Surf. Sci. 231 (2004) 428–431. doi:10.1016/j.apsusc.2004.03.160.

[80] L. a McDonnell, S.R. Piersma, a F. MaartenAltelaar, T.H. Mize, S.L. Luxembourg, P.D.E.M. Verhaert, et al., Subcellular imaging mass spectrometry of brain tissue., J. Mass Spectrom. 40 (2005) 160–168. doi:10.1002/jms.735.

[81] S. Chandra, M.T. Bernius, G.H. Morrison, Intracellular localization of diffusible elements in frozen-hydrated biological specimens with ion microscopy., Anal. Chem. 58 (1986) 493–6. http://www.ncbi.nlm.nih.gov/pubmed/3963401.

[82] S. Chandra, SIMS ion microscopy as a novel, practical tool for subcellular chemical imaging in cancer research, Appl. Surf. Sci. 203-204 (2003) 679–683. doi:10.1016/S0169-4332(02)00790-0.

[83] J.N. Quong, M.G. Knize, K.S. Kulp, K.J. Wu, Molecule-specific imaging analysis of carcinogens in breast cancer cells using time-of-flight secondary ion mass spectrometry, Appl. Surf. Sci. 231-232 (2004) 424–427. doi:10.1016/j.apsusc.2004.03.156.

[84] M. Fartmann, S. Dambach, C. Kriegeskotte, H.P. Wiesmann, A. Wittig, W. Sauerwein, et al., Characterization of cell cultures with ToF-SIMS and laser-SNMS, Surf. Interface Anal. 34 (2002) 63–66. doi:10.1002/sia.1253.

[85] G.D. Mazzucchelli, N.A. Cellier, V. Mshviladzade, R. Elias, Y.H. Shim, D. Touboul, et al., Pores formation on cell membranes by hederacolchiside a1 leads to a rapid release of proteins for cytosolic subproteome analysis, J. Proteome Res. 7 (2008) 1683–1692. doi:10.1021/pr7006973.

[86] E. Gazi, J. Dwyer, N. Lockyer, P. Gardner, J.C. Vickerman, J. Miyan, et al., The combined application of FTIR microspectroscopy and ToF-SIMS imaging in the study of prostate cancer., Faraday Discuss. 126 (2004) 41–59; discussion 77–92. doi:10.1039/b304883g.

[87] E. Gazi, N.P. Lockyer, J.C. Vickerman, P. Gardner, J. Dwyer, C.A. Hart, et al., Imaging ToF-SIMS and synchrotron-based FT-IR microspectroscopic studies of prostate cancer cell lines, Appl. Surf. Sci. 231-232 (2004) 452–456. doi:10.1016/j.apsusc.2004.03.170.

[88] M.J. Baker, M.D. Brown, E. Gazi, N.W. Clarke, J.C. Vickerman, N.P. Lockyer,

Discrimination of prostate cancer cells and non-malignant cells using secondary ion mass spectrometry., Analyst. 133 (2008) 175–179. doi:10.1039/b712853c.

[89] H. Nygren, B. Hagenhoff, P. Malmberg, M. Nilsson, K. Richter, Bioimaging TOF-SIMS: High resolution 3D imaging of single cells., Microsc. Res. Tech. 70 (2007) 969–974. doi:10.1002/jemt.

[90] and M.H. Friedegund Meier, Kapaettu Satyamoorthy, Mark Nesbit, Mei-Yu Hsu, Birgit Schittek, Claus Garbe, MOLECULAR EVENTS IN MELANOMA DEVELOPMENT AND PROGRESSION, Front. Biosci. (1998) 1005–1010. doi:10.1007/s11655-011-0934-5.

[91] H.R. Byers, T. Etoh, J.R. Doherty, A.J. Sober, M.C. Mihm, Cell Migration and Actin Organization in Cultured Human Primary , Recurrent Cutaneous and Metastatic Melanoma Time-lapse and Image Analysis, 139 (1991) 423–435.

[92] G. Weder, M.C. Hendriks-balk, R. Smajda, D. Rimoldi, M. Liley, H. Heinzelmann, et al., Increased plasticity of the stiffness of melanoma cells correlates with their acquisition of metastatic properties, Nanomedicine Nanotechnology, Biol. Med. (2013) 1–8. doi:10.1016/j.nano.2013.07.007.

[93] I. Horcas, R. Fernández, J.M. Gómez-Rodríguez, J. Colchero, J. Gómez-Herrero, a. M. Baro, WSXM: A software for scanning probe microscopy and a tool for nanotechnology, Rev. Sci. Instrum. 78 (2007). doi:10.1063/1.2432410.

[94] M. Lekka, K. Pogoda, J. Gostek, O. Klymenko, S. Prauzner-Bechcicki, J. Wiltowska-Zuber, et al., Cancer cell recognition–Mechanical phenotype, Micron. 43 (2012) in press. http://www.scopus.com/inward/record.url?eid=2-s2.0-84858254502&partnerID=40&md5=05ab0f469a5a78279ceb335287baac79.

[95] L. Bozec, A. Hammiche, H.M. Pollock, M. Conroy, Localized photothermal infrared spectroscopy using a proximal probe, 90 (2001) 5159–5166. doi:10.1063/1.1403671.

[96] A. Hammiche, L. Bozec, H.M. Pollock, M. German, M. Reading, Progress in near-field photothermal infra-red microspectroscopy, J. Microsc. 213 (2004) 129–134. doi:10.1111/j.1365-2818.2004.01292.x.

[97] M. Reading, D. Grandy, A. Hammiche, L. Bozec, H.M. Pollock, Thermally assisted nanosampling and analysis using micro-IR spectroscopy and other analytical methods, 29 (2002) 257–260.

[98] J.G. Mo, M.D. Eddleston, P.S. Belton, D.Q.M. Craig, Analysis of single particle photodegradation using photothermal infrared microspectroscopy, (2013) 2315–2322. doi:10.1039/c3an36686c.

[99] M.E. Tipping, C.M. Bishop, Probabilistic Principal Component Analysis, J. R. Stat. Soc. Ser. B (Statistical Methodol. 61 (1999) 611–622. doi:10.2307/2680726.

[100] R. Bro, A.K. Smilde, Principal component analysis, Anal. Methods. 6 (2014) 2812. doi:10.1039/c3ay41907j.

[101] M. Ringnér, What is principal component analysis?, Nat. Biotechnol. 26 (2008) 303–304. doi:10.1038/nbt0308-303.

[102] A.M. Belu, D.J. Graham, D.G. Castner, Time-of-flight secondary ion mass spectrometry: Techniques and applications for the characterization of biomaterial surfaces, Biomaterials. 24 (2003) 3635–3653. doi:10.1016/S0142-9612(03)00159-5.

[103] R. a van den Berg, H.C.J. Hoefsloot, J. a Westerhuis, A.K. Smilde, M.J. van der Werf, Centering, scaling, and transformations: improving the biological information content of metabolomics data., BMC Genomics. 7 (2006) 142. doi:10.1186/1471-2164-7-142.

[104] J.R. Ramos, J. Pabijan, R. Garcia, M. Lekka, The softening of human bladder cancer cells happens at an early stage of the malignancy process, Beilstein J. Nanotechnol. 5 (2014) 447–457. doi:10.3762/bjnano.5.52.

[105] M.E. Dokukin, N. V Guz, I. Sokolov, Quantitative Study of the Elastic Modulus of Loosely Attached Cells in AFM Indentation Experiments, Biophysj. 104 (2013) 2123–2131. doi:10.1016/j.bpj.2013.04.019.

[106] Z. Zhou, C. Zheng, S. Li, X. Zhou, Z. Liu, Q. He, et al., AFM nanoindentation detection of the elastic modulus of tongue squamous carcinoma cells with different metastatic potentials, Nanomedicine Nanotechnology, Biol. Med. 9 (2013) 864–874. doi:10.1016/j.nano.2013.04.001.

[107] E.C. Faria, N. Ma, E. Gazi, P. Gardner, M. Brown, W. Clarke, et al., Measurement of elastic properties of prostate cancer cells using AFM, (2008) 1498–1500. doi:10.1039/b803355b.

[108] K. Hayashi, M. Iwata, Stiffness of cancer cells measured with an AFM indentation method, J. Mech. Behav. Biomed. Mater. 49 (2015) 105–111. doi:10.1016/j.jmbbm.2015.04.030.

[109] Q.S. Li, G.Y.H. Lee, C.N. Ong, C.T. Lim, Biochemical and Biophysical Research Communications AFM indentation study of breast cancer cells, 374 (2008) 609–613. doi:10.1016/j.bbrc.2008.07.078.

[110] A. Lityńska, M. Przybyło, E. Pocheć, P. Laidler, Adhesion properties of human bladder cell lines with extracellular matrix components: the role of integrins and glycosylation., Acta Biochim. Pol. 49 (2002) 643–50. doi:024903643.

[111] D. Debois, M.P. Bralet, F. Le Naour, A. Brunelle, O. Lapr??vote, In Situ lipidomic analysis of nonalcoholic fatty liver by cluster TOF-SIMS imaging, Anal. Chem. 81 (2009) 2823–2831. doi:10.1021/ac900045m.

[112] K.A.N. Nygren, K. Richter, Y.U.N. Chen, F. Dangardt, P. Friberg, Y. Magnusson, Imaging of Lipids in Human Adipose Tissue by Cluster Ion TOF-SIMS, 835 (2007) 828–835. doi:10.1002/jemt.

[113] D.C. Walker, B.H. Brown, a D. Blackett, J. Tidy, R.H. Smallwood, A study of the morphological parameters of cervical squamous epithelium., Physiol. Meas. 24 (2003) 121–135. doi:10.1088/0967-3334/24/1/309.

[114] S. Prauzner-bechcicki, J. Raczkowska, E. Madej, J. Pabijan, J. Lukes, J. Sepitka, et al., PDMS substrate stiffness affects the morphology and growth pro fi les of cancerous prostate and melanoma cells, J. Mech. Behav. Biomed. Mater. 41 (2015) 13–22. doi:10.1016/j.jmbbm.2014.09.020.

[115] H. Haga, S. Sasaki, K. Kawabata, E. Ito, T. Ushiki, T. Sambongi, Elasticity mapping of living " broblasts by AFM and immuno # uorescence observation of the cytoskeleton, 82 (2000) 253–258.

[116] S.E. Cross, Y. Jin, J. Rao, J.K. Gimzewski, Nanomechanical analysis of cells from cancer patients, 2 (2007) 1–4. doi:10.1038/nnano.2007.388.

[117] S.E. Cross, Y. Jin, J. Tondre, R. Wong, J. Rao, J.K. Gimzewski, AFM-based analysis of human metastatic cancer cells, 384003 (2008). doi:10.1088/0957-4484/19/38/384003.

[118] C. Rotsch, M. Radmacher, Drug-Induced Changes of Cytoskeletal Structure and Mechanics in Fibroblasts : An Atomic Force Microscopy Study, Biophys. J. 78 (2000) 520–535. doi:10.1016/S0006-3495(00)76614-8.

[119] H.J. Yang, I. Ishizaki, N. Sanada, N. Zaima, Y. Sugiura, I. Yao, et al., Detection of

characteristic distributions of phospholipid head groups and fatty acids on neurite surface by time-of-flight secondary ion mass spectrometry, Med. Mol. Morphol. 43 (2010) 158–164. doi:10.1007/s00795-009-0487-2.

[120] C.R. Anderton, B. Vaezian, K. Lou, J.F. Frisz, M.L. Kraft, Identification of a lipid-related peak set to enhance the interpretation of TOF-SIMS data from model and cellular membranes, Surf. Interface Anal. 44 (2012) 322–333. doi:10.1002/sia.3806.

[121] M.J. Baker, M.D. Brown, E. Gazi, N.W. Clarke, J.C. Vickerman, N.P. Lockyer, Discrimination of prostate cancer cells and non-malignant cells using secondary ion mass spectrometry., Analyst. 133 (2008) 175–179. doi:10.1039/b712853c.

[122] G. Bellisola, C. Sorio, Infrared spectroscopy and microscopy in cancer research and diagnosis., Am. J. Cancer Res. 2 (2012) 1–21. http://www.pubmedcentral.nih.gov/articlerender.fcgi?artid=3236568&tool=pmcentrez&rendertype=abstract.

[123] A. Pacifico, L.A. Chiriboga, P. Lasch, M. Diem, Infrared spectroscopy of cultured cells: II. Spectra of exponentially growing, serum-deprived and confluent cells, Vib. Spectrosc. 32 (2003) 107–115. doi:10.1016/S0924-2031(03)00051-1.

[124] J. Hefele Wald, E. Goormaghtigh, J. De Meutter, J.M. Ruysschaert, A. Jonas, Investigation of the lipid domains and apolipoprotein orientation in reconstituted high density lipoproteins by fluorescence and IR methods, J. Biol. Chem. 265 (1990) 20044–20050.

[125] W. Pohle, D.R. Gauger, H. Fritzsche, B. Rattay, C. Selle, H. Binder, et al., FTIR-spectroscopic characterization of phosphocholine-headgroup model compounds, J. Mol. Struct. 563-564 (2001) 463–467. doi:10.1016/S0022-2860(00)00830-9.

[126] M. Diem, L. Chiriboga, P. Lasch, A. Pacifico, IR spectra and IR spectral maps of individual normal and cancerous cells, Biopolym. - Biospectroscopy Sect. 67 (2002) 349–353. doi:10.1002/bip.10109.

[127] P. Dumas, L. Miller, Biological and biomedical applications of synchrotron infrared microspectroscopy, J. Biol. Phys. 29 (2003) 201–218. doi:10.1023/A:1024448910761.

[128] P. Lasch, M. Boese, A. Pacifico, M. Diem, FT-IR spectroscopic investigations of single cells on the subcellular level, Vib. Spectrosc. 28 (2002) 147–157. doi:10.1016/S0924-2031(01)00153-9.

[129] B.H. Stuart, Infrared Spectroscopy: Fundamentals and Applications, 2004. http://books.google.com.cy/books/about/Infrared_Spectroscopy.html?id=xQVog8RrJKcC&pgis=1.

[130] M.S. Wagner, D.J. Graham, B.D. Ratner, D.G. Castner, Maximizing information obtained from secondary ion mass spectra of organic thin films using multivariate analysis, Surf. Sci. 570 (2004) 78–97. doi:10.1016/j.susc.2004.06.184.

[131] A.J. Bentley, T. Nakamura, A. Hammiche, H.M. Pollock, F.L. Martin, S. Kinoshita, et al., Characterization of human corneal stem cells by synchrotron infrared micro-spectroscopy., Mol. Vis. 13 (2007) 237–242.

[132] A. Hammiche, M.J. German, R. Hewitt, H.M. Pollock, F.L. Martin, Monitoring cell cycle distributions in MCF-7 cells using near-field photothermal microspectroscopy., Biophys. J. 88 (2005) 3699–706. doi:10.1529/biophysj.104.053926.

[133] I. Dobrzynska, B. Szachowicz-Petelska, S. Sulkowski, Z. Figaszewski, Changes in electric charge and phospholipids composition in human colorectal cancer cells, Mol. Cell. Biochem. 276 (2005) 113–119. doi:DOI 10.1007/s11010-005-3557-3.

[134] G. Eliyahu, Tamar Kreizman, Hadassa Degani, Phosphocholine as a biomarker of breast cancer: Molecular and biochemical studies, Int. J. Cancer. 120 (2007) 1721–1730. doi:10.1002/ijc.22293.

[135] E. Iorio, D. Mezzanzanica, P. Alberti, F. Spadaro, C. Ramoni, S. D’Ascenzo, et al., Alterations of choline phospholipid metabolism in ovarian tumor progression, Cancer Res. 65 (2005) 9369–9376. doi:10.1158/0008-5472.CAN-05-1146.

[136] A. Ramírez de Molina, A. Rodríguez-González, R. Gutiérrez, L. Martínez-Pieiro, J.J. Sánchez, F. Bonilla, et al., Overexpression of choline kinase is a frequent feature in human tumor-derived cell lines and in lung, prostate, and colorectal human cancers, Biochem. Biophys. Res. Commun. 296 (2002) 580–583. doi:10.1016/S0006-291X(02)00920-8.

[137] S. Shimma, Y. Sugiura, T. Hayasaka, Y. Hoshikawa, T. Noda, M. Setou, MALDI-based imaging mass spectrometry revealed abnormal distribution of phospholipids in colon cancer liver metastasis, J. Chromatogr. B Anal. Technol. Biomed. Life Sci. 855 (2007) 98–103. doi:10.1016/j.jchromb.2007.02.037.

[138] K. Pogoda, J. Jaczewska, Depth-sensing analysis of cytoskeleton organization based on

AFM data, (2012) 79–87. doi:10.1007/s00249-011-0761-9.

[139] K.R. Gehlsent, G.E. Davis, P. Sriramarao, Integrin expression in human melanoma cells with differing invasive and metastatic properties, 10 (1992) 111–120.

[140] M. Lekka, K. Pogoda, J. Gostek, O. Klymenko, S. Prauzner-Bechcicki, J. Wiltowska-Zuber, et al., Cancer cell recognition--mechanical phenotype., Micron. 43 (2012) 1259–66. doi:10.1016/j.micron.2012.01.019.

[141] E. Gazi, J. Dwyer, N.P. Lockyer, J. Miyan, P. Gardner, C. Hart, et al., Fixation protocols for subcellular imaging by synchrotron-based Fourier transform infrared microspectroscopy, Biopolymers. 77 (2005) 18–30. doi:10.1002/bip.20167.

[142] K.S. Kulp, E.S.F. Berman, M.G. Knize, D.L. Shattuck, E.J. Nelson, L. Wu, et al., Chemical and biological differentiation of three human breast cancer cell types using time-of-flight secondary ion mass spectrometry., Anal. Chem. 78 (2006) 3651–3658. doi:10.1021/ac060054c.

[143] M.J. Baker, E. Gazi, M.D. Brown, N.W. Clarke, J.C. Vickerman, N.P. Lockyer, ToF-SIMS PC-DFA analysis of prostate cancer cell lines, Appl. Surf. Sci. 255 (2008) 1084–1087. doi:10.1016/j.apsusc.2008.05.256.

[144] M. a. Robinson, D.J. Graham, F. Morrish, D. Hockenbery, L.J. Gamble, Lipid analysis of eight human breast cancer cell lines with ToF-SIMS, Biointerphases. 11 (2016) 02A303. doi:10.1116/1.4929633.

List of figures

List of publications of Justyna Bobrowska

1. M.Lekka, D.Gil, K.Pogoda, J.Dulińska-Litewka, R.Jach, **J.Gostek**, O.Klymenko, S.Prauzner-Bechcicki, Z.Stachura, J.Wiltowska-Zuber, K.Okoń, P.Laidler, "Cancer cell detection in tissue sections using AFM"; *Archives of Biochemistry and Biophysics* (2012) 518: 151-156;
2. M.Lekka, K.Pogoda, **J.Gostek**, O.Klymenko, S.Prauzner-Bechcicki, J.Wiltowska-Zuber, J.Jaczewska, J.Lekki, Z.Stachura, „Cancer cell recognition – Mechanical phenotype"; *Micron* (2012) 43(12): 1259-1266;
3. A.Mzyk, R.Major, **J.Gostek**, M.Kot, P.Wilczek, „Chemical control of polyelectrolyte film properties for an effective cardiovascular implants endothelialization"; *ACME - Archives of Civil and Mechanical Engineering* (2014) 14(2): 262-268;
4. **J.Gostek**, S.Prauzner-Bechcicki, B.Nimmervoll, K.Mayr, J.Pabijan, P.Hinterdorfer, L.Chtcheglova, M.Lekka, "Nano-characterization of two closely related melanoma cell lines with different metastatic potential"; *European Biophysics Journal* (2015) 44(1): 49-55;
5. **J.Gostek**, K.Awsiuk, J.Pabijan, J.Rysz, A.Budkowski, M.Lekka, „Differentiation between Single Bladder Cancer Cells Using Principal Component Analysis of Time-of-Flight Secondary Ion Mass Spectrometry"; *Analytical Chemistry* (2015) 87(6): 3195-3201;
6. M.G.Ayele, J.Czwartos, D.Adjei, P.Wachulak, Inam Ul Ahad, A.Bartnik, Ł.Węgrzynski, M.Szczurek, R.Jarocki, H.Fiedorowicz, M.Lekka, K.Pogoda, **J.Gostek**, "Contact Microscopy using a Compact Laser Produced Plasma Soft X-Ray Source"; *Acta Physica Polonica A* (2016) 129(2): 237-240;
7. **J.Bobrowska**, J.Pabijan, J.Wiltowska-Zuber, B.R.Jany, F.Krok, K.Awsiuk, J.Rysz, A.Budkowski, M.Lekka, "Protocol of single cells preparation for time of flight secondary ion mass spectrometry"; *Analytical Biochemistry* (2016) 511: 52-60;
8. **J.Bobrowska**, J.Pabijan, J.Wiltowska-Zuber, B.R.Jany, F.Krok, K.Awsiuk, J.Rysz, A.Budkowski, M.Lekka, "Data on step-by-step atomic force microscopy monitoring of changes occurring in single melanoma cells undergoing ToF SIMS specialized sample preparation protocol"; *Data in Brief* (2016) 8: 1322-1332;